ELECTROCHEMICAL DETERMINATION OF THE STANDARD FREE ENERGY OF FORMATION OF ALUMINA AT STEELMAKING TEMPERATURES

By

DEBABRATA S. GHOSH, B.Tech., M.Eng.

A Thesis
Submitted to the School of Graduate Studies
in Partial Fulfilment of the Requirements
for the Degree
Doctor of Philosophy

McMaster University
August 1975

STANDARD FREE ENERGY OF FORMATION

OF ALUMINA

DOCTOR OF PHILOSOPHY (1975) McMASTER UNIVERSITY
(Metallurgy & Material Science) (Hamilton, Ontario)

TITLE: Electrochemical Determination of the Standard Free Energy of Formation of Alumina at Steelmaking Temperatures

AUTHOR: Debabrata S. Ghosh, B.Tech. (Indian Institute of Technology, Bombay)

M.Eng. (McMaster University)

SUPERVISOR: Professor D. A. R. Kay

NUMBER OF PAGES: (xv), 182

ABSTRACT

A high temperature electrochemical formation cell

$$Pt_{(s)}, Al_{(\ell)} \mid Al_2O_3 \text{ in } CaF_{2(\ell)} \mid O_{2(g)}, Pt_{(s)}$$

has been used to determine the standard free energy of formation of alumina at steelmaking temperatures. The temperature variation of the free energy was determined as

$$\Delta G^\circ_f(Al_2O_3) = -398,560 + 80.02T(\pm 1,800) \text{ cal/mole}$$

in the temperature range 1700°-1850°K. These results are in good agreement with those reported in the literature at ~1300°K using a similar technique but are 3.3% more positive than the generally accepted thermochemical value at 1800°K. In order to confirm the absence of any systematic errors in the above cell, the following cell was designed and operated in the temperature range 1641°-1785°K

$$C_{gr}, Al_{(\ell)} \mid Al_2O_3 \mid \underset{(O^{2-})}{\text{Electrolyte containing}} \mid Al_2O_3 \mid Fe\text{-}C_{satd}, CO_{(g)}, C_{gr} .$$

The results from this cell are in good agreement with those of the first cell within the experimental error.

The Third Law analysis of the present data gives an average value of the standard heat of formation of alumina at 298°K, ΔH°_{298}, of −392.6 (± 0.92) kcal/mole which is in good agreement with the Third Law analysis of lower temperature cell (~1300°K) data and the values of ΔH°_{298} calculated from phase equilibria and solution calorimetric data in mineralogical systems. All these values are at variance with the presently accepted "best" value of ΔH°_{298} = −400.40 (± 0.3) kcal/mole from oxygen bomb calorimetry, although the average of <u>all</u> bomb calorimetric data is in agreement. Using the presently determined ΔG°_f (Al_2O_3), the temperature dependence of $K = h^2_{Al} \cdot h^3_O$, the aluminum deoxidation constant, can be calculated as

$$\log K = -\frac{62{,}160}{T} + 20.86 \ (\pm 0.2 \text{ at } 1873^\circ\text{K}) \ .$$

The value of $K = 4.7 \times 10^{-13}$ at 1600°C is in good agreement with the most recent work of Jacquemont et al. (1973) and is an order of magnitude higher than previous calculations. An independent calorimetric determination of ΔH°_{298} using a method other than oxygen bomb calorimetry is therefore suggested.

ACKNOWLEDGEMENTS

The author wishes to express his gratitude to Dr. D. A. R. Kay for his guidance and encouragement during the course of this study. Grateful acknowledgements are also due to Mr. W. A. R. Drappo for his assistance with Cell II experiments.

The author would like to thank members of the staff and graduate students of McMaster Metallurgy Department who through many discussions contributed to the solution of various problems. Special thanks are due to Mr. P. Apté for his helpful criticism and assistance with the thesis and to Ms. Erie Long for her accurate rapid typing of the thesis.

TABLE OF CONTENTS

TABLE OF CONTENTS - continued

TABLE OF CONTENTS - continued

TABLE OF CONTENTS - continued

LIST OF TABLES

LIST OF TABLES - continued

LIST OF ILLUSTRATIONS

LIST OF SYMBOLS

s, ℓ, g	(subscripts) indicate the physical state of the material, i.e., solid, liquid and gas, respectively
$\Delta G°$	change in the Gibbs standard free energy
$\Delta H°$	change in the standard enthalpy
$\Delta S°$	change in the standard entropy
T	absolute temperature in degrees Kelvin
f	(subscript) formation of the product from the elements
K	equilibrium constant for the reaction as written
[ ]	represents a component in solution in liquid iron
1 w/o	(subscript) refers to the 1 wt. pct. standard state
h_i & f_i	Henrian activity and activity coefficient of component i, respectively
[%i]	concentration of component i in wt. pct.
K'	deoxidation "constant" (obtained by replacing activities in K by concentrations)
a_i	Raoultian activity of component i
C_p	specific heat at constant pressure
p_i	partial pressure of gaseous species i
f_i^j	gives the effect of solute j on the activity coefficient of i ($f_i = \prod_{j=1}^{n} f_i^j$ where j=1 to n represents n solutes in iron)
e_j^i	interaction parameter, $e_i^j = \dfrac{\partial \log f_i}{\partial [\%j]}$
γ_i	Raoultian activity coefficient of solute i
γ_i^0	γ_i at infinite dilution (i.e. slope of the Henry's-law line)
E	electromotive force of an electrochemical cell
E^0	standard cell EMF, i.e. when all the constituents are in their standard states

R	gas constant, 1.987 cal/mole-deg.
F	Faraday, 96494 coul./mole
n	number of electrons involved in the cell reaction
gef_T	Gibbs energy function, $(G^\circ - H^\circ_{298})/T$
μ_i	chemical potential of element i
M	atomic weight
$\vdots$	indicates a porous plug or an ion selective membrane

CHAPTER I

INTRODUCTION

Making steel is a succession of reductions and oxidations. The iron oxide of the ore is first reduced by carbon in the blast furnace, the hot metal produced containing elements such as silicon, manganese, phosphorus and sulphur in addition to carbon. Making steel from this hot metal consists of removing these elements, with the exception of sulphur, by oxidation in an open hearth or a basic oxygen furnace. Finally, the unavoidable excess oxygen in the steel is reduced by a process known as deoxidation. Being the last step in the process, deoxidation practices have a considerable influence on the mechanical properties of the final steel.

Deoxidation is accomplished by the addition of elements whose oxides are more stable than those of iron. These elements are called deoxidizers and one of the most powerful deoxidizers used commercially is aluminum.

Aluminum deoxidation has become increasingly important with the advent of new steel processes. It is being used extensively in vacuum degassing and in continuous casting. The product of deoxidation with aluminum is usually solid alumina, the exception being the formation of the spinel $FeAl_2O_4$ (hercynite) when not enough aluminum is added to the steel. Aluminum deoxidation with the formation of alumina can therefore be represented by the reaction

$$2[Al]_{1w/o} + 3[O]_{1w/o} \rightleftarrows Al_2O_{3(s)} \tag{1.1}$$

where [ ] represents a component in solution in liquid iron and "1w/o" refers to the standard state. Under equilibrium conditions the soluble oxygen is related to the soluble aluminum through the equilibrium constant 1/K where K is given by

$$K = h_{Al}^2 \cdot h_O^3 / a_{Al_2O_3}$$

$$= [\%Al]^2 \cdot [\%O]^3 \, f_{Al}^2 f_O^3 \quad \text{when} \quad a_{Al_2O_3} = 1 \tag{1.2}$$

where $a_{Al_2O_3}$ is the Raoultian activity of alumina;

h_i and f_i are the Henrian activity and activity coefficient of the component i, respectively; and

[%i] is the concentration of component i in iron in weight percent.

There have been many direct determinations of the equilibrium constant K and the product, $K' = [\%Al]^2[\%O]^3$, reported in the literature. The experimental procedure generally consisted of analysing samples from Fe-Al-O melts, equilibrated with solid alumina, for aluminum and oxygen and determining values of K' and K. However, agreement in the results reported is poor, values of both K' and K varying from 10^{-9} to 10^{-14}. The main reasons for these discrepancies are summarized below.

(1) Aluminum is a strong deoxidizer and the equilibrium concentrations of aluminum and oxygen are very small. Using the value of $K = 10^{-14}$ an oxygen activity of 5 ppm is obtained for an aluminum activity of 0.01 wt% at 1600°C. The errors in aluminum and oxygen analysis at these

concentrations can be quite large.

(2) It is difficult to ensure that samples are taken from a "clean" melt, as the melt invariably contains some fine suspended alumina particles.

(3) Some of the investigations were carried out under "inert" argon atmospheres which could have provided the oxygen for the continuous oxidation of aluminum and the formation of suspended alumina particles.

(4) It has been suggested[25] that the high values of K ($\sim 10^{-9}$) obtained when aluminum is added to an oxygen containing melt are due to the large supersaturation required to nucleate the solid reaction product alumina in the liquid iron. In other words a metastable equilibrium is attained.

(5) The deoxidation product K' may vary since the Al-O interactions in iron are not taken into account. However, these corrections are not very significant at low concentrations.

(6) Because of the low concentrations of the reactants involved, the deoxidation reaction may not have reached equilibrium in many experimental investigations.

From this discussion it is apparent that, for a strong deoxidizer such as Al, direct determinations of deoxidation equilibria are subject to considerable error. In such cases, a more reliable value of the equilibrium constant can be obtained from a knowledge of the standard free energy change of the deoxidation reaction, e.g. equation (1.1). The following thermodynamic data are required to calculate the free energy change for reaction (1.1)

$$Al_{(\ell)} \rightleftarrows [Al]_{1w/o} \qquad \Delta\overline{G}_{Al} \qquad (1.3)$$

$$\frac{1}{2}\, O_{2\,(g)} \rightleftarrows [O]_{1w/o} \qquad \Delta\overline{G}_{O} \qquad (1.4)$$

$$2Al_{(\ell)} + \frac{3}{2}\, O_{2\,(g)} \rightleftarrows Al_2O_{3\,(s)} \qquad \Delta G^\circ_f\ (Al_2O_3)\ . \qquad (1.5)$$

There are several determinations of $\Delta\overline{G}_{Al}$ and $\Delta\overline{G}_{O}$ at 1600°C and the "best" values have been compiled[7,58,166]. However, there are no direct determinations of the standard free energy of formation of alumina, ΔG°_f, at steelmaking temperatures, the highest temperatures at which such determinations are reported being at aluminum extraction temperatures ∿1000°C[74,110-114]. Moreover, these values are consistently more positive than the presently accepted thermochemical data[58,59], except for the work of Thonstad[114].

The thermochemical calculation of the standard free energy of formation at any temperature essentially requires the determination of two quantities, the standard enthalpy of formation at 298°K, ΔH°_{298}, and the specific heats (Cp) of the products and the reactants. The value of ΔH°_{298} for alumina has been determined at least nine times[43-51] by oxygen "bomb" calorimetry since the first determination by Berthelot[42] in 1901. The spread in the values obtained is more than 27 kcal/mole. The currently accepted "best" value[58,59] is −400.4 ± 0.3 kcal/mole and is based on the data of Holley and Huber[49] (−400.29 kcal/mole) and Mah[51] (−400.48 kcal/mole). Although these values are in excellent agreement, there is some doubt as to their accuracy.

In general, the determination of specific heats is relatively accurate and the error in the free energy calculations arise from those from the determination of ΔH°_{298}. An error of 10 kcal/mole in the free energy of formation of alumina at 1600°C would result in an order of magnitude difference in the value of the equilibrium constant. For these reasons it was decided to determine the standard free energy of formation of alumina directly at steelmaking temperatures.

One of the methods of generating accurate thermodynamic data is the use of electrochemical cells, provided certain reversibility conditions are ensured. The following high temperature formation cell was therefore studied

$$\text{Cell I} \qquad Pt_{(s)},\ Al_{(\ell)} \left|\ \begin{matrix}\text{electrolyte satd with} \\ Al_2O_3\end{matrix}\ \right| O_{2\,(g)},\ Pt \qquad (1.6)$$

from which ΔG°_f (Al_2O_3) could be directly obtained. In order to check the reversibility of the oxygen electrode and the predominantly ionic conductivity of the CaF_2-Al_2O_3 electrolyte used in this cell, another cell with different electrodes and electrolyte was also studied. This cell can be represented as

$$\text{Cell II} \quad C_{gr},\ Al_{(\ell)}|Al_2O_{3\,(s)}|\begin{matrix}\text{electrolyte} \\ (O^{2-})\end{matrix}|Al_2O_3|Fe\text{-}C_{satd.},\ CO_{(g)},\ C_{gr} \qquad (1.7)$$

for which the following cell reaction can be written

$$2Al_{(\ell)} + 3CO_{(g)} \rightleftarrows Al_2O_{3\,(s)} + 3C_{(s)} \ . \qquad (1.8)$$

Thus, the standard free energy of alumina can be calculated from the cell EMF using the well established values[59] of the standard free energy of formation of CO.

CHAPTER II

LITERATURE REVIEW

2.1 Introduction

This chapter reviews the work reported in the literature related to this investigation. This review is divided into three main sections:

(A) The first section deals with the thermodynamics of deoxidation of iron with aluminum. The many experimental determinations of the product, $K' = [\%Al]^2[\%O]^3$, and the equilibrium constant, $K = h_{Al}^2 \cdot h_O^3$, by direct and indirect means, are reviewed. Calculations of the equilibrium constant from thermochemical data are also reviewed.

(B) The second section reviews the existing thermochemical data required to calculate the standard free energy of formation of alumina, ΔG_f°, at steelmaking temperatures and the free energy of solution of Al and O in iron. The standard heat of formation of alumina at 298°K, ΔH_{298}°, and the heat capacities of aluminum, oxygen and alumina in the temperature range 0-1900°K are required to calculate ΔG_f° in the same temperature range.

(C) The final section deals with previous experimental determinations of ΔG_f° of alumina using electrochemical formation cells.

(A) Aluminum Deoxidation of Iron

2.2 Introduction

As there exist quite a few good reviews on the general topic of deoxidation[1-7], no attempt has been made to make this section exhaustive. Rather, it will endeavour to highlight problems in the determination of the deoxidation thermodynamics of a strong deoxidizer such as aluminum.

Deoxidation of iron by aluminum can be represented by the equation

$$2[Al]_{1w/o} + 3[O]_{1w/o} \rightleftarrows Al_2O_{3(s)} \qquad (2.1)$$

for which an equilibrium constant, 1/K, can be written as

$$K = h_{Al}^2 \cdot h_O^3 / a_{Al_2O_3}$$

$$= f_{Al}^2 f_O^3 [\%Al]^2 [\%O]^3 \qquad (2.2)$$

when $a_{Al_2O_3} = 1$, where the symbols have the same meaning as before. Assuming Henrian activity coefficients of aluminum and oxygen (f_{Al} and f_O) to be unity, a quasi-deoxidation constant, K', given by the product

$$K' = [\%Al]^2 [\%O]^3 \qquad (2.3)$$

can now be written in terms of oxygen and aluminum analyses of iron in equilibrium with alumina. However, as the interaction in iron between a strong deoxidizer, such as aluminum, and oxygen cannot be neglected, this "constant" will vary with the aluminum content of iron at a constant temperature. The experimental determination of K' and K at steelmaking temperatures is now considered.

2.3 Experimental Determinations of Deoxidation "Constant", K'

2.3.1 By direct determination of oxygen

The many experimental determinations of deoxidation "constant", K', reported in the literature, are summarized in Table 2.1 and Figure 2.1. The early experimental attempts of Hessenbruch[8] and Herty et al.[9] were followed by a more systematic study of Wentrup and Hieber[10]. Wentrup and Hieber added aluminum to liquid iron of high oxygen content in an induction furnace and considered that 10 minutes were sufficient to reach equilibrium and to float out the deoxidation products from the melt. Parts of the melts thus obtained were poured into a copper mould and analysed for total aluminum and oxygen (soluble and insoluble forms), assuming that insoluble parts were in solution at the temperatures at which samples were taken. Their results show considerable scatter, the maximum and minimum values of K' differing by factors of 10 to 15 at each temperature.

The following sources of error were present in the work of Wentrup and Hieber:

(1) As we will see later from the work of Repetylo et al.[11], the

TABLE 2.1

EXPERIMENTAL VALUES OF DEOXIDATION "CONSTANT", $K' = [\%Al]^2 \cdot [\%O]^3$

Authors	Reference	log K'	$K'_{1873°}$	Notes
Hessenbruch	8	-	$\approx 10^{-9}$	Atm: Air
Herty et al.	9	-	6.3×10^{-9}	Atm: Air
Wentrup and Hieber	10	$-71200/T + 27.98$	0.9×10^{-10}	Equilibrated only 10 min. Atm: Air at 10-20 torr.
Hilty and Crafts	12	$-58600/T + 22.75$	2.91×10^{-9}	Large scatter. Reaction product contained hercynite. Argon atm.
Repetylo et al.	11	-	10^{-9}	Large scatter. Atm: Argon + O_2
		-	5×10^{-13}	Pure Argon atm.
Swisher	13	$(-45500/T + 11.55)$	$\approx 10^{-13}$ (1853°)	$K'_{1853°}$ at 0.01%Al combined with data of refs. 14 & 15
Rohde et al.	27	-	3.5×10^{-11}	Without slag. Argon atm.
		-	7.1×10^{-14}	With $CaO-Al_2O_3$ slag. Argon atm.
Geller and Dicke	17	$-58600/T + 18.90$	4.1×10^{-13}	Oxygen determined indirectly from C-O equilibrium
Shibata and Yagihashi	19	$-12675/T - 2.85$	2.4×10^{-10}	Carbon satd. melt. oxygen from C-O equilibrium
Braun et al.	28	-	5×10^{-14}	Mechanical stirring and long equilibration

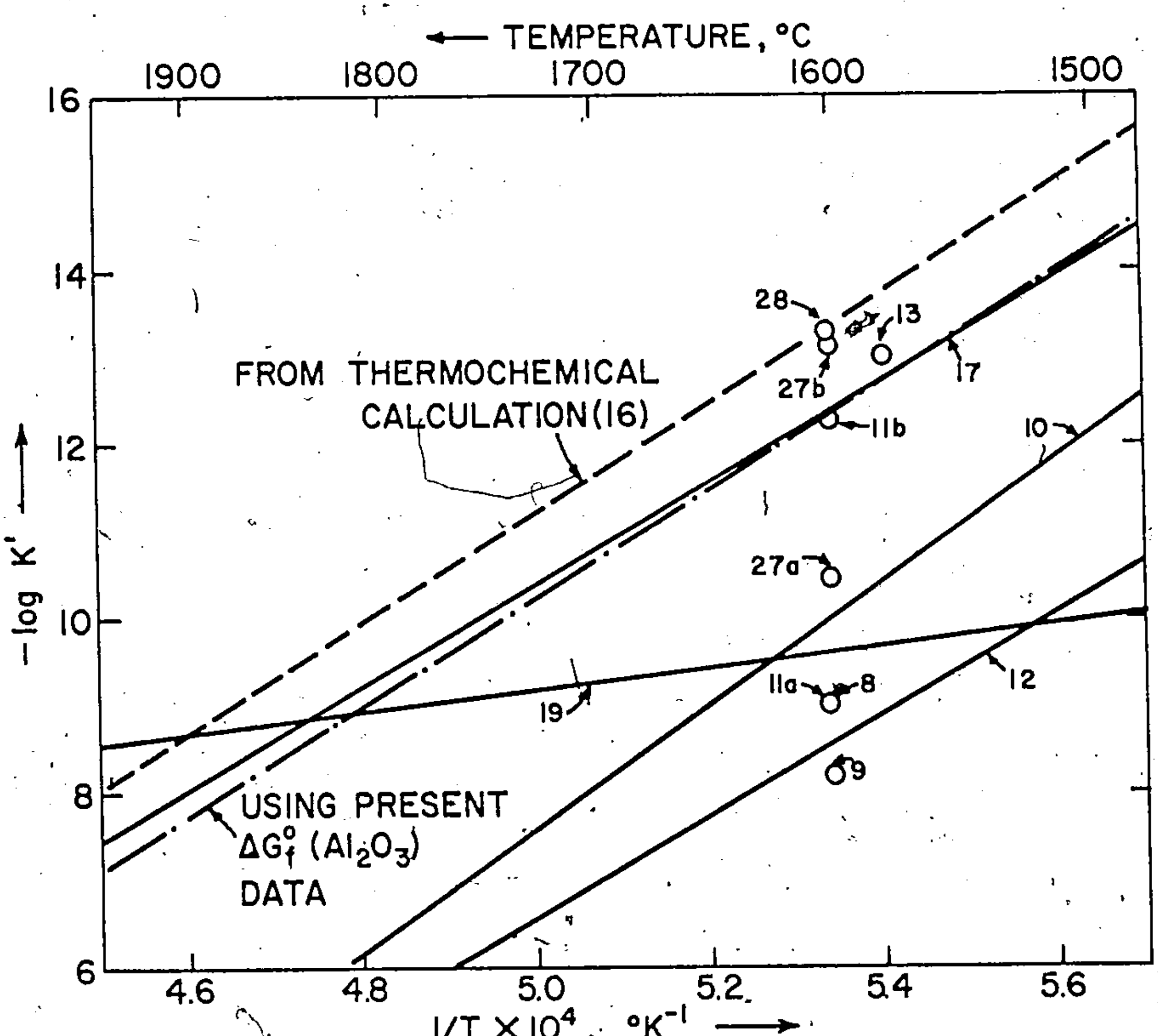

Figure 2.1: Experimental determinations of deoxidation product, $K' = [\%Al]^2[\%O]^3$. (Numbers in the figure indicate reference sources).

furnace atmosphere used by Wentrup and Hieber, consisting of air at 10-20 mm Hg pressure, is a serious source of continuous oxidation resulting in a higher oxygen content of the steel.

(2) It is doubtful if the melt equilibrated in the short period of 10 minutes. Also, fine deoxidation products take much longer to separate out of the melt. This will give rise to higher than equilibrium values of aluminum and oxygen.

(3) The temperature was measured by a Bioptex colour pyrometer which they assumed gave a direct reading of the true temperature of liquid metal. Thus, there could be considerable error in temperature measurement.

(4) Difficulties in the analysis of small quantities of aluminum and oxygen in iron, especially oxygen.

Hilty and Crafts[12] determined the solubility of oxygen in liquid iron containing aluminum in an inert argon atmosphere, using a rotating induction furnace. Metal samples, taken with a fast quenching "Taylor sampler", were analysed for total aluminum and oxygen. Samples of the reaction product ("slag"), frozen at the tip of a cold steel rod, were examined by X-ray diffraction. Their results also showed great scatter, the deoxidation product (K') varying by a factor of more than 50. From the X-ray diffraction study of their "slag" (and the reaction product found on the inner surfaces of their alumina crucibles) which generally contained hercynite, it is clear that their melt was not in equilibrium with alumina. Their samples, quenched rapidly to prevent precipitation, sometimes contained fine alumina indicating some melt contamination. Although their melts were clearly not in equilibrium with alumina, their results expressed as deoxidation product $[\%Al]^2[\%O]^3$ are included in Table 2.1 and Figure 2.1.

To understand why the deoxidation products obtained by Hilty and Crafts and from most industrial experiments ($K' = 10^{-9}$ at 1600°C) are substantially different from deoxidation constants obtained from thermochemical data ($K = 10^{-14}$ at 1600°C), Repetylo and coworkers(11) performed two types of experiments.

(1) Kinetic experiments. Aluminum was added to an iron melt containing oxygen and samples were taken for analysis at convenient intervals. These experiments were done in a high purity argon atmosphere to prevent any aluminum reoxidation. Results show that the product $[\%Al]^2[\%O]^3$ continuously dropped with time, the lowest figure obtained being $K' = 5\times10^{-13}$. This is believed to be due to continuous floating out of deoxidation product alumina. However, as a completely clean melt is almost impossible to get, the true K' cannot be obtained even after a long time.

(2) Deoxidation under an oxygen containing atmosphere. Samples for analysis were taken every 10 minutes from a melt to which Al was added periodically. The atmosphere used was argon containing some oxygen. There was quite a large scatter in the value of the deoxidation product obtained, the average value being quite close to 10^{-9}, in good agreement with that of Hilty and Crafts and industrial practice. This difference in result is believed to be due to the formation of an alumina suspension being continuously produced by reaction with

absorbed oxygen.

Finally, Swisher[13] has reported values of K' at 1580°C from equilibration studies, with the aluminum content of the metal as high as 10%. A variation of K' with Al content was observed, but the scatter was too large to permit an evaluation of K by extrapolation to zero weight percent Al. The value of K' at 0.01% Al has been combined with the data of Gokcen and Chipman[14] and d'Entremont et al.[15] to yield a temperature dependence of K', shown in Table 2.1.

Swisher used a vacuum fusion technique to analyse for oxygen which was never larger than 10 ppm in his samples. This is close to the limit of analysis of this method. Secondly, as pointed out by d'Entremont et al.[15] and Fruehan[16], the vacuum fusion technique is not suitable for oxygen analysis at high aluminum concentrations, because of absorption of gas by the aluminum distilled from the sample and vaporization of Al_2O which condenses at lower temperatures.

2.3.2 By indirect determination of oxygen

As we have seen above, the oxygen content of iron in equilibrium with an aluminum content which can be reasonably analysed in steel, say 0.01%, is ~5 ppm. This cannot be determined by conventional analytical techniques. This is why some workers have used the C-O equilibrium

$$[C]_{1w/o} + [O]_{1w/o} \rightleftarrows CO_{(g)} \qquad (2.4)$$

$$K_4 = \frac{p_{CO}}{h_C h_O} = \frac{p_{CO}}{[\%C][\%O]f_C f_O} = \frac{K_4'}{f_C f_O} \tag{2.5}$$

when p_{CO} = 1 atm., to calculate the oxygen content of iron in equilibrium with certain Al and C contents.

Geller and Dicke[17] equilibrated iron containing aluminum and 0.4-1.1% carbon in alumina crucible with CO gas at 1 atm., and studied the equilibrium

$$3[C]_{1w/o} + Al_2O_{3(s)} \rightleftarrows 2[Al]_{1w/o} + 3CO_{(g)} \tag{2.6}$$

$$K_6 = \frac{h_{Al}^2}{h_C^3} = \frac{[\%Al]^2 f_{Al}^2}{[\%C]^3 f_C^3} \tag{2.7}$$

K_6 was determined in the temperature range 1575-1775°C by analysing for aluminum and carbon in the equilibrated metal and assuming the activity coefficients f_{Al}, f_C, to be unity. The results were combined with the data on the C-O equilibrium (eq. (2.5)) published by Geller[18] to obtain deoxidation constant K'

$$K_6'/(K_4')^3 = [\%Al]^2[\%O]^3 = K' \ . \tag{2.8}$$

Their results are shown in Figure 2.1 and Table 2.1. The following sources of error were present in their work:

(1) The assumption that activity coefficients f_{Al}, f_C, f_O, are unity is not valid (see Section 2.4.2).

(2) The data on the C-O equilibrium used (Geller[18]) are not very accurate.

Yagihashi and Shibata[19] equilibrated carbon saturated iron containing about 2% Al with CO gas in graphite crucibles in the temperature range 1650-2060°C. The quenched melts were analysed for aluminum and carbon. Their data were analysed in the same manner as above and results are shown in Table 2.1 and Figure 2.1.

This work also suffers from the same problem as the earlier work of Geller and Dicke, i.e. concentrations rather than activities have been used to determine the equilibrium constants. In fact, in this work much higher concentrations of carbon (4.2 to 5.8%) and aluminum (1.1 to 2.7%) used will result in much larger errors. The scatter in the data, however, is much less, probably due to smaller variation in composition.

2.4 Experimental Determinations of the Equilibrium Constant K

2.4.1 By direct determination of oxygen

One of the earliest determinations of the equilibrium constant of aluminum deoxidation was done by Gokcen and Chipman[14] who equilibrated iron containing an initial charge of aluminum in alumina crucibles with controlled atmospheres of H_2O and H_2. The resulting melts were quenched to retain the equilibrium concentrations of aluminum and oxygen and subsequently analysed for these elements. Relatively high temperatures of 1695°, 1760° and 1866°C were chosen to obtain concentrations of aluminum and oxygen high enough for analysis. The following (simultaneous) equilibria were assumed to have been attained in the period of 8 hours at the reaction temperature:

(1) $Al_2O_{3(s)} \rightleftarrows 2[Al]_{1w/o} + 3[O]_{1w/o}$

$$K_1 = h_{Al}^2 h_O^3 = K_1' f_{Al}^2 f_O^3 \tag{2.10}$$

(2) $Al_2O_{3(s)} + 3H_{2(g)} \rightleftarrows 2[Al]_{1w/o} + 3H_2O_{(g)}$

$$K_2 = h_{Al}^2 (p_{H_2O}/p_{H_2})^3 = K_2' f_{Al}^2 \tag{2.11}$$

(3) $H_{2(g)} + [O]_{1w/o} \rightleftarrows H_2O_{(g)}$

$$K_3 = (p_{H_2O}/p_{H_2})(1/h_O) = K_3'/f_O \tag{2.12}$$

The activity coefficient of oxygen, f_O, in the Fe-Al-O alloys, determined from equation (2.12) and the data of Dastur and Chipman[20], was found to be extremely low indicating some systematic error in oxygen analysis or gas composition. The variation of log K_3' with aluminum was, therefore, used to determine e_O^{Al}, assuming f_O^O to be unity. However, the results are extremely sensitive to slight errors in oxygen analysis.

Assuming the self-interaction coefficients, f_O^O and f_{Al}^{Al}, to be unity, the following equation was derived

$$\log K_1 = \log K_1' + 3e_O^{Al}(1.12[\%O] + [\%Al]) \tag{2.13}$$

from which another set of values of e_0^{Al} was obtained. These values are, however, independent of gas composition but dependent on aluminum analysis. The values of e_0^{Al} thus obtained are substantially different from the earlier values, indicating the very approximate nature of the results. The average values at 1866°, 1760° and 1695°C have been extrapolated to give $e_0^{Al} = -12$ at 1600°C.

There is too much scatter in the data to yield values of e_{Al}^0 from the variation of log K_2' with oxygen content and so e_{Al}^0 has been calculated from the value of e_0^{Al} above.

The equilibrium constant K_1 is finally found from K_1' using the interaction coefficients determined above. The average value of log K_1 at each temperature has been compared with that calculated from thermochemical data. The agreement is fair and no change in equation is suggested. The results are summarized in Table 2.2.

McLean and Bell[21] have redetermined the equilibrium constant and the solution thermodynamics of the Fe-Al-O system by the same method as Gokcen and Chipman except for the following modifications:

(1) Argon was used to dilute the H_2-H_2O gas mixture to give a ratio of Ar:H_2 of 6:1. This is known to reduce errors due to thermal diffusion which was probably a serious source of error in Gokcen and Chipman's work inspite of their preheating the gas.

(2) The vapour pressure of water over saturated solutions of LiCl has been redetermined. The values are somewhat different from those used by Gokcen and Chipman.

TABLE 2.2

EXPERIMENTAL VALUES OF EQUILIBRIUM CONSTANT, $K = h_{Al}^2 \cdot h_O^3$

Authors	Reference	log K	$K_{1873°}$	e_O^{Al} at 1873°K	Notes
Gokcen and Chipman	14	-11.78 (1968°K) -11.13 (1996°K) -11.18 (2033°K) -9.85 (2139°K)	(2×10^{-14})	-12	Equilibration with H_2/H_2O and alumina
McLean and Bell	21	-11.62 (1996°K) -10.13 (2096°K)	-	-4.6	Equilibration with H_2/H_2O & alumina
d'Entremont et al.	15	-11.18 (2013°K) -9.71 (2183°K)	-	-1.0	Equilibration with alumina under argon
Bůzek	24	-	3.2×10^{-14}	-1.15	- do -
Schenck et al.	25	-49500/T + 17.21	7.1×10^{-10}	-0.22	Precipitation experiment
		-	3.3×10^{-12}	-	Reduction with 100 torr. CO
Rohde et al.	27	-64000/T + 20.57	2.7×10^{-14}	-1.17	Using $CaO-Al_2O_3$ slag and Ar atm.
Chipman and Langenberg	29	2.8×10^{-13} (1973°K)	3.6×10^{-14}	-	C satd. Fe-C-Si-Al melt equilibrated with $Al_2O_3-SiO_2-CaO$
Sawamura et al.	30	-62500/T + 19.70	2.1×10^{-14}	-	Recalculation of data from ref. 17
Fruehan	16	-	5.6×10^{-14}	-3.90	Using an electrochemical oxygen cell
Jacquemont et al.	32	-	1.2×10^{-13}	-	- do -

McLean and Bell analysed their data in the same manner as Gokcen and Chipman above. Their results are shown in Table 2.2. The interaction parameter e_{O}^{Al} was calculated to be -4.6 at 1600°C by extrapolation of data at higher temperatures. This is not in good agreement with the value of -12 for the same quantity reported by Gokcen and Chipman. This is not surprising considering the fact that in both investigations the results were extremely sensitive to small errors in analysis of either element.

In order to get enough oxygen in their samples to analyse by the conventional techniques, Gokcen and Chipman and McLean and Bell restricted the aluminum content of their melts to less than 0.07%. However, this range of concentration is so limited that only a rough value of the interaction coefficient could be obtained. For this reason d'Entremont et al.[(15)] redetermined the Al-O interaction in iron containing much larger quantities of Al. Their experimental method simply consisted of equilibrating Fe-Al melts with the alumina crucible at 1740° and 1910°C under argon atmospheres for 4 hours, then quenching and analysing for Al and oxygen. However, it was noted in Section 2.3 that the vacuum fusion technique for oxygen analysis is susceptible to error at high aluminum contents. On the assumption that oxygen in steels containing an excess of aluminum is essentially all present as alumina the authors determined the alumina content as residue after dissolving the sample in acid. The total aluminum content was also determined and their results indicate a minimum in % oxygen versus % aluminum plot in the composition range of 0.2-0.5% Al. The minimum has been observed in other systems[(22)] and simply reflects the effect

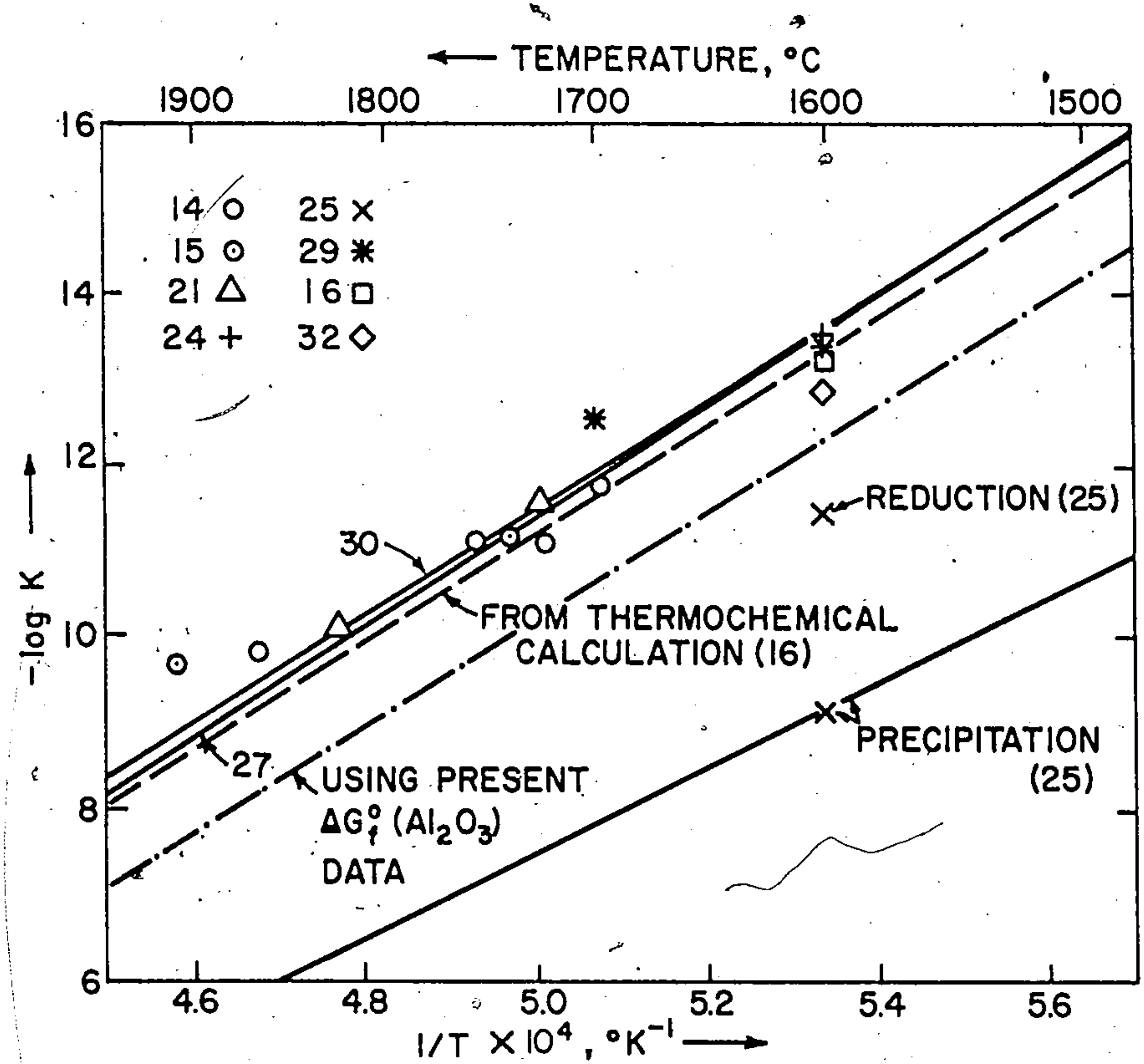

Figure 2.2: Experimental determinations of equilibrium constant $K = h_{Al}^2 \cdot h_O^3$. (Numbers in the figure indicate reference sources).

of aluminum on the activity coefficient of oxygen. In spite of considerable scatter in the data, the variation of log K' with aluminum was used to determine the interaction parameter e_O^{Al} using the value of e_{Al}^{Al} reported by Wilder and Elliott[23]. The value of $e_O^{Al} = -1$ obtained at 1600°C can be compared with -12 and -4.6 as reported by Gokcen and Chipman and McLean and Bell, respectively, for the same quantity. However, their values of the equilibrium constant are in good agreement with those of earlier workers.

Buzek[24] has reported the effects of 14 different elements on the solubility and activity of oxygen in liquid iron at 1600°C. His method also consisted of equilibrating iron alloys in alumina crucibles under argon atmospheres at 1600°C and then determining the equilibrium content of alloy and oxygen. He has incorporated the self-interaction coefficients of the alloying element and oxygen in his analysis and has solved the resulting equation for e_O^i with the help of a computer. His results with aluminum are shown in Table 2.2 and Figure 2.2.

From the values of interaction parameters shown in Table 2.2, it is now apparent that activity corrections cannot account for the large difference in the reported values of K' ($\sim 10^{-9}$) and K ($\sim 10^{-14}$) at 1600°C. To explain this difference, Schenck et al.[25] put forward the theory that a large supersaturation of aluminum and oxygen is required to nucleate alumina particles in liquid iron, thus preventing the bath from reaching equilibrium. On the other hand the reverse process of reduction of alumina should reach equilibrium. To verify their theory Schenck et al. performed the following experiments:

(1) Precipitation experiments in which aluminum was added to an iron melt containing oxygen. Samples, taken with an alumina tube at convenient intervals, were analysed for aluminum and oxygen.

(2) Reduction experiments in which iron melts held in alumina crucibles were equilibrated with CO gas at 100 torr. Melts were then quenched and analysed.

For the metastable state (precipitation runs) the following quantities were defined

$$\pi^* = (h_{Al}^2 \cdot h_O^3)_{precipitation} \tag{2.14}$$

$$(\pi^*) = [\%Al]^2[\%O]^3 \tag{2.15}$$

which were related through the equation

$$\log(\pi^*) = \log \pi^* - (2e_{Al}^{Al} + 3e_O^{Al})\cdot[\%Al] \tag{2.16}$$

where the term involving the oxygen concentration has been neglected. From the variation of $\log(\pi^*)$ with aluminum content and using the value of $e_{Al}^{Al} = 0.087$ (Belton and Fruehan[26]), the authors have found $e_O^{Al} = -0.22$ and $\log \pi^* = -9.15$ at 1600°C. Using the Gibbs-Thompson equation

$$RT(\ln \pi^* - \ln K) = 2\,\frac{\sigma}{r}\cdot\overline{V}_{Al_2O_3} \tag{2.17}$$

where σ is the interfacial tension between iron and alumina, r is the particle radius and $\overline{V}_{Al_2O_3}$ is the molar volume of alumina, Schenck et al. have calculated the difference (log π^* - log K) to be 4.02, which is close to the value 4.09 obtained above. The calculation of log K from their reduction experiments leads to an average value of -11.48 at 1600°C which, though smaller than the -9.15 obtained for log π^*, is still larger than the thermochemical value, log K = -13.24. The authors themselves point out that ±10 ppm error in their oxygen analysis could vary K between 10^{-12} and 10^{-14}.

There could be other explanations for the difference in the values of K' and K described before. The reaction product alumina could remain suspended in the melt giving rise to larger than equilibrium values of total aluminum and oxygen. Rohde et al.[27] have carried out deoxidation runs using aluminum, with and without a lime-alumina slag. Argon was used to stir the melt, and the slag, which was alumina saturated, scavenged the melt. The scatter in the results from runs without the slag was much greater than those with the slag. Average deoxidation products (K') of 3.5×10^{-11} and 7.1×10^{-14} were obtained for runs without and with slag, respectively. From the variation of log K' with aluminum content (runs with slag), values of $e_O^{Al} = -1.17$ and $K = 2.7\times10^{-14}$ were obtained at 1600°C. This value of K is close to that predicted from thermochemical data. Thus, the difference in the values of deoxidation constant is partly caused by an alumina suspension in the melt. From their electronmicroscopic examinations of the melts the authors conclude that fine particles remain in the melts even after slag treatment.

Another evidence of the fact that alumina suspensions in the melt are the cause of the large values of deoxidation constant and the scatter in the results reviewed in this section, comes from the recent work of Braun et al.[28]. These workers have shown that long equilibration times are essential for equilibrium conditions to be attained and that mechanical stirring is necessary if sampling is to be made from a clean melt. They have obtained an oxygen content of about 2 ppm in an iron melt containing 800 ppm aluminum at 1600°C, consistent with a deoxidation "constant" of

$$K' = [\%Al]^2 . [\%O]^3 = 5\times10^{-14} \tag{2.18}$$

which is close to the equilibrium constant predicted from thermochemical data, even without the use of activity coefficients.

2.4.2 By indirect determination of oxygen

Using the same principle as Geller and Dicke[17] and Yagihashi and Shibata[19], Chipman and Langenberg[29] have indirectly determined oxygen in iron in equilibrium with alumina from the C–O equilibrium. However, unlike the previous authors, Chipman and Langenberg determined aluminum and oxygen <u>activities</u> rather than concentrations and were thus able to compute the equilibrium constant. Their experiments consisted of equilibrating alumina saturated Al_2O_3-SiO_2-CaO slags with graphite saturated Fe-C-Si-Al melts under CO atmospheres at 1600° and 1700°C. The slag was analysed for its constituents while the metal was analysed for silicon and aluminum. The oxygen activity h_O in the metal was obtained from the equation

$$\log h_O = -37.2/T - 4.29 \tag{2.19}$$

which was derived from the standard free energy change for the reaction

$$C_{(gr)} + [O]_{1w/o} = CO_{(g)} \tag{2.20}$$

and by assuming unit activity of $C_{(gr)}$ and p_{CO} equal to 1 atm. The aluminum activity, h_{Al}, was determined from the analyses for aluminum and the known effects of carbon and silicon on the activity coefficient of aluminum. Thus, the equilibrium constant, $h_{Al}^2 \cdot h_O^3$, was found to be 3.6×10^{-14} at 1600°C and 2.8×10^{-13} at 1700°C.

The main advantages of this indirect method are (1) aluminum concentrations are higher than when pure iron is equilibrated with alumina and this reduces the uncertainty caused by analysing for very small quantities of aluminum; (2) accurately known oxygen potentials ($p_{CO} = 1$ in contact with graphite) are imposed, from which a good estimate of oxygen activity in iron can be obtained. Thus, errors in the composition of gas mixtures (such as H_2/H_2O) and oxygen analysis are eliminated; (3) because of the small quantities of oxygen involved melt contamination with alumina is minimized.

Sawamura et al.[30] have used recent data on the C-O equilibrium and various interaction coefficients to calculate equilibrium activities of aluminum and oxygen from the data of Geller and Dicke. The equilibrium constant thus obtained (see Table 2.2 and

Figure 2.2) is in good agreement with thermochemical data.

2.4.3 By electrochemical determination of oxygen

Since the classical work of Kiukkola and Wagner[31] solid electrolytes have been often used to determine oxygen activity in iron. Fruehan[16] and Jacquemont et al.[32] have used the ThO_2-Y_2O_3 electrolyte in the electrochemical cell

$$Cr\text{-}Cr_2O_{3(s)}|ThO_2(Y_2O_3)|Fe\text{-}Al\text{-}O_{(\ell)},\ Al_2O_{3(s)} \tag{2.21}$$

to determine oxygen and aluminum activities in equilibrium with alumina. In Fruehan's experiments, a desired amount of aluminum was added to iron at 1600°C contained in an alumina crucible. The melt was equilibrated for 30 minutes before a cell was lowered into the melt and EMF reading taken. Stable readings were obtained for the next 30 minutes after which samples were taken from the melt with silica tubes. Samples were analysed for oxygen by neutron activation while aluminum was analysed by a standard chemical method.

Results show a minimum in the [%O] versus [%Al] plot at 0.09% Al. Oxygen activity coefficients, f_O, were determined from oxygen activities for different aluminum contents, from which a value of $e_O^{Al} = -3.90$ at 1600°C was obtained. Activity coefficients of aluminum, f_{Al}, were also calculated and a value of $\log \gamma_{Al}^0 = -1.68$ was obtained at infinite dilution. The value for $K = h_{Al}^2 \cdot h_O^3$ was calculated as 5.6×10^{-14} at 1600°C.

Fruehan limited his aluminum content in iron to 1.4% in order to avoid electronic conduction in the electrolyte. Jacquemont et al.[32], on the other hand, corrected for the partial electronic conductivity of their cell using a relation given by Schmalzried[33]. A value of $K = 1.2\times10^{-13}$ has been obtained by these workers at 1600°C using an experimental method very similar to the above.

2.5 Calculations of the Equilibrium Constant

Our best values of the equilibrium constant come from calculations using thermochemical data. The following free energy data are required for the calculation

$$(1)\quad 2Al_{(\ell)} + \frac{3}{2}\,O_{2(g)} \rightleftarrows Al_2O_{3(s)} \qquad \Delta G^\circ_f \tag{2.22}$$

$$(2)\quad Al_{(\ell)} \rightleftarrows [Al]_{1w/o} \qquad \Delta\overline{G}_{Al} \tag{2.23}$$

$$(3)\quad \frac{1}{2}\,O_{2(g)} \rightleftarrows [O]_{1w/o} \qquad \Delta\overline{G}_{O}\,. \tag{2.24}$$

One of the earliest calculations was that of Schenck[34] who combined the thermodynamic data for Al_2O_3 and dissolved oxygen in iron by assuming an ideal solution. His calculated values are given in Table 2.3. Later, Chipman[35] attempted to correct for the deviation from ideality and derived an expression which led to equilibrium constants of 2×10^{-14} and 1.1×10^{-12} at 1600° and 1700°C, respectively. Since then, as more accurate thermodynamic data became available, the calculations of the deoxidation constant have been refined over the years

TABLE 2.3

CALCULATIONS OF EQUILIBRIUM CONSTANT K FROM THERMOCHEMICAL DATA

Year	Estimator	Reference	log K	K_{1873}
1933	Schenck	34	$(-81450/T + 28.80)$	2×10^{-15}
1934	Chipman	35	$-62700/T + 19.39$	8.2×10^{-15}
1944	Chipman	36	$-58400/T + 16.54$	1.35×10^{-14}
1950	Kubaschewski	38	$-49836/T + 12.28$	4.7×10^{-15}
1950	Richardson	39	$-69882/T + 24.26$	8.9×10^{-14}
1951	Chipman	37	$-64000/T + 20.48$	2×10^{-14}
1957	Sawamura et al.	30	$-69117/T + 23.84$	8.7×10^{-14}
1964	From Chipman's data	2	$-64896/T + 20.63$	9.6×10^{-15}
1966	McLean and Ward	40	$-64090/T + 20.41$	1.6×10^{-14}
1970	Fruehan	16	$-62780/T + 20.17$	4.5×10^{-14}

by many authors[2,16,30,36-40]. Their results are summarized in Table 2.3.

(B) Thermochemical Data

2.6 Introduction

This section reviews the two types of thermochemical data required to calculate the equilibrium constant: the standard free energy of formation of alumina and the free energy of solution of aluminum and oxygen in iron.

The standard free energy change for a reaction, ΔG°_T, at any temperature T°K can be obtained from the equation

$$\Delta G^\circ_T = \Delta H^\circ_T - T\Delta S^\circ_T \tag{2.25}$$

where ΔH°_T and ΔS°_T are the standard enthalpy and entropy changes for the reaction at the same temperature. The standard heat of formation, ΔH°_T, at the temperature T can be calculated from

$$\Delta H^\circ_T = \Delta H^\circ_{ref,f} + \int_{ref}^{T} \Delta C_p \, dT \tag{2.26}$$

where $\Delta H^\circ_{ref,f}$ is the standard heat formation at any reference temperature, usually 298°K, and ΔC_p is the difference between the heat capacities of the products and the reactants. Thus, if ΔH°_{ref} and the heat capacities of reactants and products are known over the whole temperature range, ΔH°_T can be calculated at any temperature T in that range. If a phase change of any component occurs in the temperature range, the heat of transformation must be included in equation (2.26) and any change in C_p value must be incorporated in ΔC_p.

The entropy change for a reaction, ΔS°_T, can be calculated from the entropies of the components at the reaction temperature. Standard entropy of any substance, S°_T, can calculated from the equation

$$S^\circ_T = \int_0^T \frac{C_p}{T}\, dT \ . \tag{2.27}$$

Thus, calculations of $\Delta G^\circ_{T,f}$ require the experimental determination of the following thermochemical quantities:

(1) the standard heat of formation, $\Delta H^\circ_{ref,f}$, at any reference temperature, usually 298°K;

(2) the heat of transformation of the components in the relevant temperature range; and

(3) the heat capacity of the components from 0°K to the required temperature.

The free energy of the reaction

$$X_{(\ell)} \rightleftarrows [X]_{1w/o} \tag{2.28}$$

can be calculated from the equation

$$\Delta\overline{G}_X = RT\ \ell n(0.5585\gamma^0_X/M) \tag{2.29}$$

where γ^0_X is the slope of the Henry's-law line or the activity coefficient of the solute X at infinite dilution and M is the atomic weight of X. Thus, a knowledge of γ^0_X as a function of temperature is required to obtain the temperature variation of free energy of solution. This requires a knowledge of heat of solution of the solute. However, if this quantity is not available, as is generally the case, a "regular solution" approximation of the constant $\Delta\overline{H}_X$, given by

$$\Delta\overline{H}_X = RT \ln \gamma_X^0 \tag{2.30}$$

is assumed when γ_X^0 is known at any temperature T.

2.7.1 The standard heat of formation of alumina

The heat of formation of metal oxides are generally obtained by combustion of the metal in excess oxygen in an apparatus known as a "bomb" calorimeter. Details of the bomb calorimeter which was first introduced by Berthelot are given elsewhere(41). In short, it consists of a steel bomb in which a precisely weighed quantity of high purity metal is placed. The bomb is then filled with high purity oxygen usually up to a pressure of 25 atmospheres. The metal is then ignited electrically with a fuse (generally Mg or Fe) and the rise of temperature of the bomb and its surroundings are measured with precision resistance thermometers. Knowing the heat capacity of the bomb, the heat of formation of the oxide can be obtained. The heat capacity of the bomb can be found by burning a material of known heat of combustion such as benzoic acid or by electrical calibration.

A survey of the literature shows that a number of determinations of the heat of formation of alumina(42-51) exist, however, with a wide variation in the values reported. Table 2.4 summarizes the type and

TABLE 2.4

THE STANDARD HEAT OF FORMATION OF ALUMINA AT 298°K, ΔH°_{298}

Worker	Year	Purity of Al, %	% Combustion	Type of Crucible	Ignition Aids Used	Form of metal	$-\Delta H^\circ_{298}$ kcal/mole	Precision %
Berthelot(42)	1901	99.6	100% (probably)	Unknown	Camphor	Foil	380.2	-
Wartenberg & Witzel(43)	1919	95.0	100	Unknown	Collodion	Powder	396.0	±0.4
Moose & Parr(44)	1924	98.37	above 99	Alundum	None	Powder	375.8	±0.2
Roth & Muller(45)	1929	99.83	above 98	Clay	Cotton thread & vaseline	Powder	380.8	±0.4
Meichener & Roth(46)	1934	99.83	above 92	Alundum	Cotton thread & vaseline	Powder	393.3	±0.4
Roth, Wolf & Fritz(47)	1940	99.83	above 95	Alundum	Cellophane	Powder	402.9	±0.3
Snyder & Seltz(48)	1945	99.993	100	Zircon lined with Al_2O_3	None	Foil	399.04	±0.24
Holley & Huber(49)	1951	99.996	99.36	Alumina	Mg fuse	Foil	400.29	±0.31
Schneider & Gattow(50)	1954	99.99			Cellophane		402.0	±0.5
Mah(51)	1957	99.998	99.14	Alundum	Filter paper	Turnings	400.48	±0.25

purity of the materials used and the results obtained by various workers. It can be observed from the table that while the estimated precision by the authors is never more than ±0.5%, the maximum divergence in these values is nearly 7%. Furthermore, three values determined by one investigator (Roth) over a period of eleven years show a range of 22 kilocalories. This serves to show the extremely sensitive nature of these calorimetric determinations. Aside from systematic errors, several possible sources of error are:

(1) the use of impure aluminum;

(2) the fluxing of the molten Al_2O_3 with the crucible material;

(3) the use of ignition aids;

(4) the difference between calibration and aluminum combustion conditions;

(5) incomplete combustion;

(6) the form of aluminum used, i.e. powder, foil, etc.; and

(7) the form of product obtained, whether α, γ, δ Al_2O_3, etc.

Further discussion on this topic is reserved till a later section (§ 5.6).

2.7.2 Heat capacity of alumina, aluminum and oxygen

Of the different experimental methods for determining high temperature heat contents and heat capacities, the method of mixtures or the "dropping method" has been most widely and frequently employed. It consists of dropping the substance under investigation from a furnace at a measured and controlled temperature into a calorimeter operating at or near room temperature. This method determines the change in total heat content (enthalpy) of a substance between the temperature of the furnace and that of a calorimeter. Heat capacities are obtained from the heat content values by some process of differentiation ($C_p = \frac{dH}{dT}$). It is, however, easier to deal with heat contents and these are therefore tabulated along with specific heats and entropies.

In order to be able to analytically integrate equations (2.26) (2.27), etc., C_p values (often enthalpy values) are fitted into expressions of the form

$$C_p = a + bT + cT^2 + dT^{-2} + eT^{-\frac{1}{2}} \qquad (2.31)$$

where a, b, c, d and e are constants. All the terms are rarely required to describe the data and the formula used depends on the temperature range of the data.

Excellent compilations of heat content, heat capacity, entropy and free energy of formation data are available[52-59]. In this section the data on alumina, aluminum and oxygen that were chosen are discussed.

<u>Alumina</u>: As α-Al_2O_3 ("Corundum" or synthetic sapphire) is used as a calorimetric standard over the temperature range 10° to 1800°K, there are numerous reports of enthalpy measurements of α-alumina in the literature. However, the majority of these measurements are restricted

to the lower temperature range of 0°-1200°K, only a few being reported[63-66] in the range 1200°-2000°K of interest in this study.

The lower temperature data have been adequately reviewed by Furukawa et al.[60] and Ditmars and Douglas[61] who have compared their results with those of other workers. Furukawa et al.[60] used an adiabatic calorimeter from 13° to 380°K and a drop method with a Bunsen ice calorimeter from 273° to 1170°K. Their values have been used in several compilations[58,59] though Ginnings[62] discovered a slight error in these data above 850°K due to a phase transformation in their sample capsule. Ditmars and Douglas[61] at NBS have redetermined the relative enthalpy of α-Al_2O_3 over the range 273°-1173°K by the drop method using an ice calorimeter. Their data, estimated to be accurate to 0.1%, have been compared with those from more than 20 references.

The high temperature relative enthalpy of alumina has been determined by Shomate and Naylor[63] (400°-1800°K), Hoch and Johnston[64] (1200°-2000°K), Ferrier and Olette[65] (1200°-2100°K) and by Kantor et al.[66] (1200°-2500°K). The following relative enthalpy and C_p values for alumina in the temperature range 1200°-2300°K were selected from the work of Kantor et al.:

$$H_T - H_{298} = 30.333T + 8.403\times10^{-4}\ T^2 + 2.816\times10^6\ T^{-1}$$

$$- 15280\ \text{cal/mole} \qquad (2.32)$$

$$C_p = 30.333 + 16.806\times10^{-4}\ T - 2.816\times10^6\ T^{-2}\ . \qquad (2.33)$$

Aluminum: As in the case of alumina, there have been a number of determinations of the relative enthalpy and heat capacity of aluminum at lower temperatures (below 1200°K) while only one study[67], published in 1967, has extended the range to 1700°K. This is mainly due to highly corrosive nature of liquid aluminum and the difficulty of finding a suitable container material.

The low temperature data have been well documented by Kelley[53], Stull and Sinke[68], Hultgren et al.[69] and most recently by Buyco and Davis[70]. As there were insufficient data for liquid aluminum, the constant value of $C_p = 7.0$ of Awbery and Griffiths[71] was selected by most compilers for the entire liquid range. McDonald[67] measured the relative enthalpy of aluminum from 300° to 1700°K using crucibles of titanium diboride and boron nitride. Their results for liquid aluminum are given by

$$H_T - H_{298} = 7.588T - 191.2 \text{ cal/mole} \tag{2.34}$$

$$C_{p(\ell)} = 7.59 \text{ cal/mole.deg } (933°\text{-}1650°\text{K}) . \tag{2.35}$$

Oxygen: High-temperature heat contents and specific heats of gases may be calculated statistically from spectroscopic data with a high degree of accuracy. The properties of gases for which complete energy level data are not available often may be obtained from a knowledge of the molecular configuration and the fundamental interatomic vibration frequencies.

The function for C_p adopted here is from Kelley's compilation[53]

$$C_p = 7.16 + 1.0\times10^{-3}\ T - 0.40\times10^{5}\ T^{-2} \tag{2.36}$$

which is valid in the range 298°-3000°K.

2.7.3 The standard free energy of formation of alumina

Since the early estimates[72,73] of the standard free energy of formation of alumina at elevated temperatures, a number of calculations of this quantity have appeared as more and more thermochemical data became available. Some of these calculations will be reviewed here, including some of the compilations of thermodynamic data.

Treadwell and Terebesi[74] have calculated ΔH_f° and ΔG_f° for alumina in the temperature range 293°-2600°K and have compared their calculated values with available experimental data at different temperatures. The results of their calculations are shown in Table 2.5 along with those of other estimators. The value of ΔH_{298}° has been included in Table 2.5 as it is the single largest source of error in free energy calculations and differences in the values of free energy changes can generally be traced to the choice of this quantity. Treadwell and Terebesi have reviewed the values of ΔH_{298}° obtained from heats of reactions involving alumina and from bomb calorimetry. Roth's value of ΔH_{298}° from bomb calorimetry was chosen. Their calculations compare well with the $\Delta G_f^\circ(Al_2O_3)$ calculated from the data of Fischer

TABLE 2.5

THE STANDARD FREE ENERGY OF FORMATION OF ALUMINA, ΔG°_T, FROM THERMOCHEMICAL DATA

Estimator or Compiler	Reference	ΔH°_{298} used kcal/moles	ΔG°_T, cal/mole	Range, °K
Treadwell & Terebesi	74	-293.2	$-396,678 + 78.17T$	930-2320
Chipman	76	?	$-399,800 + 74.8T$	930-2320
DeKay Thompson	52	-388.1	$-376,000 + 61.56T$	929-2073
Richardson & Jeffes	56	?	$-386,250 + 66.45T$	930-2318
Elliott et al.	58	-400.4	$-401,500 + 76.91T$	1500-2000
Wicks and Block	55	-400.29	$-408,660-2.69T\ln T$ $-0.78\times10^{-3}T^2+3.93\times10^5T^{-1}$ $+102.38T$	931.7-1300
Kubaschewski et al.	57	-400.0	$-405,760-3.75T\log T$ $+92.22T$	923-1800
JANAF	59	-400.4	Approx. same as (58)	1500-2000

and Gewehr[75] for the reaction

$$Al_2O_{3(s)} + 6HCl_{(g)} \rightleftarrows 2AlCl_{3(g)} + 3H_2O_{(g)} \tag{2.37}$$

and their own experimental results at 1118°-1378°K for the cell

$$Al_{(\ell)}|Al_2O_3 \text{ in cryolite}|O_{2(g)} \; . \tag{2.38}$$

The agreement of their calculations with the data at high temperatures (1800°-2300°K) for the reaction

$$Al_2O_{3(s)} + 3C_{(s)} = 2Al_{(\ell)} + 3CO_{(g)} \tag{2.39}$$

is fair.

The following estimate of the free energy of formation of alumina was given by Chipman[76] in 1942

$$\Delta G^\circ_T = -399{,}800 + 74.8T \; . \tag{2.40}$$

However, the values and sources of thermochemical data used were not specified.

DeKay Thompson[52] in his monograph "The Total and Free Energies of Formation of the Oxides of Thirty-Two Metals" has combined ΔH°_f and ΔG°_f calculated from thermochemical data with the available experimental data to give the "best" line given in Table 2.5. The value of ΔH°_{298} taken was the mean value of a number of values from the literature while the C_p data was taken from Kelley[53].

One of the early systematic compilations of thermodynamic data was by Richardson and Jeffes[56] whose value for alumina in the appropriate temperature range is given in Table 2.5. Data were mostly taken from DeKay Thompson[52].

Elliott and coworkers[58] have compiled thermochemical data of selected elements and compounds from the literature. They have used the value of ΔH°_{298} reported by Mah[51] and the C_p data of alumina from Furukawa et al.[60]. Other data have been taken from earlier compilations.

The compilation by Wicks and Block[55] uses $\Delta H^\circ_{298} = -400.29$ by Holley and Huber[49] while the C_p data have been taken from Kelley[53].

Kubaschewski et al.[57] have reviewed the data on ΔH°_{298} and have chosen 400.0±1.5 k cal/mole as the "best" value. C_p values have all been taken from Kelley's compilations[53]. When the reaction involves a relatively large value of ΔC_p, as is the case in the formation of alumina, they prefer to introduce an extra term involving T log T into the linear equation for ΔG°_T. Their equation for alumina is given in Table 2.5.

Finally, free energy data from a recent comprehensive compilation[59] is also included in the table. The recently available data for C_p for liquid aluminum[67] have been used in the calculations. Comparison with earlier calculations[55,58] indicate very little effect of this change on the final free energy. From Table 2.5 the importance of choice of ΔH°_{298} on the free energy calculated is also apparent.

2.8.1 The free energy of solution of aluminum

In order to calculate the free energy change for the reaction

$$Al_{(\ell)} \rightleftarrows [Al]_{1w/o} \tag{2.41}$$

the slope of the Henry's Law line, γ^0_{Al}, in Fe-Al system is required. The earliest study of the activity coefficient of aluminum in liquid iron was made by Chipman[35] who measured the distribution ratio of aluminum between liquid iron and liquid silver at 1600°C. It was assumed that the activity of aluminum in liquid silver was equal to its mole fraction, an assumption which is not justified. Chou and Elliott[77] calculated activities in the Ag-Al system by combining activities calculated from the phase diagram of the Pb-Ag system with data on distribution of silver between liquid lead and liquid aluminum which was determined by Lorenz and Erbe[78]. The data on the distribution of aluminum between liquid silver and liquid iron were then used to determine its activity in the latter solution. A value of $\gamma^0_{Al} = 0.04$ was obtained at 1600°C.

Activities in solid Al-Ag alloys have been reported by Hillert et al.[79] at temperatures upto 527°C from measurements on an electrochemical cell. Chipman and Floridis[80] extrapolated this data to liquid Ag-Al alloys at 1600°C and calculated activities in the Fe-Al system using this data and data on partition of aluminum. Their results are given in Table 2.6 along with those of other workers. Chipman and Floridis also determined the effect of carbon and silicon on the activity of aluminum in iron alloys.

TABLE 2.6

FREE ENERGY CHANGE FOR THE REACTION, $Al_{(\ell)} \rightleftarrows [Al]_{1w/o}$

Author(s)	Reference	Quantity	Value	$\Delta\bar{G}_{Al}$, cal/mole
Chipman	35	γ^{0}_{Al}	0.014	-15,900 - 7.71T
Chipman & Floridis	80	γ^{0}_{Al}	0.031	-13,000 - 7.71T
Hultgren et al.	69	γ^{0}_{Al}	0.035	-12,500 - 7.71T
Wilder & Elliott	81	γ^{0}_{Al}	0.063	-10,300 - 7.71T
Vachet et al.	83	γ^{0}_{Al}	0.053	-10,970 - 7.71T
Woolley & Elliott, (and ref. 81)	84	ΔH^{M}_{Al}	-15,350 cal/mole	-15,350 - 5.05T
Belton & Fruehan	85	γ^{0}_{Al}	0.024	-15,100 - 6.67T

In order to directly determine activities in liquid Ag-Al alloys, Wilder and Elliott[81] studied the cell

$$Al_{(\ell)}|Al^{3+} \text{ in } KCl+NaCl|Al\text{-}Ag_{(\ell)} \tag{2.42}$$

between 700°-980°C. Their data agree quite well with Hultgren et al.'s[69] recalculation of Chou and Elliott's work using Kleppa's[82] calorimetrically determined heats of solution for the Pb-Ag system. Using the distribution data of Chipman and Floridis[80], Wilder and Elliott have redetermined γ_{Al} in Fe-Al, Fe-Al-C and Fe-Al-C-Si systems.

Vachet et al.[83] have redetermined the partition of Al between iron and silver at 1600°C and have used the data of Wilder and Elliott to determine activities in the Fe-Al system. Their results on the partition of aluminum are in good agreement with Chipman and Floridis.

The value of the partial molar heat of mixing of aluminum in iron is essential in calculating the temperature dependence of γ_{Al}. This quantity has been determined by Woolley and Elliott[84] using a high temperature solution calorimeter at 1600°C. Using a value of $\log \gamma^0_{Al} = -1.20$ (Wilder and Elliott) and $H^M_{Al} = -15{,}350$ cal/mole determined by them, Woolley and Elliott calculated the free energy change for the reaction (2.41) as

$$\Delta\overline{G}_{Al} = -15{,}350 - 5.05T \,. \tag{2.43}$$

Belton and Fruehan[85] have directly determined activities in the Fe-Al and Ag-Al systems at 1600°C using a mass spectrometer. From their Ag-Al data and the distribution ratios of Chipman and Floridis, they also calculated activities in the Fe-Al system, which are in good agreement with their direct determination. Both their sets of results are given in Table 2.6 along with other workers. The following calculations[16] can be made using their data

$$\Delta\bar{G}_{Al} = RT \ \ell n(0.5585 \ \gamma^{0}_{Al}/M) = -27,600 \text{ cal/mole (at } 1600°C)$$

$$\Delta\bar{H}_{Al} = -15,100 \text{ cal/mole (at } 1600°C \text{ - Woolley \& Elliott)}$$

and $$\Delta G^{\circ}_{Al} = -15,100 - 6.67T \qquad (2.44)$$

Finally, Fruehan[16] determined oxygen activities in the Fe-Al-O system using the cell

$$Cr\text{-}Cr_2O_{3(s)} | ThO_2(Y_2O_3) | Fe\text{-}Al\text{-}O_{(\ell)}, \ Al_2O_{3(s)} \qquad (2.45)$$

from which the aluminum activity could be derived. His value of $\log \gamma^{0}_{Al} = -1.68$ obtained at 1600°C is slightly different from $\log \gamma^{0}_{Al} = -1.62$ determined by Belton and Fruehan, the difference being well within the error in the data used for the free energy of formation of alumina and Cr_2O_3.

2.8.2 The free energy of solution of oxygen

The free energy change for the reaction

$$\frac{1}{2}\, O_{2(g)} \rightleftarrows [O]_{1w/o} \quad \Delta\bar{G}_O \tag{2.46}$$

can be obtained by studying the H_2/H_2O equilibrium with iron, given by

$$H_{2(g)} + [O]_{1w/o} \rightleftarrows H_2O_{(g)} \tag{2.47}$$

$$K_{47} = p_{H_2O}/p_{H_2} \cdot f_O[\%O] \tag{2.48}$$

and combining this data with the well known standard free energy of formation of H_2O. There have been many determinations of the above equilibrium reported in the literature; however, there will be no attempt to review them here as they have been adequately dealt with elsewhere[86,87].

One of the early investigations of reaction (2.46) by Chipman[88] showed that the equilibrium ratio K'_{47} varied with oxygen content indicating a deviation in the behaviour of oxygen from Henry's law in dilute solutions. While this was confirmed by some investigators, a number of studies indicated Henrian behaviour of oxygen in iron (see ref. 87). Errors in oxygen analysis and thermal diffusion in H_2/H_2O mixtures are some of the reasons for these discrepancies.

Careful work by Floridis and Chipman[86] confirm slight non-Henrian behaviour of oxygen in liquid iron, the activity coefficient being given by the relation

$$\log f_O = -0.20[\%O] \ . \tag{2.49}$$

The values of K_{47} obtained at 1550° and 1600°C were 4.68 and 3.65, respectively. Combination with the previous data of Dastur and Chipman[20] gives the following temperature dependence of K_{47}

$$\log K_{47} = 7050/T - 3.20 \tag{2.50}$$

$$\therefore \qquad \Delta G^\circ_{47} = -32,200 + 14.63T \ . \tag{2.51}$$

Combining this with the free energy of formation[2] of $H_2O_{(g)}$ -

$$H_{2(g)} + \frac{1}{2}\, O_{2(g)} \rightleftarrows H_2O_{(g)} \tag{2.52}$$

$$\Delta G^\circ = -60,200 + 13.94T \tag{2.53}$$

the free energy for reaction (2.46) is given by

$$\Delta\overline{G}_O = -28,000 + 0.69T \ . \tag{2.54}$$

(C) Electrochemical Cells in Molten Electrolytes

2.9 Introduction

In recent years electrochemical cells have been developed to determine the thermodynamic properties of high temperature systems. Most of this work has been carried out on simple salt mixtures and these have been reviewed by, for example, Lumsden[89], Blander[90], Sundheim[91] and Delimarskii and Markov[92].

The simplest of electrochemical cells is a "formation cell", given by

$$M|M_aX_b \text{ in electrolyte}|X_{2(g)} \tag{2.55}$$

whose cell reaction involves the formation of M_aX_b from its elements, as

$$aM + \frac{b}{2} X_{2(g)} \rightleftarrows (M_aX_b)_{electrolyte} \tag{2.56}$$

The EMF of such a cell, in which both the electrodes are reversible to their ionic constituent in the electrolyte, is given by

$$E = E^\circ - \frac{RT}{nF} \ln \frac{a_{M_aX_b}}{a_M^{a} \cdot p_{X_2}^{b/2}} \tag{2.57}$$

Thus, the cell can be used under the following experimental conditions to obtain different thermodynamic data:

(1) Both the electrodes and M_aX_b are at unit activity, i.e. pure M electrode, X_2 gas at 1 atm. and pure M_aX_b as electrolyte (or electrolyte saturated with M_aX_b). Under these conditions, the standard free energy of formation of M_aX_b can be calculated from cell EMF, E°, by

$$\Delta G^\circ = - nF\ E^\circ \tag{2.58}$$

where nF is the number of Faradays involved in the cell reaction.

(2) When only the electrodes are at unit activity, the cell can be used to determine solution thermodynamics of M_aX_b in the electrolyte. The cell EMF is related to the activity of M_aX_b by equation (2.57) where a_M and p_{X_2} have been put to unity. By studying temperature variation of EMF the enthalpy and entropy of the electrolyte solution can be obtained which gives insight into its structure.

(3) When the gas electrode and M_aX_b are at unit activity, the cell EMF can be used to calculate the activity of M in an alloy electrode. The Gibbs-Duhem equation can then be used to calculate the activity of the other component in the alloy. Again, the variation of EMF with temperature can be used to determine the enthalpy and entropy of solution of the alloy components.

A concentration cell can be set up by combining two formation cells back-to-back, for example

$$Ag|AgCl(a_I),\ NaCl|Cl_2|AgCl(a_{II}),\ NaCl|Ag \tag{2.59}$$

where the cell EMF is given by the expression

$$E = -\frac{RT}{nF}\,\ln\frac{a_I}{a_{II}} \tag{2.60}$$

the "cell reaction" being the reversible transfer of AgCl from solution II to solution I. If a_{II} is made unity, the cell gives a direct measure of activity of AgCl in solution I. This is a cell "without transference" as there is no physical transfer of materials in the compartments.

In the above cell two electrodes are required to be reversible to the electrolyte. However, in practice this is not always possible. In such cases, one of the electrodes can be eliminated by the use of cells "with transference", such as

$$Ag|AgNO_3(a_I),\ NaNO_3\ \vdots\ AgNO_3(a_{II}),\ NaNO_3|Ag \tag{2.61}$$

where the solutions I and II are separated by a porous plug or an ion-selective membrane. This cell, however, will contain an additional liquid junction potential which involves transfer properties of the ions. Because of the high temperatures and mobilities involved in fused salt systems, often the liquid junction potential is small and can be neglected. The cell EMF then is given by equation (2.60).

The cells of the type

$$Ag|AgCl\ \vdots\ PbCl_2|Pb \tag{2.62}$$

containing a liquid junction between two salts are known as "Daniell

Cells". In these cells, however, the liquid junction potential can be substantial and can be estimated if the measurements on the corresponding formation cells are possible. For example, Laity[93] compared the EMFs of the cells Ag|AgCl|Cl_2, C and Pb|$PbCl_2$|Cl_2, C with those of cell (2.62) to obtain a liquid junction potential of 22 mV at 525°C. This value can then be compared to that calculated from irreversible thermodynamics.

Measurements on a large number of cells in molten salts are reported in the literature. These have been well reviewed in the books quoted above and in articles by Reddy[94], Solomons[95], Laity[93], Dijkhuis et al.[96], etc. In this section the cells containing an oxygen electrode and alumina formation cells will be reviewed.

2.10 Oxygen Electrode

The use of oxygen electrodes in fused electrolytes at high temperatures has been adequately reviewed by Laity[93], Reddy[94], Delimarskii and Markov[92] and Laitinen and Bhatia[97]. One of the early investigations which attempted to establish the reversibility of the oxygen electrode in fused melts was by Lux[98]. He used two oxygen electrodes (with Pt contacts) in a concentration cell containing an eutectic mixture of sodium and potassium sulphates as electrolytes and different quantities of Na_2O in the compartments. His work is, however, criticized by Flood et al.[99] because of rapid evaporation of the alkali oxide and attack on the alumina crucible during the experiment. Another early work by Csáki and Dietzel[100] who used Pt-oxygen electrodes in borate melts has also been criticized by Flood et al. for failing to give quantitative evidence of the potential determining reaction. These and further work of Lux, however, indicated the feasibility of using the oxygen electrode in sulphate, phosphate and borate melts.

In carefully designed experiments, using CO_2-O_2 gas mixtures on platinum electrodes, Flood et al.[99] demonstrated the reversibility of the oxygen electrode in the Na_2SO_4-Na_2CO_3 system. They showed that the cell potential varied with oxide ion activity according to the Nernst equation in the sulphate-carbonate mixtures although that was not strictly the case in potassium chromate-dichromate mixtures. Oscillation of the cell EMF with gas bubbling was observed. This disappeared when the furnace atmosphere was made the same as the gas in the electrodes.

Didtschenko and Rochow[101] were the first to use Pt-oxygen electrodes in silicate melts in which the electrode was found to be reversible. The potential was found to vary with the concentration and the basicity of the oxide added. Hill and co-workers[102] combined an oxygen electrode (on Pt) with a metal-metal oxide electrode in Li-K sulphate mixtures containing dissolved CaO in the temperature range 550°-750°C. The EMF was found to be close to that derived from thermochemical data for Fe, Cu and Ni indicating cell reversibility. Some variation in EMF was observed with stirring and was thought to be due to the poisoning of the Pt-O_2 electrode.

Although Antipin[103] has used anodized graphite rod as the oxygen electrode in a cryolite melt, graphite held in oxygen did not act as reversible oxygen electrode in LiCl-KCl melts[97].

Ito and Yanagase[104], Minenko and Ivanova[105] and Sridhar and Jeffes[106] successfully used the Pt-O_2 electrode in the lead silicate system around 1000°C. Using liquid lead as the other electrode they have determined the thermodynamics of PbO and PbO-SiO_2 melts. Sridhar and Jeffes also reported EMF oscillations with gas bubbling which was eliminated when the Pt wire was slightly retracted within the refractory tube. Lepinskikh and Esin[107] have used a similar cell with a Pt-O_2 electrode to determine the thermodynamic properties of PbO-B_2O_3 melts while Delimarskii and Andreeva[108] have studied PbO-$NaPO_3$ melts by the same method.

An oxygen electrode was also found to be reversible in NiO-alkali silicate melts[109] at 900°-1000°C. The variation of cell EMF with oxygen partial pressure from 1 atm. upto 5×10^{-3} atm. and with NiO concentration was found to follow an exact Nernst relationship. The enthalpy and entropy of solution of NiO in the silicate was also determined.

2.11 Alumina Formation Cells

A number of workers[74,110-114] have determined the standard free energy of formation of alumina around 1000°C by using the cell

$$Al_{(\ell)} | Al_2O_3 \text{ in cryolite} | O_{2(g)}, Pt \quad . \qquad (2.63)$$

Their results are summarized in Table 2.7.

Treadwell and Terebesi[74] used a 3 mmD Pt tube inside a closed end porcelain tube as the oxygen electrode. This electrode was dipped into an alumina saturated cryolite melt contained in a MgO crucible which was placed inside a larger MgO crucible containing liquid aluminum. Thus the electrodes and the electrolyte were separated from each other using MgO and porcelain diaphragms. They also tried a burnt lime diaphragm instead of the MgO diaphragm but with no success. The EMF was found to be constant with oxygen flow rate and the variation with temperature is given in Table 2.7.

Drossbach[110] using a 10% alumina-cryolite electrolyte found the cell EMF to be 2.06 at 1060°C. His experimental arrangement consisted of aluminum and Pt-O_2 electrodes separated from the electrolyte using closed end alumina tubes. Holes at the side of the alumina tubes let the electrolyte into the electrodes.

Mashovets and Revazyan[112] used two sintered alumina crucibles, one inside the other, to separate the cathode and anode compartments. Oxygen or O_2-N_2 mixtures were passed over a platinum wire inside an alumina tube. Contact with liquid aluminum was made with Mo wire and the cell EMF was corrected for the Mo-Pt thermal EMF thus introduced. The change in EMF with p_{O_2} did not strictly follow the Nernst equation, however, the Pt-O_2 electrode was believed to be substantially reversible. They have also measured the EMF of similar cells with the oxygen electrode replaced by Pt-CO_2, C-CO_2 or C-O_2 electrodes. Results compatible with the first cell were obtained. However, in the cells using the graphite electrode, larger than final stable EMFs were

TABLE 2.7

DETERMINATIONS OF STANDARD FREE ENERGY OF FORMATION, $\Delta G°$, FROM

ELECTROCHEMICAL CELLS

Workers	Temperature °C	Temperature °K	Cell EMF, E°, Volts	$\Delta G° = -nFE°$ kcal/mole	$\Delta H°_{298}$ from Third Law Analysis of $\Delta G°$ Data
Treadwell & Terebesi[74] (1933)	845	1118	2.215	-306.467	-390.93
	980	1253	2.169	-300.103	-395.24
	1015	1288	2.143	-296.505	-394.40
	1090	1363	2.113	-292.355	-396.16
	1105	1378	2.108	-291.663	-396.64
Drossbach[110] (1934)	1060	1333	2.06	-285.022	-386.46
Baimakov et al.[111] (1937)	1000	1273	2.12	-293.323	-390.04
Mashovets & Revazyan[112] (1957)	1015	1288	2.12	-293.323	-391.22
Ray[113] (1965)	957	1230	2.20	-304.392	-397.71
Thonstad[114] (1968)	1000	1273	2.205	-305.084	-401.80

obtained initially which was attributed to chemisorbed oxygen on the graphite electrode.

Ray[113] separated the aluminum and the oxygen electrodes from the electrolyte using zirconia or alumina sheaths. The electrolyte was also placed inside the oxygen electrode in which the Pt tube was immersed. The oxygen electrode was tested for reversibility and reproducibility against a silver reference electrode.

Finally, Thonstad[114] used a three electrode system - aluminum and oxygen working electrodes and a reference aluminum electrode in the same system. The oxygen electrode consisted of the usual Pt wire in an alumina tube whose dimensions were varied without any effect. Similarly, the diameters of the Pt wire, the depths of immersion and rates of bubbling were changed without affecting the cell EMF. Thonstad, however, did not get a stable and reproducible EMF when no external current was applied. He obtained the standard cell EMF by taking the initial reading from a potential decay curve after switching off the electrolysis current.

Other workers (see ref. 114) have determined the decomposition potential of alumina in cryolite from extrapolation of the current-voltage curve. These values, although often identified as $E°(Al_2O_3)$, contain overvoltage terms over and above E°.

CHAPTER III

EXPERIMENTAL APPARATUS AND PROCEDURE

3.1 Introduction

As mentioned in Chapter I the following high temperature electrochemical cells were used in this study to determine the standard free energy of formation of alumina in the temperature range 1400°-1560°C

$$\text{Cell I} \quad Pt_{(s)}, Al_{(\ell)} \mid Al_2O_3 \text{ satd. slag} \mid O_{2(g)}, Pt_{(s)} \tag{3.1}$$

$$\text{Cell II} \quad C_{(gr)}, Al_{(\ell)} \mid Al_2O_3 \mid \underset{(O^{2-})}{\text{electrolyte}} \mid Al_2O_3 \mid Fe\text{-}C_{satd.}, CO_{(g)}, C_{gr}. \tag{3.2}$$

This chapter describes the considerations leading to the design of these cells, their working and the difficulties involved in making measurements on high temperature cells.

3.2 Design of Cell I

The design of Cell I is largely governed by the choice of the liquid slag electrolyte. At steelmaking temperatures this slag

(1) must conduct ionically;

(2) must not be reduced by aluminum;

TABLE 3.1

PHYSICAL PROPERTIES OF ALUMINUM AND CaF_2-Al_2O_3 ELECTROLYTE

Property	Aluminum	CaF_2-Al_2O_3 electrolyte
Melting point	660°C[59]	CaF_2: 1423°C[179] Al_2O_3: 2042°C[59] Eutectic[121] at 1368°C and 10 w/o Al_2O_3
Density at 1500°C	2.1 g/ml[180]	CaF_2: 2.5 g/ml[122] CaF_2-30 w/o Al_2O_3[122] ∿2.85 g/ml
Vapour pressure at 1500°C	0.7 mmHg[57]	0.21 mmHg[57]
Compatibility with container materials	Attacks almost all metals. Can be contained in graphite and some refractories.	Attacks almost all refractories. Can be contained in graphite and some metals (Pt, Mo, etc.)

(3) must be chemically stable with a low vapour pressure; and

(4) must be saturated with alumina.

A study of the properties of calcium fluoride shows that it satisfies the above requirements quite well (for further discussion see sect. §5.2). It was therefore decided to use calcium fluoride saturated with alumina as the liquid electrolyte in Cell I. The properties of aluminum and the electrolyte which influence the cell design are given in Table 3.1.

It is apparent from the density of the materials at 1500°C that a simple cell design used by workers in other systems[104-108,114] cannot be used in this system. The liquid aluminum will float on the electrolyte and has to be isolated from the atmosphere and the oxygen electrode. Furthermore, aluminum melts at a much lower temperature than the electrolyte. These considerations led to the final cell design shown diagrammatically in Figure 3.1 which was adopted after trying a number of preliminary designs.

The cell assembly essentially consists of a container, an aluminum electrode and an oxygen electrode. In the following sections these components are described in detail.

3.2.1 The container

The container, shown in detail in Figure 3.2, consists of a graphite crucible ($2\frac{1}{4}$" OD × $1\frac{3}{4}$" ID × $2\frac{1}{4}$") set within a silica crucible using alumina powder as insulating material. Alundum cement was used

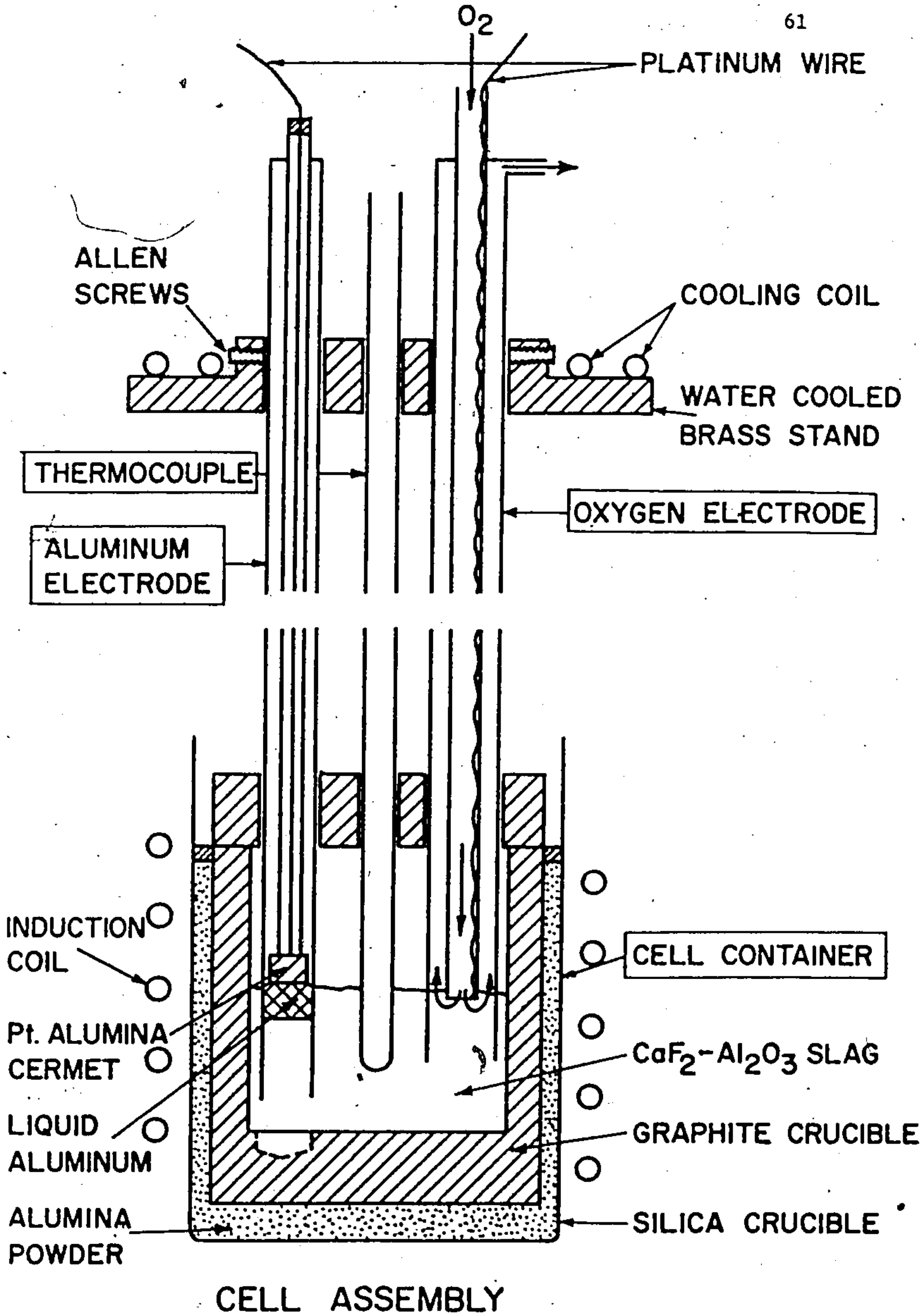

Figure 3.1: A schematic diagram of cell assembly - Type I.

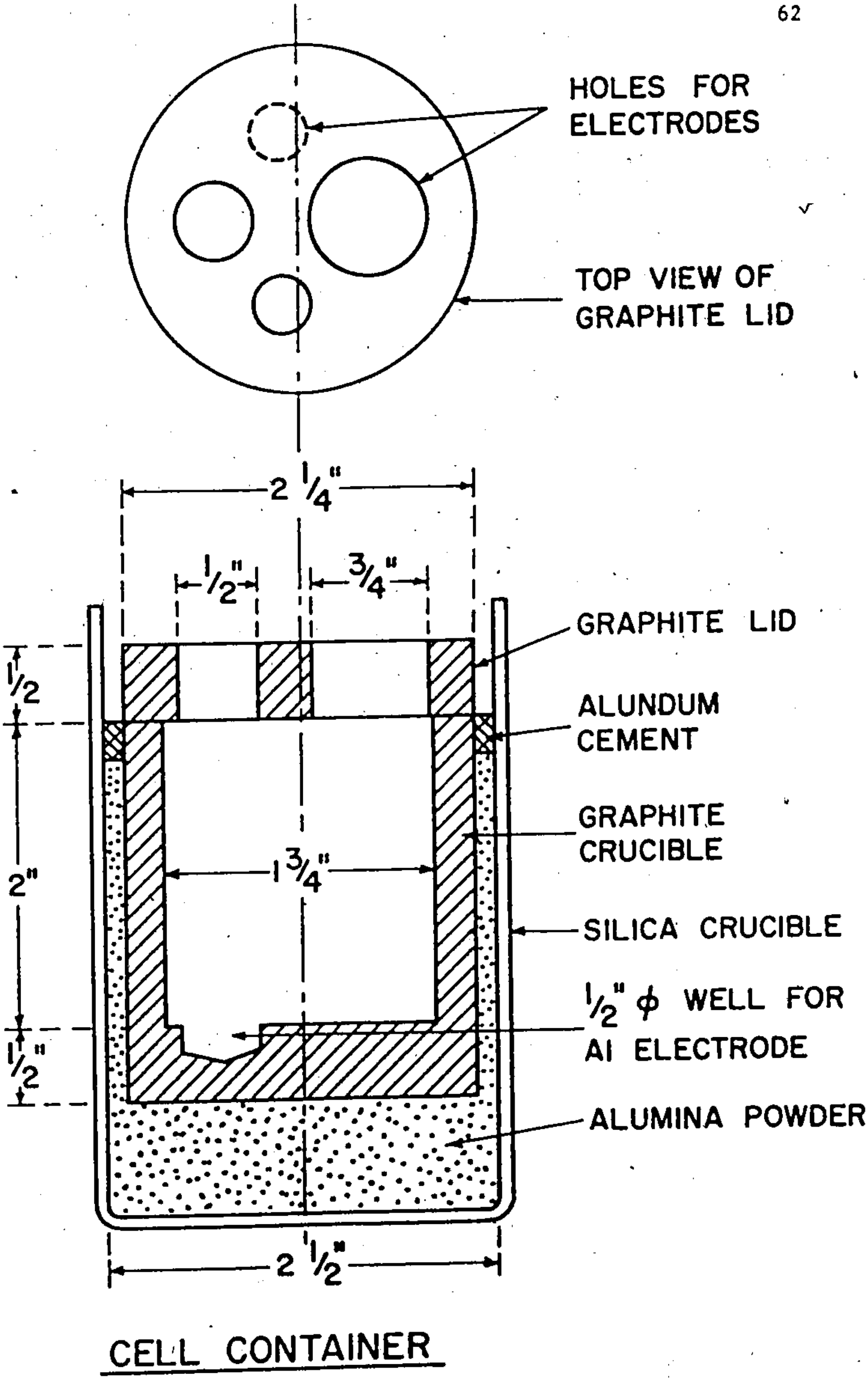

Figure 3.2: The container.

to fix the graphite crucible to the silica crucible. This arrangement protected the graphite crucible from oxidation while keeping the cell design simple.

A $\frac{1}{4}$" deep well, drilled in the bottom of the graphite crucible, provided a seal for the alumina tube of the aluminum electrode during the initial stages of an experiment before the electrolyte became molten.

A graphite lid ($2\frac{1}{2}$" D × $\frac{1}{2}$") with holes for the electrodes and thermocouple was used to cover the crucible.

3.2.2 The aluminum electrode

The two types of aluminum electrode used in Cell I are shown diagrammatically in Figure 3.3. These designs were chosen to satisfy the following conditions:

(1) aluminum will float on the liquid slag (see Table 3.1);

(2) aluminum melts at a lower temperature than the slag electrolyte;

(3) electrical contact has to be made with liquid aluminum; and

(4) aluminum must be protected against excessive oxidation.

Conditions (1) and (2) are satisfied by placing the outer alumina tube of the electrode in the well at the bottom of the graphite container, and surrounding it with crushed, pre-fused electrolyte. Aluminum placed inside this tube melts first and is contained in it while the slag is still solid. When the slag becomes molten the tube is raised out of the well in order to allow the aluminum to float on top of the electrolyte inside the tube.

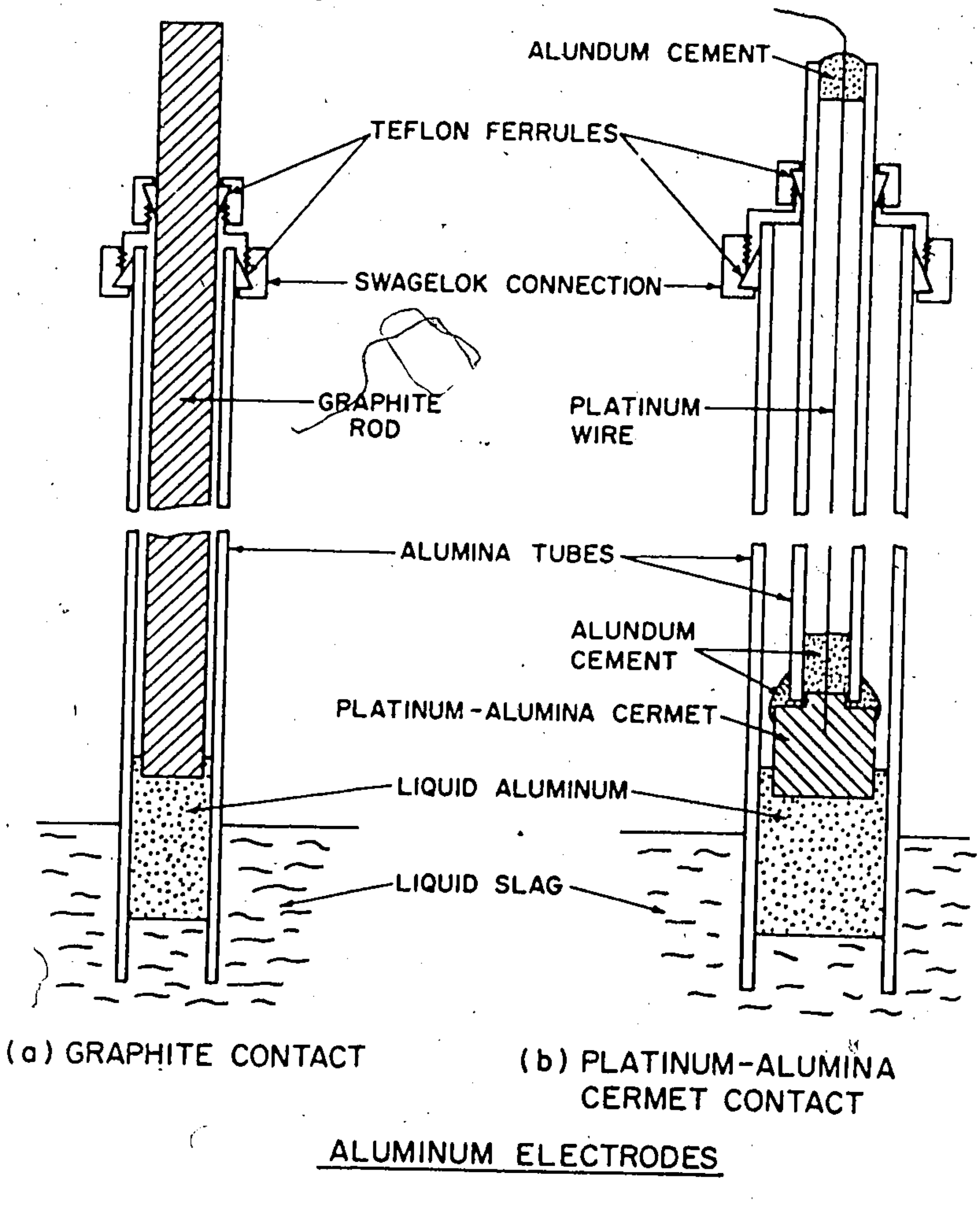

Figure 3.3: The two types of aluminum electrodes used in Cell I.

Graphite was used to make electrical contact with liquid aluminum in the initial experiments (see Figure 3.3a). However, this introduced a thermal EMF with the platinum contact of the oxygen electrode. Although this platinum-graphite thermal EMF was experimentally determined and the measured EMF corrected for this quantity, it acts as an additional source of error and is better eliminated. Since platinum is rapidly attacked by liquid aluminum at 1500°C, a ceramic-metal pellet (cermet) resistant to liquid aluminum attack was developed as a contact. Preparation of this cermet is described in Section 3.9. The design of the aluminum electrode using the cermet as a contact is shown in Figure 3.3b.

The construction of both the types of aluminum electrodes is quite similar. The electrode with the $\frac{1}{4}$" D graphite contact used a high purity (99.8%) recrystallized alumina tube of dimensions $\frac{3}{8}$" OD × $\frac{1}{4}$" ID. The electrode with the cermet contact used a larger alumina tube ($\frac{1}{2}$" OD × $\frac{5}{16}$" ID). In both these cases, Swagelok fittings with Teflon ferrules were used to seal the electrodes gas tight while allowing the vertical motion of the respective electrical contacts. This simple arrangement was quite effective in preventing excessive oxidation of the molten aluminum during the experiment. After each experiment, the electrode was checked for the presence of aluminum metal.

3.2.3 The oxygen electrode

The main requirement of the oxygen electrode is that oxygen gas of known partial pressure must contact the electrolyte and an electrical lead (usually Pt). Oxygen flowing through a platinum tube or over a platinum wire in a refractory tube has commonly been used as an oxygen electrode(98-102,104-114). Jeffes and Sridhar(115) have critically reviewed the design of these electrodes and the one used in the present study, shown in Figure 3.4, is based on their assessment.

Oxygen gas is passed through the inner of two concentric recrystallized alumina tubes and returned through the outer tube, the dimensions of the tubes being $\frac{1}{4}$" OD × $\frac{1}{8}$" ID and $\frac{3}{4}$" OD × $\frac{5}{8}$" ID, respectively. Contact is made with the slag by a 0.020" D platinum wire passing down the inner tube, the end of the wire being retracted about 0.1" from the bottom. A brass head held the two tubes together at the top using an 'O'-ring seal and a Swagelok fitting, as shown in Figure 3.4. The $\frac{1}{4}$" Swagelok fitting with Teflon ferrules, while making a gas tight seal, allowed vertical movement of the inner tube. As discussed in Section 5.2.2, free movement in the vertical direction was quite critical in the successful operation of this electrode.

The oxygen gas was dried over silica gel and drierite before being let into the electrode. The oxygen flow rate was adjusted with the help of a fine needle valve and a rotameter. The rotameter was standardized in the usual way against a soap bubble meter.

3.3 Design of Cell II

While working with various preliminary cell designs, it was realized that recrystallized alumina has some conductivity by O^{2-} ions at high temperatures and hence can be used to isolate the anodic and cathodic compartments. While there is no agreement in the literature

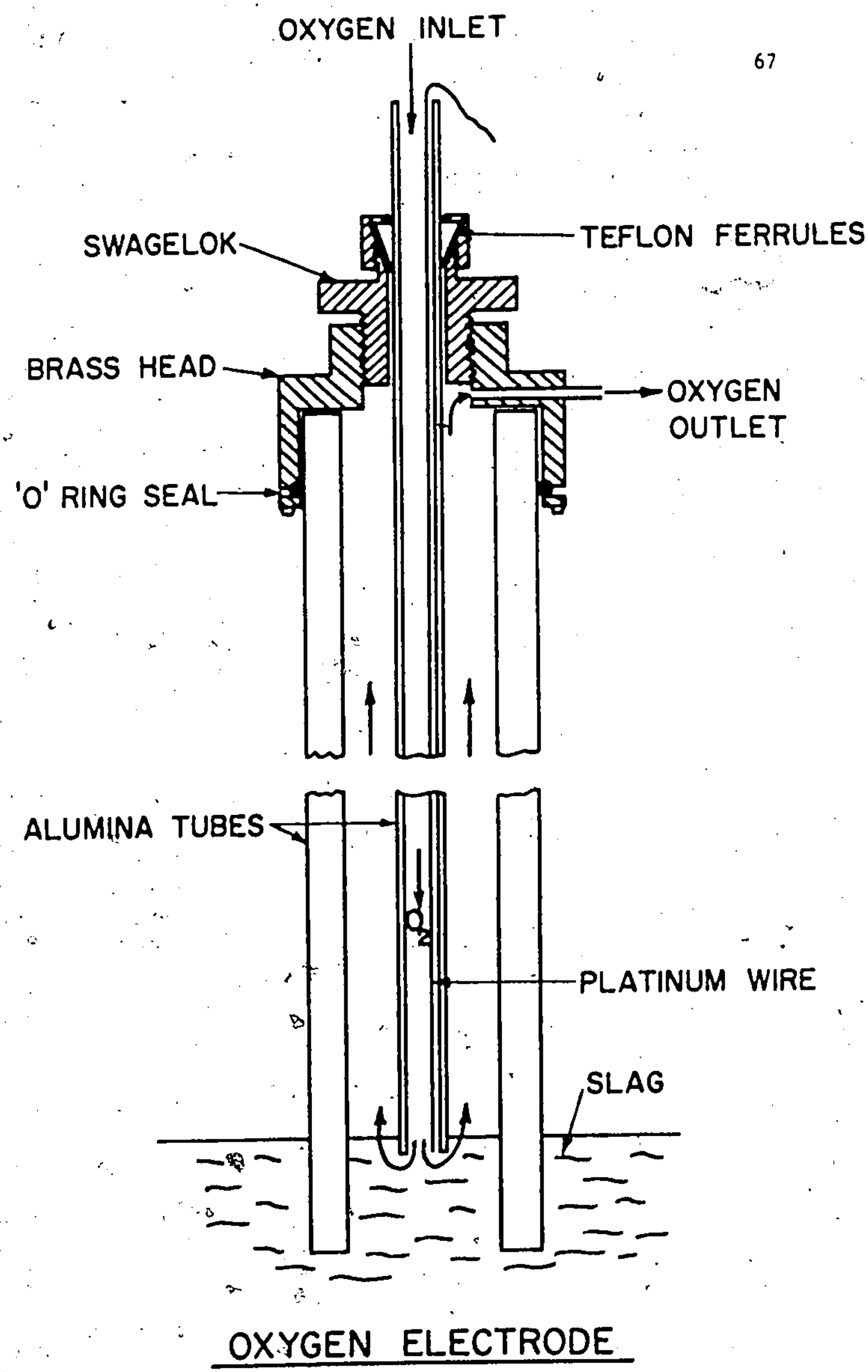

Figure 3.4: The oxygen electrode.

on the value of the transport number for oxygen ions in alumina, it is generally believed that there is considerable electronic conductivity at 1600°C. However, as long as a predominantly ionic electrolyte is interposed between the electrodes, it will "block out" any electronic short-circuiting of the cell. The designs of cells based on this principle have already been reviewed in an earlier section (§2.11).

The design of Cell II, consisting of a container, an aluminum electrode and a C/CO electrode, is shown diagrammatically in Figure 3.5. Separation of the anode and cathode from the electrolyte removes the restrictions on the electrolyte, i.e. that it must not be reduced by aluminum and that it must be saturated with alumina. Thus other electrolytes containing O^{2-} ions were also used in this cell.

3.3.1 The container

The container used in this cell is identical to the one used in Cell I (see Section 3.2.1), except for the absence of the well in the bottom of the graphite crucible. Also, a $\frac{1}{4}$" thick asbestos sheet, with appropriate holes for the electrodes and the thermocouple, was used as a cover instead of the graphite lid used in the earlier version. This reduced heat loss from the top by radiation.

3.3.2 The electrodes

As can be seen from Figure 3.5 both the aluminum and C/CO electrodes are of similar construction. They consist of closed-end recrystallized alumina tubes ($\frac{3}{8}$" OD × $\frac{1}{4}$" ID) containing aluminum or

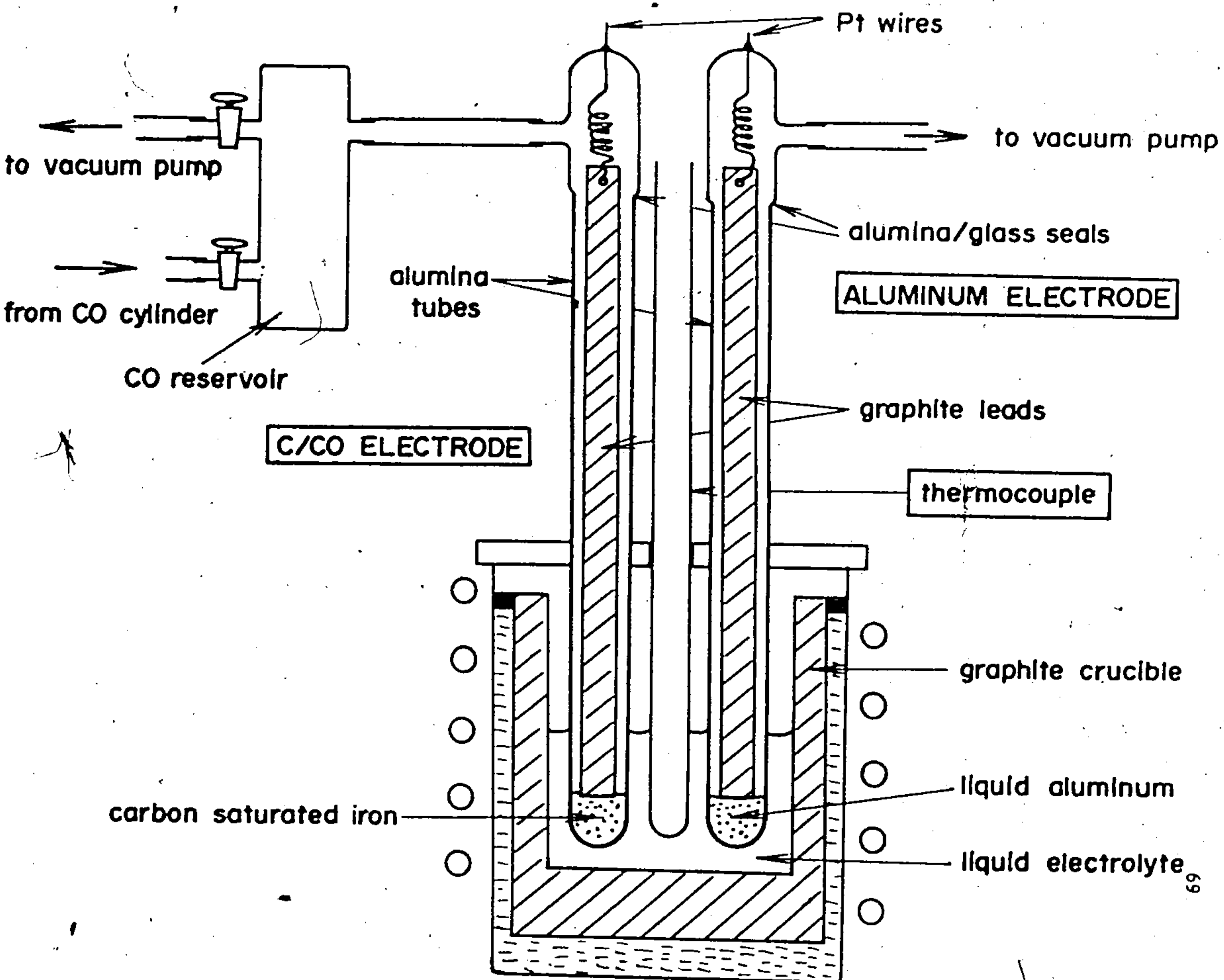

Figure 3.5: A schematic diagram of cell assembly - Type II.

carbon saturated iron. Contact with the metal phase is made by a $\frac{1}{4}$" D graphite rod. The top of the alumina tubes were sealed to glass "tops" with an opening in each to allow gas into the electrodes. Contact with the graphite rods was made by platinum wires sealed into the glass. There was some difficulty in making glass-alumina seals; however, with the proper glass (Corning #7056) and technique, reasonable seals were obtained. A picture of the glass-alumina seal on the top of one of the electrodes is shown in Figure 3.6 which also shows the graphite contact rod and the platinum wire connection. A piece of iron tube placed on the top of the graphite rod was used to push it down into the melt with the help of a magnet.

The aluminum electrode was continuously evacuated with a mechanical pump so that a pressure of $\sim 10^{-2}$ torr was maintained throughout the experiment. The C/CO electrode was connected to a reservoir ($\sim$200 ml) to take care of the expansion of gas inside the electrode during heating. Both the electrode and the reservoir were evacuated and then filled with CO gas at one atmosphere before the experiment.

Figure 3.7 is a picture of a cell assembly while in operation.

3.4 Temperature Measurement

In both cells, a platinum-platinum 13% rhodium thermocouple was used to measure the cell temperature. The 0.020" D wires used to make this thermocouple were obtained from Johnson Matthey & Mallory. The thermocouple was protected from slag attack by a high purity

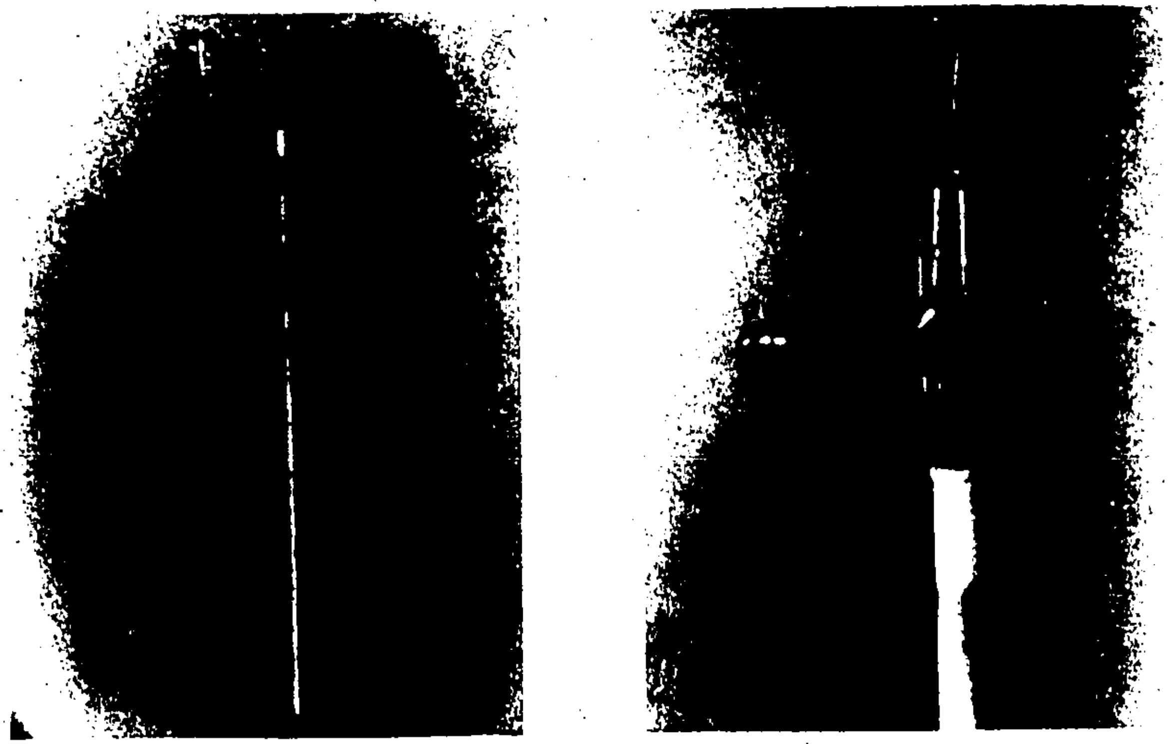

(a) (b)

Figure 3.6 Photographs showing (a) an electrode (b) details of an electrode top - cell II

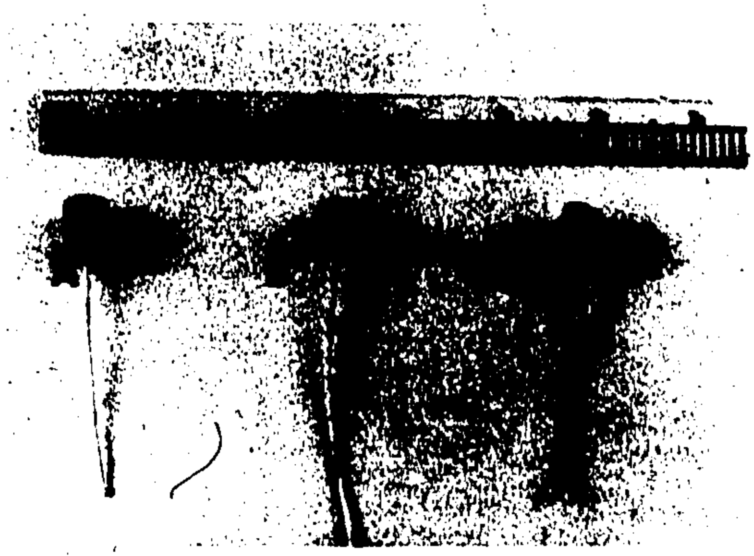

3.10

Figure 3.10 photograph showing Pt - Al_2O_3 cermet
(a) before use (b) after 30 min at 1465°C
(c) after 25 min. at [illegible]°C

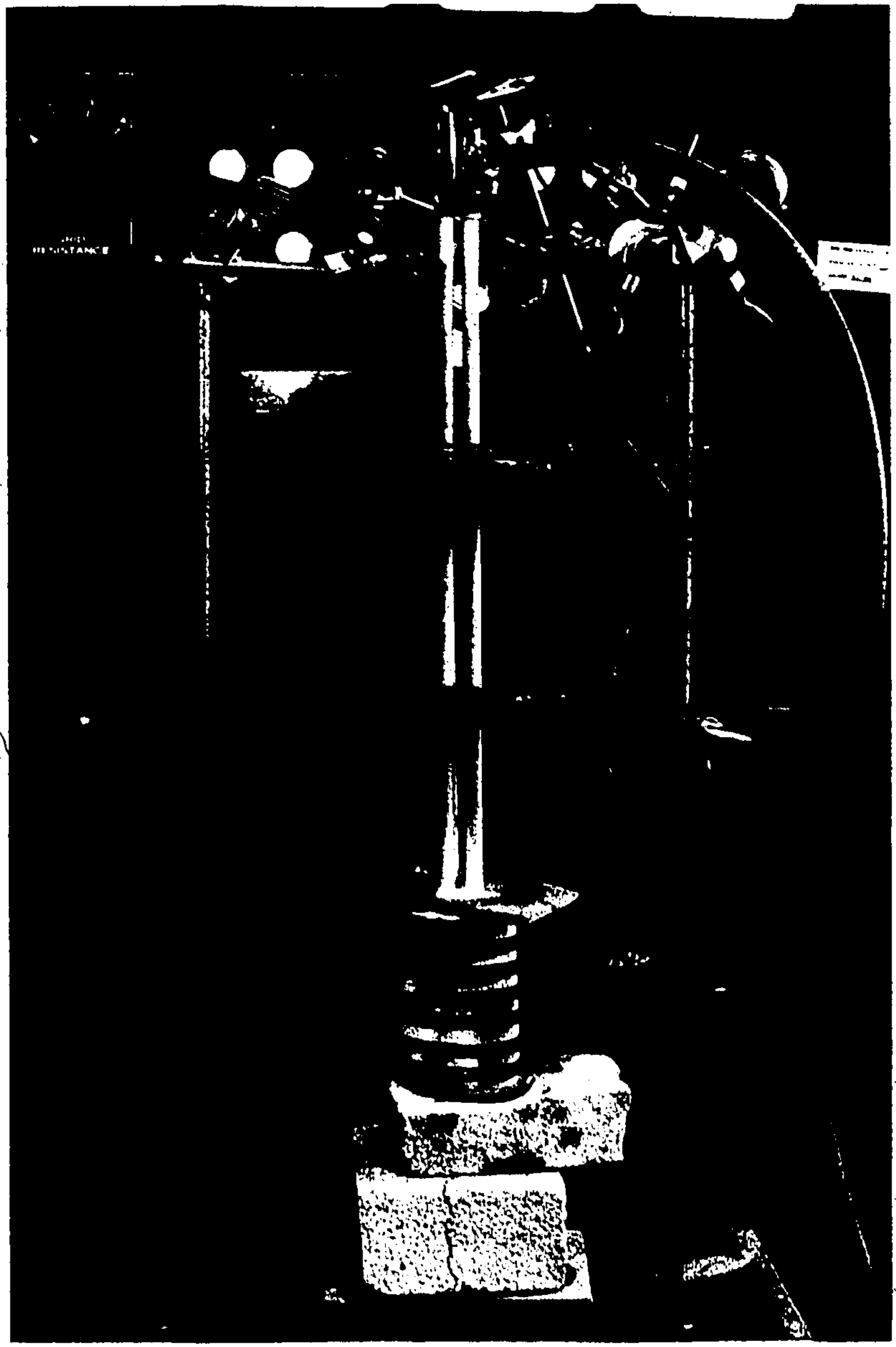

Figure 3.7: Photograph showing Cell II assembly.

recrystallized alumina sheath ($\frac{3}{8}$" OD × $\frac{1}{4}$" ID). In the earlier experiments the thermocouple with its alumina sheath was placed inside a graphite sheath to protect the alumina sheath from corrosive attack of the slag. Also, it was thought that the graphite sheath would shield the thermocouple from the high frequency field. However, this field was picked up by the unsheathed portion of the thermocouple and by the leads. This field was eliminated from the measurement circuit by the grounding the leads through capacitors as described in Section 3.7. It was also found that slag attack on the alumina sheath was not excessive and that the sheath could be easily reused a number of times before the slag corroded through it. The slag attack was more significant at the higher temperatures.

After every four experiments, $\frac{1}{2}$" from the end of the thermocouple was cut off and a fresh bead was made. This reduced any error due to rhodium evaporation from the thermocouple and from any impurity pick up.

The thermocouples were calibrated against a standard thermocouple supplied by the National Research Council. The potentiometer used for temperature measurement was frequently calibrated against a standard cell, also supplied by NRC.

3.5 The Electrode Stand

A water cooled brass electrode stand was used to position the two electrodes and the thermocouple in Cell I (see Figure 3.1). Holes corresponding to those on the crucible lid were drilled on a brass disc (4" D × $\frac{1}{4}$") and the electrodes were clamped in place using Allen screws.

In the case of Cell II a $\frac{1}{4}$" thick asbestos sheet with three holes drilled in it was used as the stand. Clamps were used to hold the electrodes in place.

3.6 The Power Supply and Temperature Control

Power supply of a crystal growing unit (Taylor-Winfield 'Thermonic') was used to heat the graphite cell to the required temperature. It was a medium frequency induction furnace with a fine temperature control, its output specifications being: 450 kHz, 25 kW, 208 V and 144 A.

The power from this unit was manually controlled by fine adjustment of the coil current. High temperature thermal stability, with a small temperature drift ($\sim 8°C/hr$), was achieved in about fifteen to twenty minutes using this method of control. Overall temperature control is estimated at ±5°C.

3.7 EMF Measurement

In order to obtain a reversible value, the cell EMF must be measured in 'open-circuit' using a null balance potentiometer. However, high impedance electrometers (input impedance 10^{11} to 10^{14} ohms), drawing a small cell current, have been used previously to measure cell EMF[106,116]. Although not nominally a zero-current method, current drawn by electrometer is usually less than the current flowing in a null-balance potentiometer circuit, particularly when the latter is slightly off-balance. The speed of response, convenience and continuity of reading of the electrometer are great advantages when an accuracy better than 0.1% is not required. In this investigation both the instruments have been used to measure cell and thermocouple EMFs.

The circuit diagram for Cell I is shown in Figure 3.8. A type P3 Croydon potentiometer was connected in parallel with a Keithley Model 616 high impedance electrometer (2×10^{14} ohms) through a double pole double throw switch. The double pole double throw switch allowed cell and thermocouple readings to be taken on the electrometer within seconds of each other. This was especially critical in the case of Cell II where the power had to be shut off before taking a cell EMF reading.

The EMF of Cell I (~2 volts at 1500°C) was out of the range of the potentiometer (0-1.8 V) and could be read on the electrometer only to ±10 mV. For this reason a Weston (Eppley) Standard cell (1.0183 V at 20°C) was introduced in the measuring circuit in opposition to the formation cell (see Figure 3.8) so that the resultant EMF, given by

$$E_{\text{measured}} = E_{\text{Cell}} - E_{\text{Standard}} \tag{3.3}$$

could be measured within ±1 mV on both the instruments.

Measurements of the cell EMF taken independently on the potentiometer and the electrometer generally agreed to within ±2 mV. As the difference between the two instruments was within the experimental error, the potentiometer was only used to check the electrometer readings at convenient intervals.

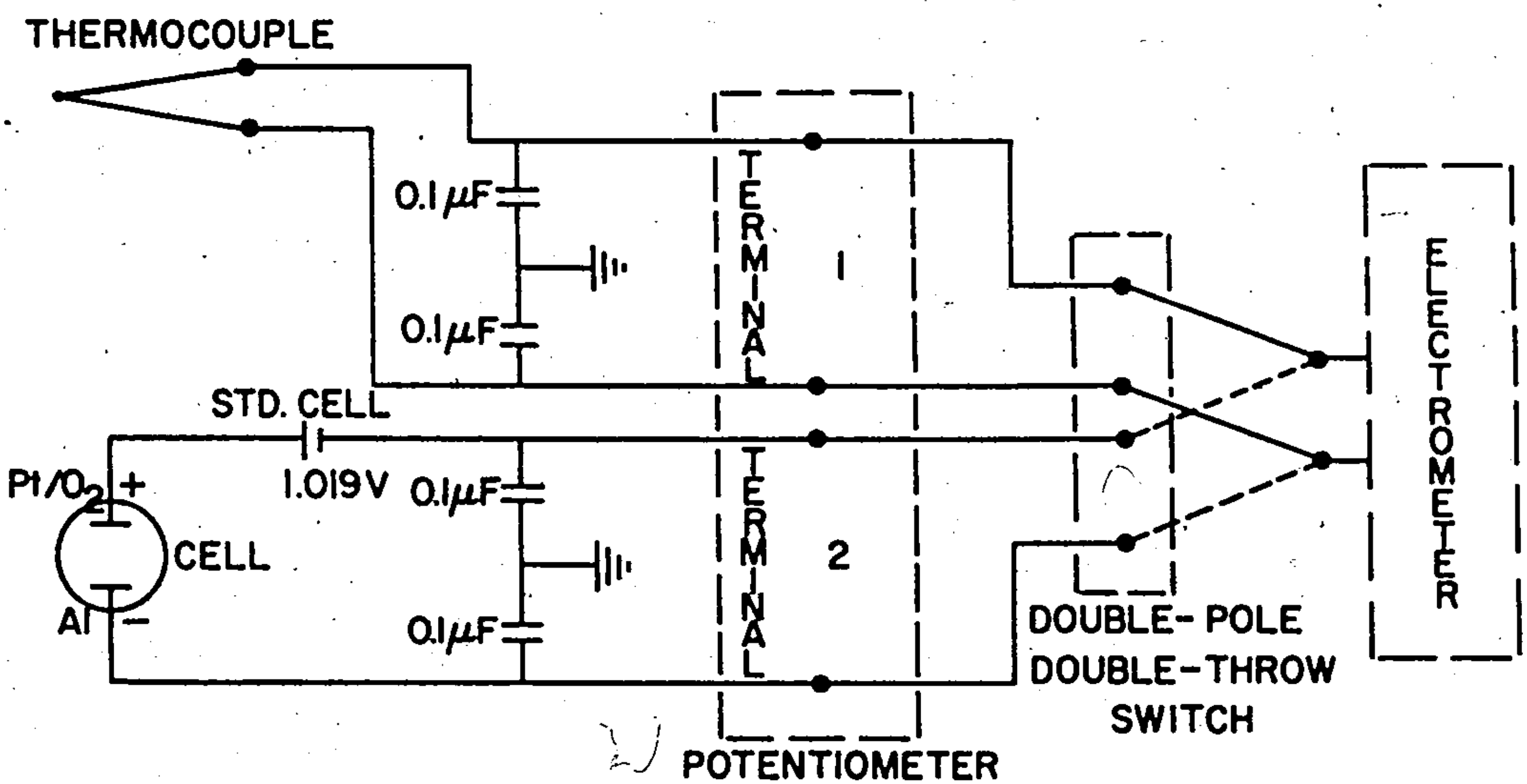

CIRCUIT DIAGRAM

Figure 3.8: The circuit diagram.

Thermocouple and cell EMF readings were initially hampered by the large amount of noise pick-up from the induction unit. A number of shielding arrangements were tried but with little success. The problem was solved in the case of Cell I by grounding all the thermocouple and cell leads through 0.1 μF capacitors as shown in Figure 3.8. Tests on the oscilloscope indicated that the high frequency signal was effectively eliminated by this procedure. The cell and thermocouple readings were checked by taking readings with the furnace off.

In the case of Cell II, however, grounding the leads through capacitors did not remove all the high frequency signals. Readings therefore could only be taken by momentarily shutting the induction unit off. Thus, the circuit diagram in the case of Cell II was essentially the same as Figure 3.8, minus the standard cell and the capacitors in the cell circuit.

The potentiometer and the electrometer were frequently calibrated against a standard cell supplied by NRC. Thus, with the arrangement used in this study, the thermocouple EMF was accurately measured to ±0.01 mV and the cell EMFs to ±1 mV. This does not take into account the error in the Cell II EMF due to a drop in cell temperature.

3.8 Materials

High purity aluminum metal (99.995% Al) used in this investigation was obtained from ALCAN in the form of $\frac{1}{2}$" thick rolled slab. Rods of required dimensions ($\frac{1}{4}$" D or $\frac{5}{16}$" D) were machined from $\frac{1}{2}$" × $\frac{1}{2}$" bar cut from this material. About $\frac{1}{2}$" long pieces were cut from these rods and used in the aluminum electrode.

The slag was made by mixing pure CaF_2 and Al_2O_3 in required proportions. Calcium fluoride (grade 'extra pure') was obtained from BDH Chemicals with the following specified maximum limits of impurities: Chloride (Cl), 0.005%; Iron (Fe), 0.005%; Lead (Pb), 0.005%; Silica (SiO_2), 0.05%; and Sulphate (SO_4), 0.01%. Assay (except Ca) after ignition was reported to be not less than 99%. Anhydrous alumina powder (grade 'certified') was supplied by Fisher Scientific with the following maximum limits of impurities: Chloride (Cl), 0.004%; Iron (Fe), 0.003%; Heavy Metals (such as Pb), 0.002%; Sulphate (SO_4), 0.07%; Silicate, (0.01%); and Alk. & Earths, 0.14%. Slags for Cell II were made out of reagent grade lime, alumina and silica powders obtained from Fisher Scientific.

Oxygen gas of purity greater than 99.6% was obtained in compressed cylinders from Canadian Liquid Air (grade 'Extra Dry'). The gas was dried over silica gel and drierite before use in the oxygen electrode. CO gas of purity greater than 99% (grade 'Technical') was obtained from Mattheson.

Graphite crucibles were machined out of 3" D bars (grade 'CS') obtained from Union Carbide. A higher grade of graphite (grade 'ECV', Union Carbide) was used for the $\frac{1}{4}$" D graphite contact rods and the 2" D graphite block in the thermal EMF measurement. The limits of impurities for the 'CS' grade are between 0.24% and 1.3% including the ash content while for 'ECV' grade they are between 0.03% and 0.11%.

All the alumina tubes used in this investigation were high purity (99.8% Alumina) recrystallized alumina tubes obtained from McDanel. This high density recrystallized material was quite resistant to the slag attack except at higher temperatures. This material was also gas tight. The chemical analysis of this grade was reported to be: Al_2O_3, 99.8%; SiO_2, 0.070%; MgO, 0.050%; Na_2O, 0.005%; CaO, 0.030%; Fe_2O_3, 0.025%; Ga_2O_3, 0.009%; TiO_2, 0.004%; and MnO, 0.001%.

Silica crucibles were made out of $2\frac{1}{2}$" ID × 0.08" wall transparent fused quartz tubes obtained from Quartz Scientific. Alundum cement was supplied by Fisher Scientific.

High purity platinum powder used for making the cermets was obtained as sponge from Johnson, Matthey and Mallory Ltd. The metallic impurity content of this 'Grade I' platinum is reported to be 5 ppm maximum. Alumina powder used in the cermets was Fisher Scientific 'certified' grade.

Platinum and 13% rhodium-platinum .020" D thermocouple wires were also obtained from Johnson, Matthey and Mallory. The maximum deviation from standard calibration between 1400°C and 1600°C is guaranteed by the supplier to be within ±3°C for this thermocouple. The EMF change when heated at 1450°C for a prolonged period is specified as 10 microvolts.

3.9 Cermet Preparation

In order to avoid the introduction of any thermal EMF in the measurements on Cell I, which contained a platinum lead in the oxygen electrode, contact with liquid aluminum had to be made with platinum. However, platinum rapidly dissolves in liquid aluminum at steelmaking temperatures as indicated by the platinum-aluminum phase diagram[117]. Sintered ceramic-metal rods ('cermet') have been previously used[116,118] to make electrical contacts with corrosive liquid metals. The ceramic network in cermets inhibits the attack of the liquid metal while still maintaining good electrical conductivity.

The ideal ceramic material for a cermet in this study is alumina as it is already present in the cell. However, as a platinum-alumina cermet was not commercially available, the technique of making this cermet had to be developed. Initially, fine platinum powder was chemically obtained by dissolving high purity platinum wires in aqua regia and precipitating the platinum as $(NH_4)_2PtCl_6$ with ammonium chloride

$$H_2PtCl_6 + 2NH_4Cl \rightleftarrows (NH_4)_2PtCl_6 + 2HCl \ . \qquad (3.4)$$

This hexachloroplatinate precipitate is then ignited at 1000°C in a silica crucible to give fine platinum powder. However, as there was considerable loss of platinum in this process, later batches of cermets were made from platinum powder obtained by grinding platinum sponge supplied by Johnson, Matthey and Mallory in a mortar and pestle. Fine alumina powder was obtained from Fisher Scientific.

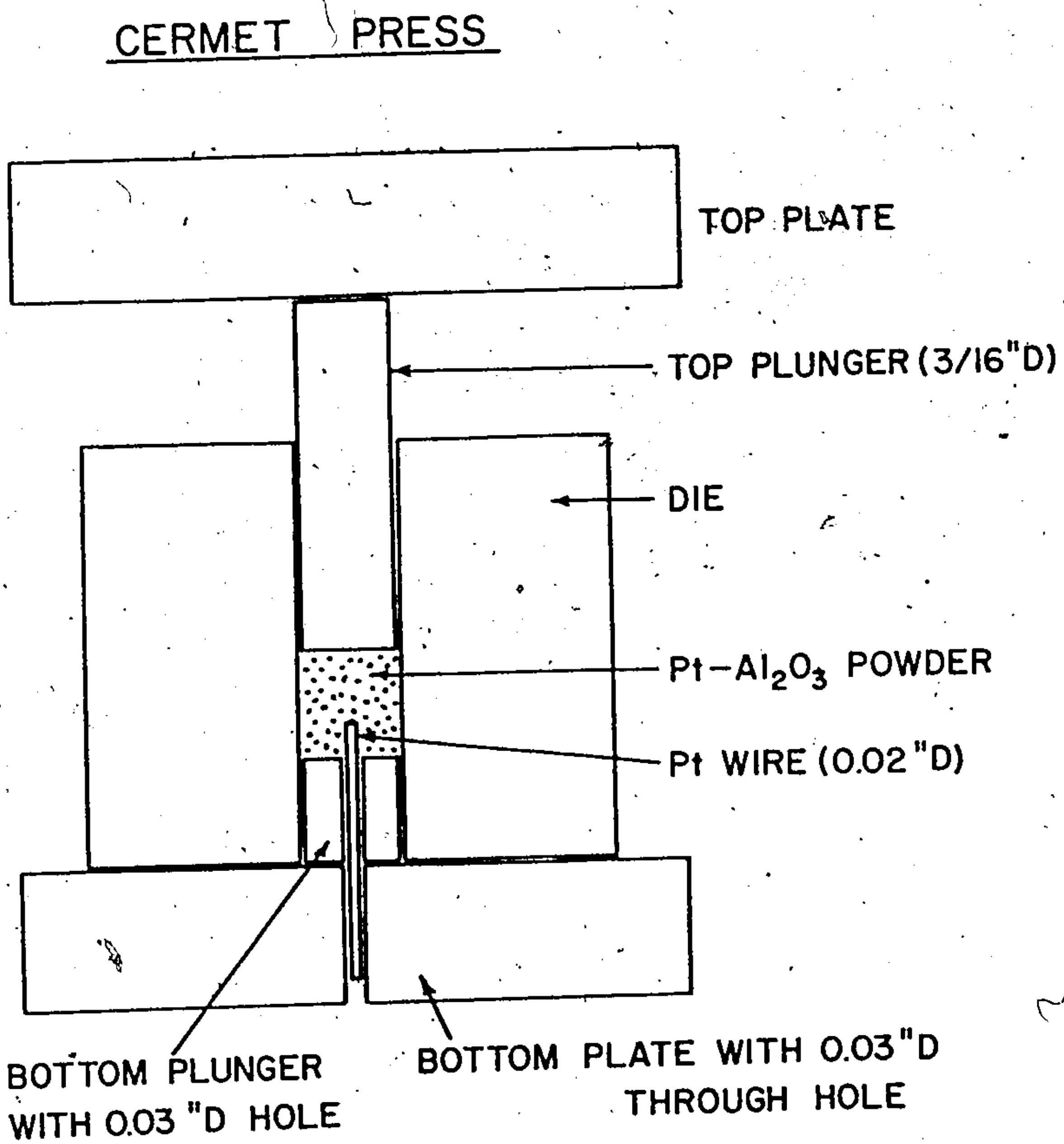

Figure 3.9: The cermet press.

Platinum and alumina powders were taken in 70:30 proportion by weight and throughly mixed for six hours on a ball mill. About 0.6 g of this mixture was placed in the die shown in Figure 3.9 and pressed into a pellet, $\frac{3}{16}$" D, at a pressure of about 100 k.p.s.i.. A 0.020" platinum wire lead was passed through a hole in the base plate and the bottom plunger of the die before pressing and formed an integral part of the cermet. The 'green' cermet was then sintered at 1500°C for twelve hours with the platinum wire embedded in it.

The cermet thus produced had good strength and electrical conductivity. It could be machined on the lathe at very small feed rates. Its resistance to attack by liquid aluminum was quite good at 1500°C as we can see from Figure 3.10.

A required length of platinum wire was welded to the wire on the cermet. This wire was protected from aluminum attack by an alumina tube ($\frac{1}{4}$" OD × $\frac{1}{8}$" ID) sealed to the cermet by alundum cement, see Figure 3.3, the top of the cermet being machined to fit the inside diameter.

3.10 Slag Preparation

One requirement of slag used in Cell I is that it should be alumina saturated. The CaF_2-Al_2O_3 system is reported to be a simple eutectic system with no terminal solid solubilities[119-121]. However, considerable disagreement exists as to the eutectic temperature and composition, as can be seen from Figure 3.11. The disagreement is probably due to varying quantities of CaO present in 'pure' CaF_2.

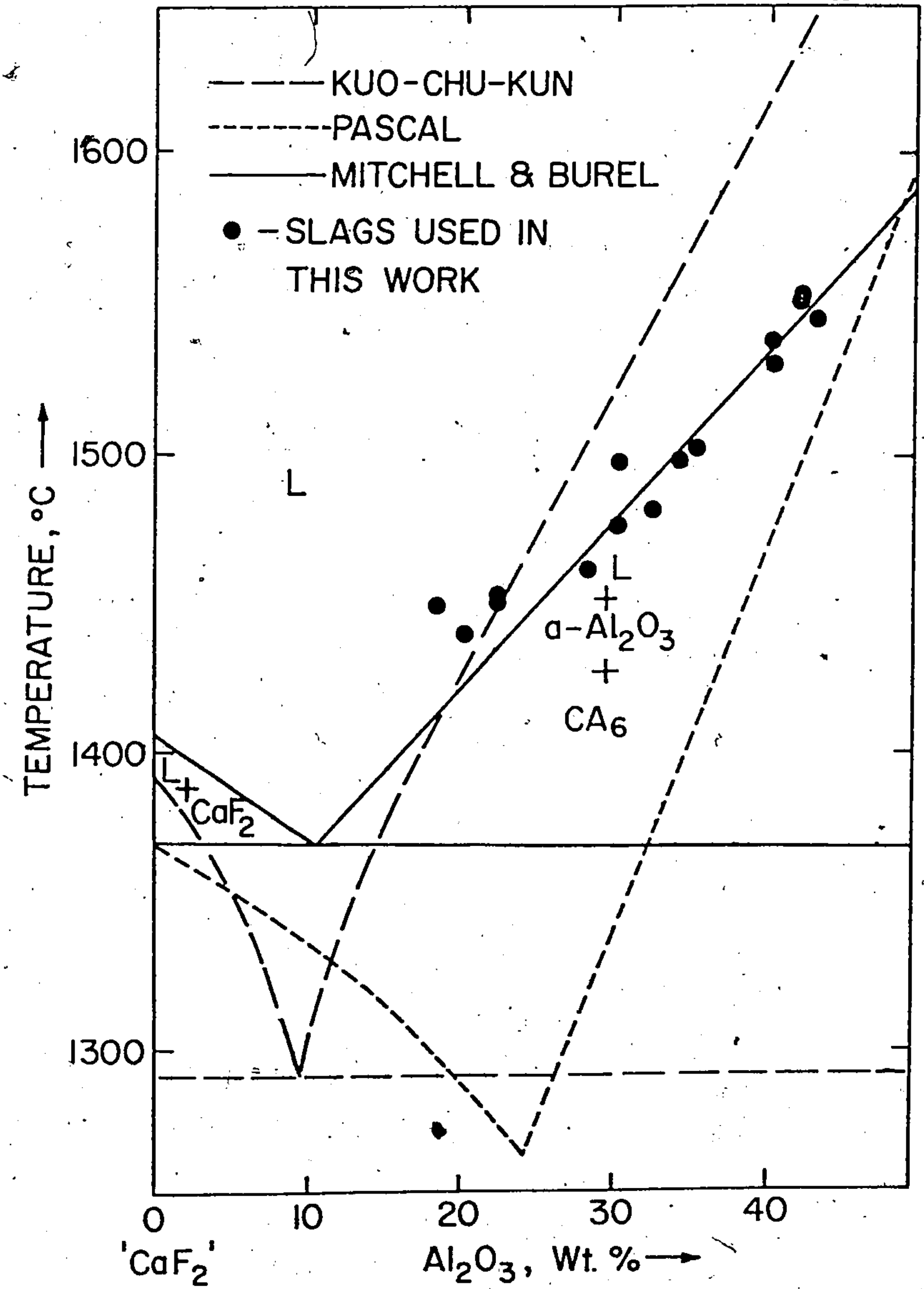

Figure 3.11: The 'CaF_2'-Al_2O_3 phase diagram. (The points indicate the composition of the slags used in Cell I.)

In designing slags for Cell I, the alumina saturated liquidus of Mitchell and Burel[121] was preferred and the compositions of the slags chosen are shown in Figure 3.11. It can be seen that a large excess of alumina in the slag was avoided as that would reduce the slag fluidity.

A slag of required composition was made by mixing weighed quantities of the two powders (CaF_2 and Al_2O_3) in a ball mill for two hours. Calcium fluoride was premelted in a graphite crucible in an induction furnace and poured into a steel mould to solidify. It was then crushed and ground in a disc grinder to the desired size. Alumina powder was used as supplied.

The amount of slag required was calculated based on the slag density and the volume required to give 1" height of molten slag in the graphite crucible. Measurements of densities in this system (CaF_2-Al_2O_3) at high temperatures have been reviewed[122] and, since all the slag compositions used were within the range 17% to 43% alumina, an average value of 2.85 g/ml was chosen for the calculations. The height of the slag was found to be close to the calculated value of 1".

CaF_2-Al_2O_3 slags used in Cell II were also made in the same way as described above. CaO-Al_2O_3-SiO_2 slags were made by premelting the required quantities of reagent grade powders in a graphite crucible and then pouring it into a steel mould to solidify. The slags were crushed and ground before use.

3.11 Metal and Slag Analysis

Aluminum in the anode of Cell I was analysed for platinum by a gravimetric method described by Vogel[123]. A weighed sample was dissolved in aqua regia and the solution was evaporated to dryness, dissolved in HCl and again evaporated to dryness to remove the nitrate ions. The residue was dissolved in water and the platinum was precipitated from the solution as metal by the addition of formic acid and sodium acetate. After ensuring complete precipitation, the solution was filtered through a quantitative filter paper which was washed until free from chloride and dried and ignited in a silica crucible. It was then weighed as metallic platinum.

Washing the precipitate and the filter paper throughly before drying was found to be important, failing which a fine white powder (alumina) was found with the dark platinum powder. These samples were redissolved and analysis carried out again.

Samples of slag taken from different regions of the solidified melt were crushed and ground before analysing by X-ray diffraction. Diffraction patterns were then compared with the patterns of 'pure' starting materials to identify phases present in the slag.

3.12 The Platinum-Graphite Thermal EMF Measurement

The use of a graphite lead in one of the aluminum electrode designs (Figure 3.3a) introduced a platinum-graphite thermoelectric EMF into the measured EMF. As no values of this quantity at the experimental temperatures are reported in the literature, they were determined directly using the cell illustrated in Figure 3.12. It consisted of a graphite block (2" D × 2") set in a silica crucible ($2\frac{1}{2}$" ID × 4") with alumina powder rammed in between as insulation. A $\frac{1}{4}$" graphite rod which screwed onto the graphite block made electrical contact with it. The other contact was made by a platinum-alumina cermet tightly fitting into a well in the graphite block. The graphite rod was protected from oxidation by an alumina tube sealed to the rod at the top by an air tight Swagelok fitting. The temperature of the graphite block was measured by a 0-13 Pt-Rh thermocouple protected by an alumina sheath.

The graphite block was heated by a 450 kHz induction furnace. The EMF between the graphite rod and the platinum wire and the thermocouple EMF were measured simultaneously as the block was raised to the required temperature. Measurements were taken using techniques described in Section 3.7.

3.13 Procedure

3.13.1 Cell I

A cell container was made as described in Section 3.2.1 and placed within the induction coil. Refractory brick shields were placed below and around the cell in order to prevent excessive heat losses.

The cell was then set up by placing a cylindrical piece of high purity aluminum in the alumina tube of the aluminum electrode the bottom of which was sealed in the well of the graphite crucible. A

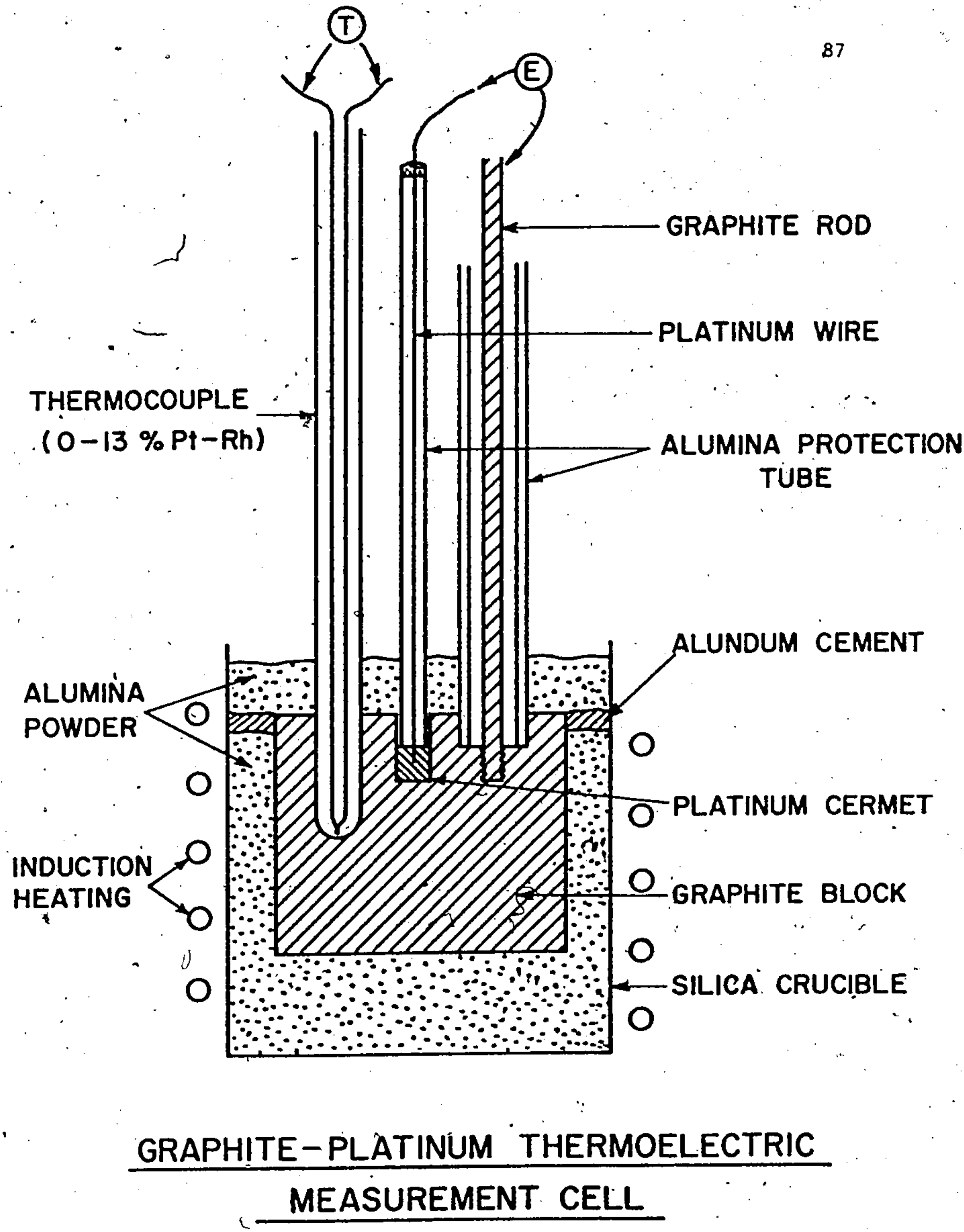

Figure 3.12: A schematic diagram of the cell used for the measurement of platinum-graphite thermal EMF.

slag mixture of predetermined composition was then poured into the container, with the thermocouple sheath in position and the oxygen electrode positioned above the slag, using the water-cooled brass electrode holder, Figure 3.1. The induction unit was then switched on and the temperature raised to approximately that of the experiment in about 45-60 minutes. The melt was equilibrated for a further 15-20 minutes by which time a thermal steady state, with negligible thermal drift was achieved.

The aluminum electrode was then raised and the oxygen electrode lowered into the melt until the outer alumina tube was below the surface of the slag. The inner alumina tube was lowered into the slag with the oxygen flowing at a predetermined rate, until a reading was obtained on the electrometer. When the inner tube was pushed too far into the melt the "saw-tooth" EMF associated with the oxygen bubbling through the melt[99,115] was obtained. The inner tube was then pulled up until the "saw-tooth" variation of EMF disappeared.

After the electrodes were in position (time zero), the cell and thermocouple EMFs were alternately monitored on the electrometer and check measurements made at convenient intervals with the potentiometer.

After an experiment the electrodes were sectioned and checked for slag attack. The aluminum electrode was checked for the presence of aluminum metal and the cermet condition recorded. Finally, metal samples were analysed for platinum and slag samples by X-ray diffraction.

3.13.2 Cell II

The cell container was made and set up in the induction coil as in the case of Cell I. The slag mixture was then poured into the crucible and the electrodes positioned above the slag. The C/CO electrode was evacuated and filled with CO at one atmosphere while the aluminum electrode was continuously evacuated. The cell was raised to the experimental temperature in 45-60 minutes and then equilibrated for further 10-15 minutes. The electrodes were then lowered and the EMF of the cell and thermocouple monitored as before.

CHAPTER IV

EXPERIMENTAL RESULTS

4.1 Standardization of the Experiment

The Pt-Pt13%Rh thermocouples used in this study were calibrated against a Pt-Pt10%Rh thermocouple which was previously calibrated upto 1100°C by the National Research Council within ±0.3°C on the IPTS-48 scale. At 1100°C the Pt-Pt13%Rh thermocouples gave a temperature reading about 1.5°C lower than that indicated by the calibrated thermocouple. As no calibration above this temperature was available, a constant correction of 2°C was applied to all experimental measurements at the higher temperatures. Thus, all temperatures quoted in this study are referred to IPTS-48 scale[181].

The potentiometer and the electrometer used for EMF measurements were frequently calibrated against an Eppley standard cell. The EMF of this standard cell was checked against an accurately known EMF from a Metra Blansko Weston Standard cell (#4828080) and was found to be correct within the limits of accuracy of the potentiometer i.e. ±0.1%. Thus, temperature could be measured to an accuracy of ±2°C at 1500°C although, for the reasons given below, the cell temperatures could not be measured with this accuracy.

In a preliminary experiment, the temperature gradient along the cell axis was measured and the results are shown in Table 4.1 and Figure 4.1. Within the electrolyte (slag) layer itself there was a temperature gradient of at least 5°C at 1450°C (probably larger at

TABLE 4.1

TEMPERATURE GRADIENT IN THE CELLS

Distance from the crucible bottom, inches	Temperature, mV (Ref. 0°C)	Temperature, °C
0.0	16.69	1452
0.25	16.68	1451.2
0.50	16.665	1450
0.75	16.65	1449
1.00	16.62	1447
1.125	16.595	1445

TABLE 4.2

PLATINUM-GRAPHITE THERMAL EMF

Temperature, °C (IPTS-48)	Pt-gr thermal EMF, mV
937	10.7
1081	14.9
1164	17.3
1197	18.1
1215	18.6
1360	22.9

Note: (1) Cold junction at 30°C

(2) Polarity: Graphite +ve
Platinum −ve

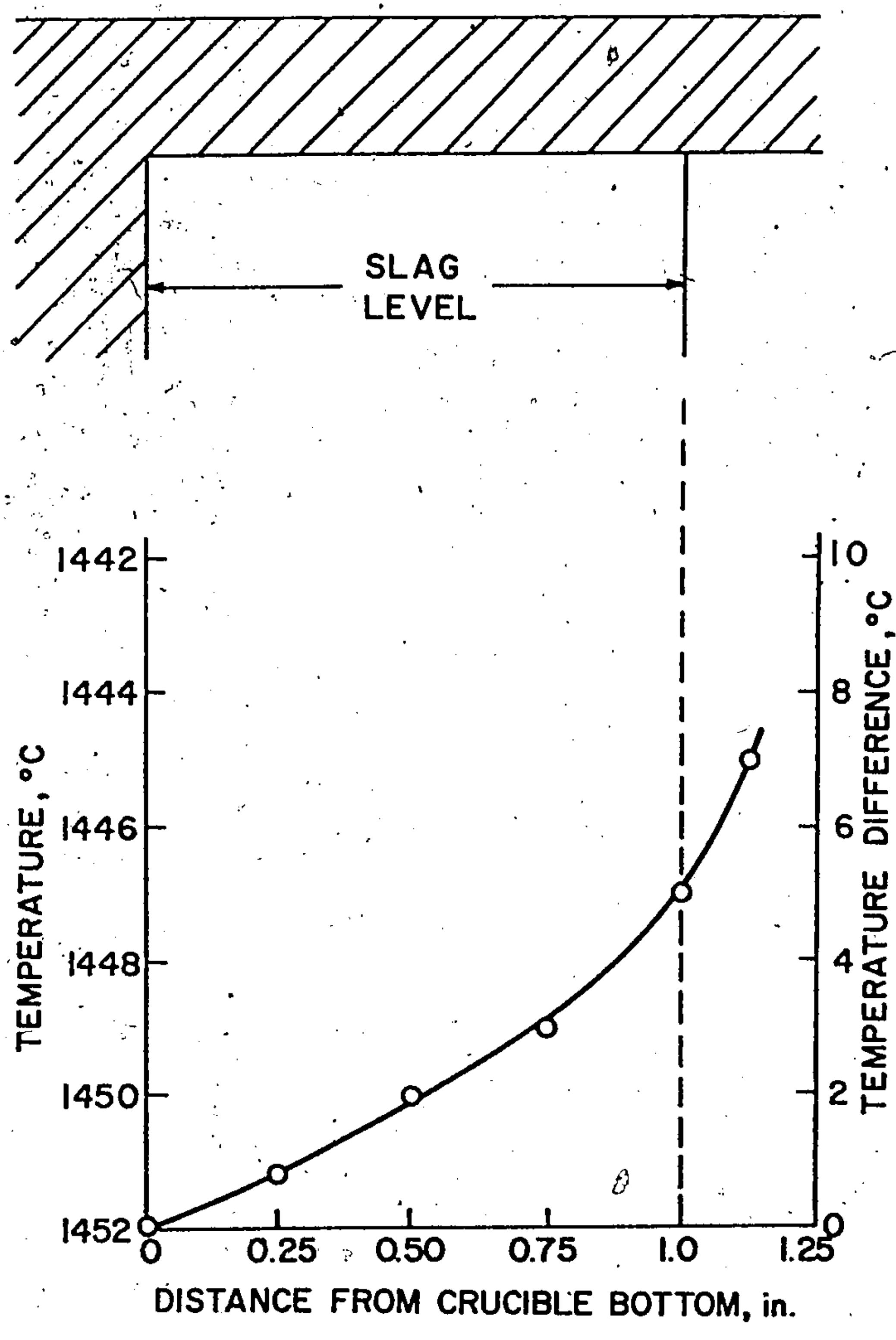

Figure 4.1: The temperature gradient in the cell.

higher temperatures). The gradient in the radial direction was not measured but is not believed to be much different. As the thermocouple was placed midway in the slag layer, an overall accuracy of only ±5°C can be claimed for cell temperature measurements.

The cell could be raised to the experimental temperature near 1500°C in about 45-60 minutes after which it required a further 15-20 minutes to achieve a thermal steady state condition. Subsequently a small temperature drift of about 8°C/hour could be corrected for by fine manual adjustment of the coil current. Overall temperature control is estimated at ±5°C.

The rotameter used in Cell I for the control of the oxygen flow rate was calibrated using a soap bubble flow meter. The flow rate of oxygen in the electrode was changed from 10 ml/min to 120 ml/min without significantly affecting the cell EMF. At higher flow rates there was spurting or freezing of the liquid electrolyte inside the oxygen electrode, while shutting off the oxygen flow made the cell EMF erratic. From the preliminary experiments oxygen flow rates of between 20 ml/min and 40 ml/min were found to be suitable.

4.2 Platinum-graphite Thermal EMF

The results of measurements of the platinum-graphite thermal EMF by the method indicated in Section (3.12) are shown in Table 4.2. These values are plotted against temperature in Figure 4.2, which indicates a linear variation of EMF in the temperature range shown.

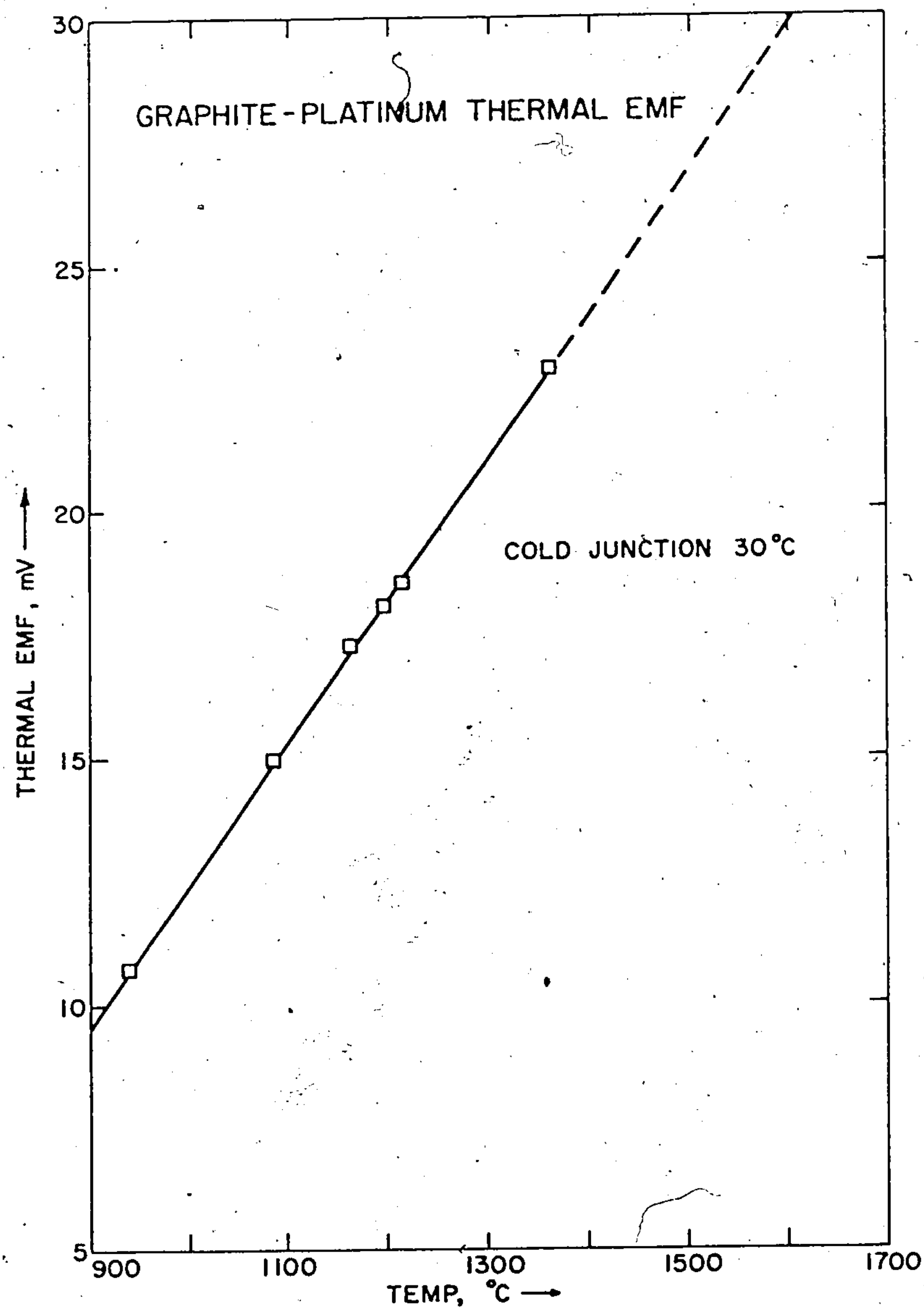

Figure 4.2: The graphite-platinum thermal EMF (reference 30°C). (Graphite +ve, platinum -ve).

This variation of Pt-graphite thermal EMF, e_t, can be expressed as

$$e_t = 2.91\times10^{-2}t - 16.73 \text{ (mV)} \tag{4.1}$$

where t is temperature in degrees Celsius. Because of the failure of this cell above 1400°C, equation (4.1) was used to extrapolate the thermal EMF to the required experimental temperature. The accuracies of the temperature and EMF measurements are the same as those given above.

4.3 Compatibility of Cell Components

In Cell I, when an alumina saturated electrolyte was used, the attack on alumina refractories was found to be very small upto temperatures around 1500°C. At 1550°C the attack was more significant and at 1600°C it was so rapid that experiments could not be satisfactorily performed.

In the case of Cell II the attack on the alumina refractories was more significant even at 1500°C. However, the cell could be satisfactorily operated at these temperatures for over two hours.

The electrolytes used in Cells I and II, in CaF_2-Al_2O_3 and CaO-Al_2O_3-SiO_2 systems, were found to be stable at the experimental temperatures, although some vapourization in the CaF_2-Al_2O_3 system was observed at higher temperatures. Slight changes in electrolyte composition due to dissolution of alumina or evaporation of CaF_2 are not expected to affect the results.

In both cells, the graphite crucible was virtually intact after the experiment and was reused a number of times. The dissolution of graphite in the slags used is known to be small[135] and its effect can be neglected. Similarly graphite is virtually insoluble in liquid aluminum[125,126]. Although platinum is extensively soluble in aluminum at the experimental temperatures[127] very little attack was observed on the platinum-alumina cermet. Figure 3.10 is a photograph showing an unused cermet (A) and cermets used at 1448°C (B) and 1551°C (C). The cermet used at 1448°C can be seen to be virtually intact while some deterioration of cermet C used at 1551°C is visible. Cermet C was still working when the experiment was terminated and subsequent analysis showed very little (~2.5%Pt) dissolution of platinum in the aluminum (see Table 4.3).

The platinum wire used in the oxygen electrode in Cell I was found to have lost its shiny lustre in the portion subjected to high temperatures. There were, however, no visible signs of slag attack. An inch was cut off from the lower end of the platinum wire and a fresh surface exposed to the slag in every experiment.

The loss of aluminum by oxidation from the electrode was found to be between 10 and 20% in Cell I, while it was even smaller in Cell II. This surprisingly small quantity of aluminum loss, inspite of the simple electrode design used in Cell I, is believed to be due to a protective layer of alumina formed on liquid aluminum.

TABLE 4.3

PLATINUM ANALYSIS OF ANODE ALUMINUM

METAL FROM CELL I

Run No.	Weight of the sample, g	Wt of the Pt precipitate, g	%Pt in Al sample (by weight)	Mole fraction of Pt in Al
2	0.8426*	0.0037	0.44	0.00061
9	0.7564	0.0068	0.90	0.00126
13	0.1503	Not detected	-	-
14	0.8032**	0.0053	(0.66)	(0.00092)
15	0.7750	0.0047	0.61	0.00085
17	0.7624	0.0122	1.60	0.00225
18	0.6366	0.0162	2.54	0.00361
19	0.7205	0.0157	2.18	0.00309
21	0.7801	0.0164	2.10	0.00297

* White powder with Pt precipitate. Redissolved and reprecipitated

** Slag entrapped in sample

4.4 Metal and Slag Analysis

The aluminum used in Cell I designs with a Pt cermet contact was analysed for Pt by a gravimetric method described in Section 3.11 and the results are shown in Table 4.3. The maximum dissolution of platinum was observed in run #18 which contained 2.54%Pt by weight i.e. 0.0036 mole fraction of Pt. This is not believed to alter the aluminum activity significantly.

Fine white alumina powder was found with dark Pt powder after ignition at 1000 C while analysing the sample from run #2. The alumina was believed to have formed by the oxidation of unwashed aluminum chloride in the precipitate. The platinum in the precipitate was dissolved in aqua regia and reprecipitated before being weighed.

The weight of metal in sample #14 was uncertain as some slag was found trapped within it. The platinum content of the sample would be somewhat higher than the value indicated.

The electrolytes and the pure starting materials were analysed by X-ray diffraction on a diffractometer and results are given in Appendix AI. The X-ray analysis revealed the presence of the compound calcium hexa-aluminate ($CaO \cdot 6Al_2O_3$) in the CaF_2-Al_2O_3 electrolytes. The presence of this compound in these slags has been reported before[121] and is believed to be due to small quantities of CaO invariably present in 'pure' CaF_2.

4.5 Variation of Cell EMF with Time

In the case of Cell I, the cell EMF was found to be stable for an initial period of between 6-15 minutes duration after which it slowly deteriorated. A typical variation of cell EMF with time is shown in Table 4.4 and Figure 4.3. The figure also shows the results of cell reversibility tests performed by momentarily imposing a greater EMF than the equilibrium value or by discharging the cell through an external circuit. In each case the EMF returned to its "open circuit" equilibrium value within a few seconds. This plateau EMF has been taken as the reversible cell EMF.

In the case of Cell II, stable cell voltages were obtained once the cell attained equilibrium. The voltage stability was checked for a period of over two hours until the experiment had to be terminated due to slag attack on the alumina refractory. The cell reversibility was checked in the following manner: (1) an EMF greater or less than the equilibrium value was impressed, as in the case of Cell I. On removal of this constraint the cell voltage returned to its original value. (2) The same EMF was observed when the equilibrium was approached from a higher or lower temperature.

4.6 EMF Data from Cell I

Results from type I cells using the graphite contact in the anode are summarized in Table 4.5. The composition of the slag, the cell temperature and the platinum-graphite thermal EMF correction,

TABLE 4.4

VARIATION OF CELL EMF WITH TIME

(RUN #19)

Experimental Conditions: Cell temperature, 1554°C;

slag, 58% CaF_2, 42% Al_2O_3; Pt contact; E_{std}=1.019

Time, min	EMF measured, $E_M = E_{Cell} - E_{std}$, volts	Comments
0.0	-	Electrodes lowered; time zero
1.0	0.842	
2.0	0.807	
3.0	0.796	
4.0	0.794	Check reading on potentiometer
5.0	0.794	External EMF imposed
5.5	0.793	
6.0	0.793	Check reading on potentiometer
7.0	0.794	External EMF imposed
7.5	0.790	
8.0	0.793	
9.0	0.791	
10.0	0.792	
11.0	0.790	Checked on potentiometer
12.0	0.787	
13.0	0.781	
14.0	0.774	
15.0	0.764	
16.0	0.752	
17.0	0.737	
18.0	0.720	

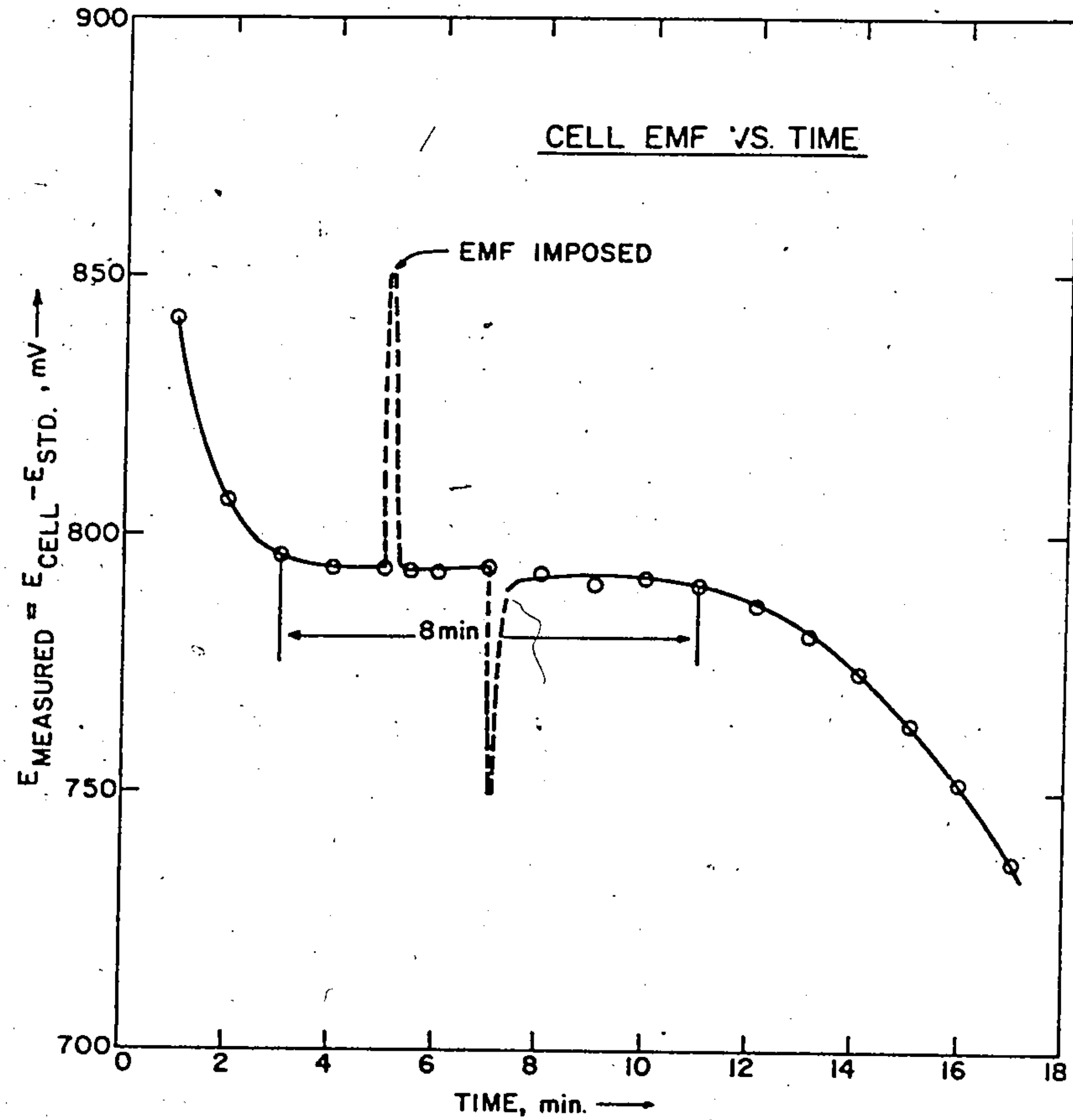

Figure 4.3: The variation of EMF of Cell I with time.

determined previously, are also given in Table 4.5. Results from cells with the platinum cermet contact in the anode are shown in Table 4.6. EMFs from all type I cells are plotted against the cell temperature in Figure 4.4. The least square line through the data, which can be represented by the equation

$$E^{\circ}_{cell} = 2.8806 - 5.784\times10^{-4}T \text{ volts} \tag{4.2}$$

is also shown in the figure along with the 95% confidence limits. The standard free energies of formation of alumina calculated from the cell EMFs are summarized in Table 4.7. Assuming that the temperature variation of ΔH°_{f} and ΔS°_{f} in the range of temperature shown are small, an assumption which is implicit in equation (4.2), a linear regressional analysis was carried out on the ΔG°_{f} data. The results are shown in Table 4.7 and Figure 4.5, the equation of the line being

$$\Delta G^{\circ}_{f}(Al_2O_3) = -398,560 + 80.02T \text{ cal/mole } Al_2O_3 \,. \tag{4.3}$$

The following quantities were also obtained from the regressional analysis: (1) the standard deviation about the line, 1800 cal/mole; (2) the correlation coefficient, 0.882; (3) the 95% confidence limit of slope, ±27.0 cal/mole-deg; and (4) the 95% confidence limit on intercept, ±47,800 cal/mole. The equations used to calculate the above quantities are summarized in Appendix AII.

TABLE 4.5

EMF FROM TYPE I CELLS USING GRAPHITE CONTACT IN THE ANODE

Run No.	$\%Al_2O_3$ in slag	Temperature, °C	Cell EMF, E°, volts		
			EMF measured	Pt-Gr EMF	Corrected EMF
1	35	1502	1.827	0.027	1.854
6	30	1498	1.857	0.027	1.884
8	34	1499	1.830	0.027	1.857
10	40	1539	1.783	0.028	1.811
12	22	1450	1.858	0.025	1.883

TABLE 4.6

EMF FROM TYPE I CELLS USING A PLATINUM

CERMET CONTACT IN THE ANODE

Run No.	$\%Al_2O_3$ in slag	Temperature, °C	Cell EMF, E°, volts
2	18	1448	1.889
9	32	1482	1.852
13	20	1440	1.878
14	30	1476	1.881
15	28	1462	1.873
17	40	1530	1.845
18	42	1551	1.834
19	42	1554	1.812
21	43	1545	1.834

TABLE 4.7

SUMMARY OF CELL I DATA WITH RESULTS OF REGRESSIONAL ANALYSIS

Run	Anode Contact*	Temperature, °K	Cell EMF, E°, volts	$-\Delta G° = 6FE°$, kcal/mole Al_2O_3	Regressional Estimate of $-\Delta G°$, kcal/mole	95% Confidence interval, ±kcal mole
13	P	1713	1.878	259.84	261.49	1.89
2	P	1721	1.889	261.36	260.85	1.71
12	G	1723	1.883	260.53	260.69	1.67
15	P	1735	1.873	259.15	259.73	1.43
14	P	1749	1.881	260.26	258.61	1.21
9	P	1755	1.852	256.24	258.13	1.13
6	G	1771	1.884	260.67	256.85	1.05
8	G	1772	1.857	256.93	256.77	1.05
1	G	1775	1.854	256.52	256.53	1.05
17	P	1803	1.845	255.27	254.29	1.35
10	G	1812	1.811	250.57	253.57	1.52
21	P	1818	1.834	253.75	253.09	1.64
18	P	1824	1.834	253.75	252.61	1.76
19	P	1827	1.812	250.71	252.37	1.83

* P – Pt cermet
G – Graphite

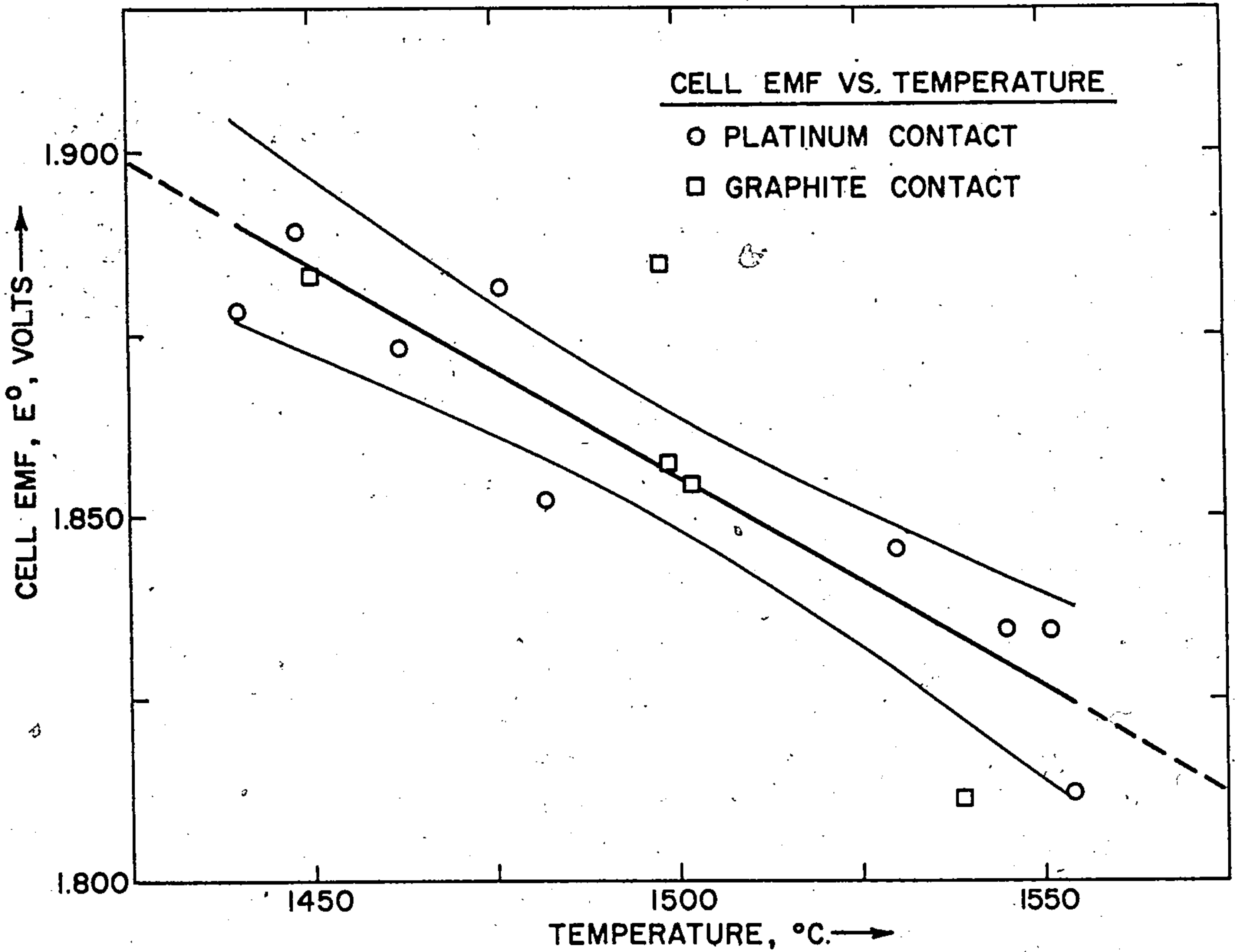

Figure 4.4: The variation of EMF of Cell I with temperature.

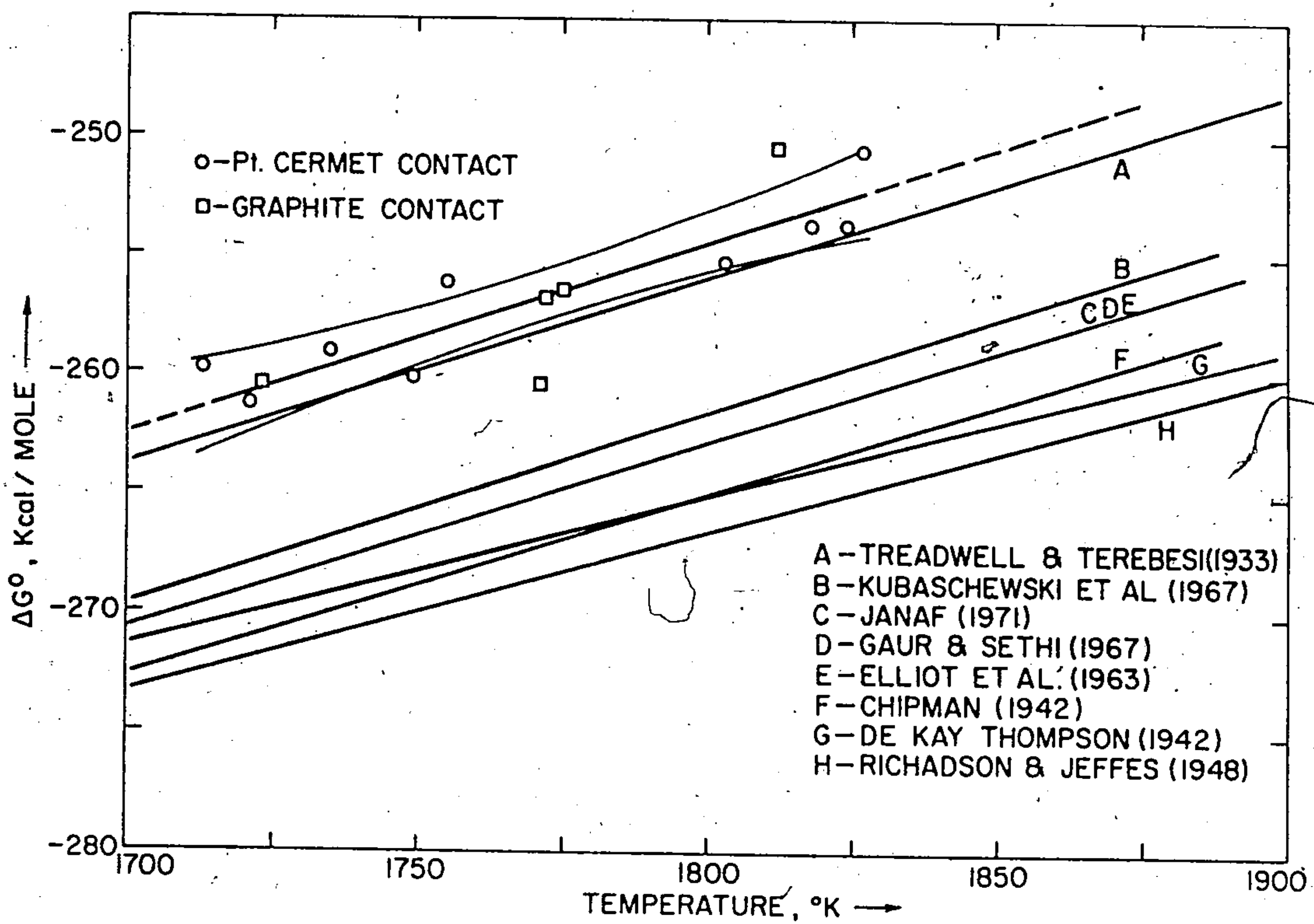

STANDARD FREE ENERGY OF FORMATION OF ALUMINA IN TEMP. RANGE 1700-1900°K.

Figure 4.5: The standard free energy of formation of alumina in the temperature range 1700°-1900°K. Comparison of Cell I data with various thermochemical values.

4.7 The Third Law Analysis of Cell I Data

The Third Law analysis of the free energy data was carried out in the following way. The Gibbs energy function, gef_T, given by

$$gef_T = (G^\circ_T - H^\circ_{298})/T \tag{4.4}$$

was determined for alumina, aluminum and oxygen using the relationship

$$gef_T = -S^\circ_T + \frac{H^\circ_T - H^\circ_{298}}{T} \tag{4.5}$$

and the thermochemical data for these substances chosen in Section 2.7.2. ΔH°_{298} is then calculated from the free energy data from the equation

$$\Delta H^\circ_{298} = \Delta G^\circ_T - T\Delta gef_T \tag{4.6}$$

where Δgef_T is given by

$$\Delta gef_T = gef_T(Al_2O_3) - 2gef_T(Al) - 1.5gef_T(O_2) \ . \tag{4.7}$$

The results of the calculations for the change in the Gibbs energy function (Δgef_T) and ΔH°_{298} are given in Table 4.8. The average value of ΔH°_{298} obtained from Cell I data is -392.55 kcal/mole Al_2O_3, the standard deviation of the data being 1.73 kcal/mole. The values of ΔH°_{298} are plotted against the experimental temperature in Figure 4.6,

TABLE 4.8

THIRD LAW ANALYSIS OF CELL I DATA

Temperature, T, °K	$-\Delta G^\circ_T$, kcal/mole	$T \times \Delta gef_T$, kcal/mole	$-\Delta H^\circ_{298}$, kcal/mole	δ, $\Delta H^\circ_{298}-(\Delta H^\circ_{298})_{Av}$, kcal/mole
1713	259.84	131.19	391.03	+1.52
1721	261.36	131.81	393.17	-0.63
1723	260.53	131.97	392.50	+0.05
1735	259.15	132.90	392.05	+0.50
1749	260.26	133.99	394.25	-1.70
1755	256.24	134.46	390.70	+1.85
1771	260.67	135.70	396.37	-3.82
1772	256.93	135.78	392.71	-0.16
1775	256.52	136.01	392.53	+0.01
1803	255.27	138.19	393.46	-0.91
1812	250.57	138.89	389.46	+3.09
1818	253.75	139.35	393.10	-0.56
1824	253.75	139.82	393.57	-1.02
1827	250.71	140.05	390.76	+1.79

Note: $(\Delta H^\circ_{298})_{Av}$ = - 392.55 kcal/mole Al_2O_3

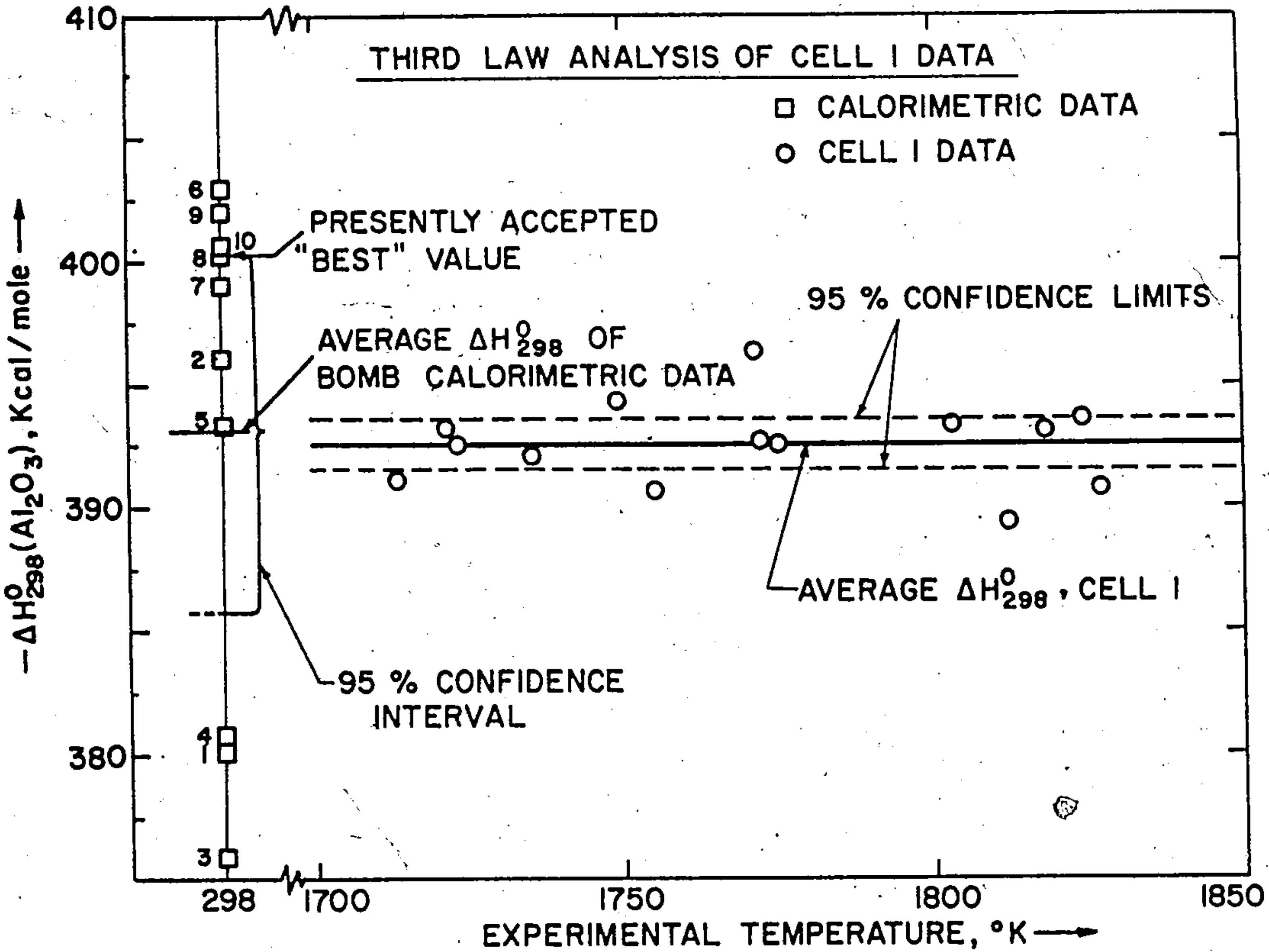

Figure 4.6: The standard heat of formation of alumina at 298°K, ΔH^o_{298}, from Third Law analysis of Cell I data.

the average ΔH°_{298} and the 95% confidence limits being indicated. The average of many determinations of ΔH°_{298} from bomb calorimetry (see §2.7.1) is also shown with its 95% confidence limits.

4.8 EMF Data from Cell II

The EMF of type II cells using $CaF_2-Al_2O_3$ and $CaO-SiO_2-Al_2O_3$ electrolytes are summarized in Table 4.9. The standard free energy of the cell reaction

$$2Al_{(\ell)} + 3CO_{(g)} \rightleftarrows Al_2O_3 + 3C_{(s)} \tag{4.8}$$

is shown in the fourth column. The fifth column gives the standard free energy of formation of carbon monoxide, $\Delta G^{\circ}_{f}(CO)$, given by

$$\Delta G^{\circ}_{f}(CO) = -27{,}925 - 20.22T \text{ cal } (1500°-2000°K) \tag{4.9}$$

which was obtained from JANAF Tables[59]. Combining this data with the free energy change for the cell reaction the standard free energy of formation of alumina, $\Delta G^{\circ}_{f}(Al_2O_3)$, is obtained and shown in the sixth column.

The values of the standard free energy of formation of alumina obtained in this manner from Cell II EMFs are plotted along with the data from Cell I in Figure 4.7. Thermochemical values from JANAF for the same quantity are also included in this figure for comparison.

TABLE 4.9

EMF OF TYPE II CELLS AND CALCULATION OF

$\Delta G^\circ_f(Al_2O_3)$ FROM THE DATA

Type of electrolyte used	Temperature, °K	Cell EMF, E°, volts	$\Delta G^\circ_{cell} = -6FE^\circ$, kcal/mole (A)	$3\Delta G^\circ_f(CO)$, kcal/mole (B)	$\Delta G^\circ_f(Al_2O_3)$ kcal/mole (A+B)
CaF_2-10%Al_2O_3	1749	0.480	-66.41	-189.87	-256.28
CaF_2-15%Al_2O_3	1759	0.475	-65.72	-190.48	-256.20
CaF_2-15%Al_2O_3	1785	0.468	-64.75	-192.05	-256.81
38%CaO +	1674	0.562	-77.76	-185.32	-263.08
42%SiO_2 +	1679	0.580	-80.25	-185.62	-265.87
20%Al_2O_3	1641	0.628	-86.89	-183.32	-270.21

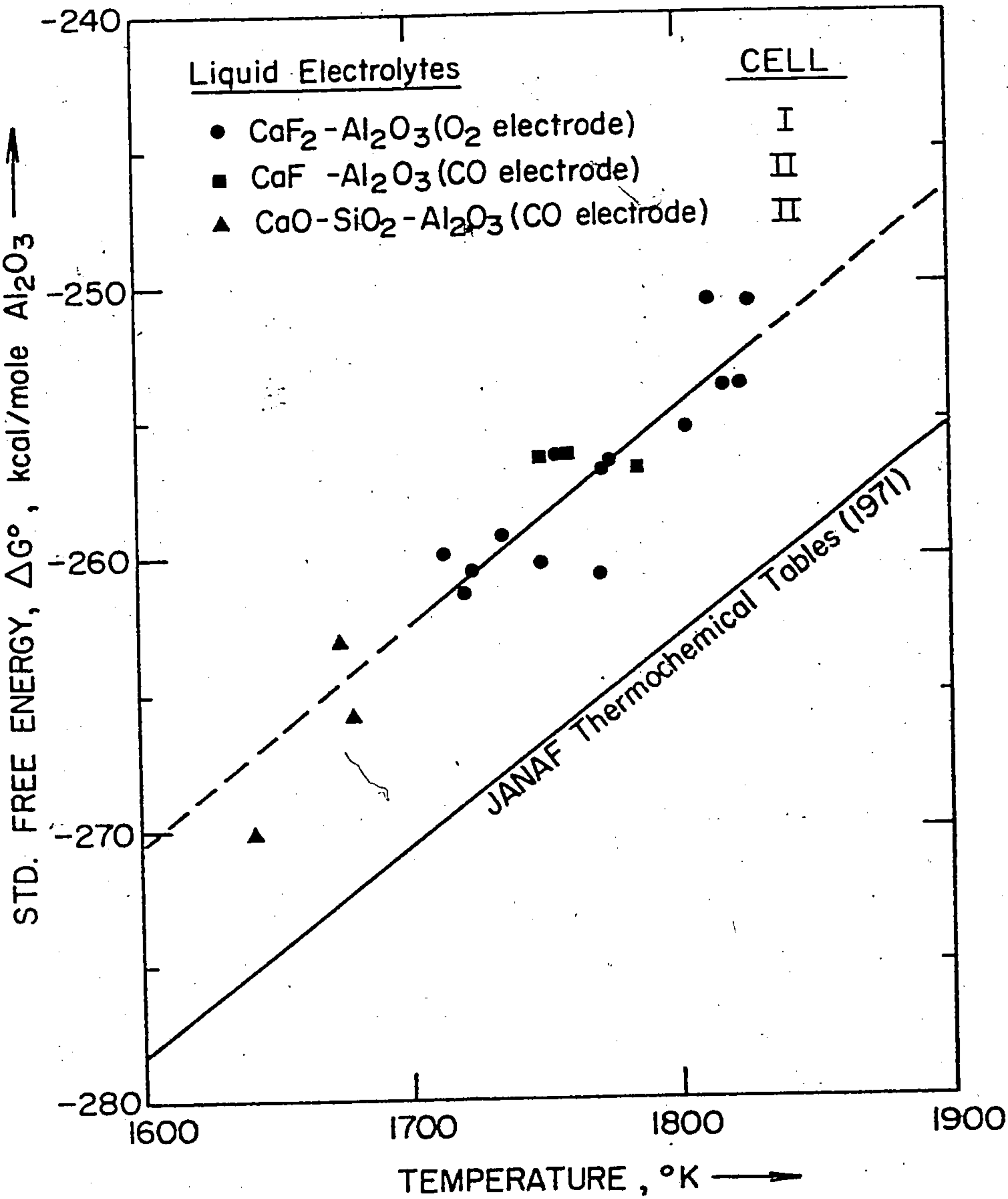

Figure 4.7: ΔG_f° (Al_2O_3) data from Cells I and II and comparison with the accepted thermochemical value.

TABLE 4.10

THIRD LAW ANALYSIS OF CELL II DATA

Temperature, T, °K	$-\Delta G^\circ_T$, kcal/mole	$T \times \Delta gef_T$, kcal/mole	$-\Delta H^\circ_{298}$, kcal/mole	$\delta = \Delta H^\circ_{298} - (\Delta H^\circ_{298})_{Av}$ kcal/mole	Type of electrolyte used
1674	263.08	128.15	391.23	+1.48	$CaO + SiO_2 + Al_2O_3$
1679	265.87	128.54	394.41	-1.70	
1641	270.21	125.58	395.79	-3.07	
1749	256.28	133.99	390.27	+2.44	$CaF_2 + Al_2O_3$
1759	256.20	134.77	390.97	+1.74	
1785	256.81	136.79	393.60	-0.89	

Note: $(\Delta H^\circ_{298})_{Av} = -392.71$ kcal/mole

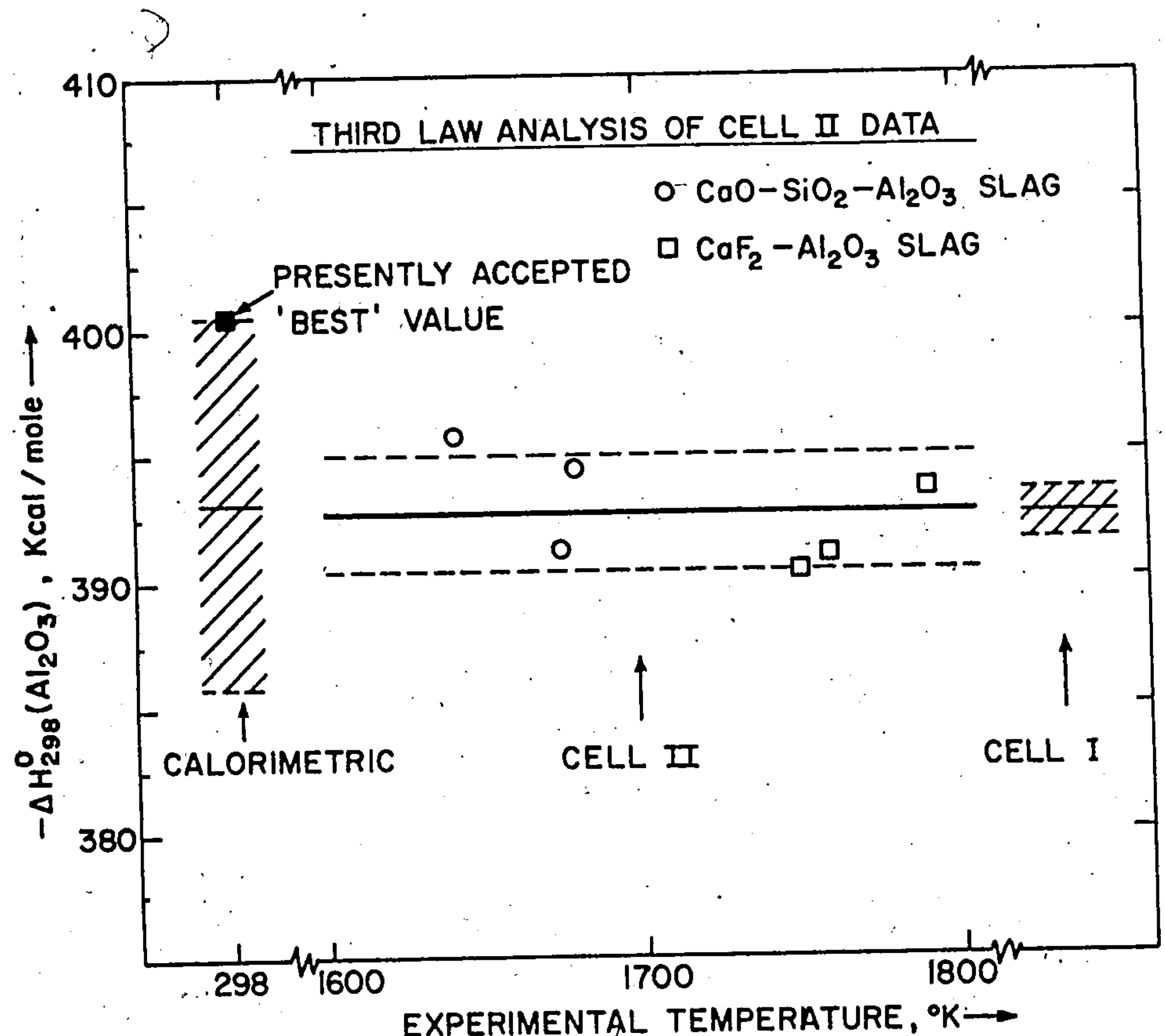

Figure 4.8: The standard heat of formation of alumina at 298°K, ΔH°_{298}, from Third Law analysis of Cell II data.

4.9 The Third Law Analysis of Cell II Data

Using the Gibbs energy functions established above, the data from Cell II were analysed by the Third Law method as before. The results are shown in Table 4.10 and Figure 4.8. The average value of ΔH°_{298} (-392.71 kcal/mole) and the 95% confidence interval (±2.3 kcal/mole) of Cell II data are shown in Figure 4.8 together with those from Cell I and bomb calorimetric determinations for comparison.

Combining the values of ΔH°_{298} calculated by the third law analysis of Cells I and II data, the following results are obtained: average ΔH°_{298} - 392.60 kcal/mole, standard deviation 1.87 kcal/mole and 95% confidence interval 0.92 kcal/mole.

CHAPTER V

DISCUSSION

5.1 Introduction

In this chapter the results presented in the last chapter are discussed vis-a-vis the work reported in the literature, and the differences in the values of standard enthalpy and free energy are critically examined. Figure 4.5 compares the values of the standard free energy of formation of alumina obtained from Cell I with the thermochemical estimation of the same quantity by various authors in the temperature range of 1700°-1900°K of interest in steelmaking. It must be noted that the scales have been expanded in Figure 4.5 to amplify the difference in the results reported by different workers. From the figure it is apparent that the present results are in excellent agreement with the early estimation of Treadwell and Terebesi[74] while they are substantially more positive than other estimations. Except for the work of Treadwell and Terebesi, the thermochemical estimates of ΔG_f° range from -261.74 kcal/mole (Kubaschewski et al.[57] 1967) to -266.64 kcal/mole (Richardson and Jeffes[56] 1948) at 1800°K, the presently accepted "best" value being -262.92 kcal/mole (JANAF Tables[59] 1971). This compares with the value of -254.52 kcal/mole at 1800°K experimentally determined in this study. Although, in percentage terms, the present data is only 3.2% more positive than the JANAF data at 1800°K, they give rise to an order of magnitude difference in the value of the equilibrium constant. Thus, it becomes necessary to examine the possible sources of error in the different types of experiments in order to arrive at the "best" value.

Following Jeffes and Sridhar(115), the conditions necessary for the satisfactory operation of the EMF cell can be enumerated:

(1) The components, i.e. aluminum, oxygen and alumina, must be in their respective standard states;

(2) the cell reaction must be unambiguous;

(3) the mutual solubility of the phases must be small and the cell components must be compatible with each other at the reaction temperature;

(4) the electrodes must be reversible; and

(5) the EMF must represent the ionic process only, i.e. electronic conductivity of the electrolyte must be small.

These conditions are now considered.

5.2 Conditions of Operation of the EMF Cell

5.2.1 Non-standard conditions

Following the discussion in Section 2.9, the EMF of Cell I can be written as

$$E = E^\circ - \frac{RT}{nF} \ln \frac{a_{Al_2O_3}}{a_{Al}^2 \cdot p_{O_2}^{3/2}} \tag{5.1}$$

where the symbols have the same meaning as before. Thus, the standard cell EMF, E°, can only be obtained if the activities of aluminum and alumina and the partial pressure of oxygen are maintained substantially close to unity. The measured cell EMF can also be in error due to the presence of an additional thermal EMF arising from non-identical electrical leads to the electrodes. Finally, the temperature gradient across the cell can give rise to errors in the cell EMF due to changes in chemical potential and the thermal EMF thus introduced. These effects are now discussed separately.

(a) *Activity of alumina in the slag.* Tables 4.5 & 4.6 & Figure 3.11 show the composition of CaF_2-Al_2O_3 slags used in Cell I at different experimental temperatures. The three versions[119-121] of the phase diagram of the 'CaF_2'-Al_2O_3 system reported in the literature are also included in Figure 3.11. While there is agreement on the nature of the system, i.e. a simple eutectic system with no terminal solid solubilities, there is no agreement as to the eutectic temperature and composition. The most recent work of Mitchell and Burel[121] is in agreement with that of Kuo and Yen[120] with respect to the eutectic composition but with a 80°C discrepancy in the eutectic temperature. These discrepancies are believed to be due to varying quantities of CaO present in 'pure' CaF_2, as can be seen from the different melting points of CaF_2 reported in Figure 3.11. There are at least ten determinations of the melting point of 'pure' CaF_2 reported in the literature (see ref. 124) and they range from 1386°C to 1423°C. As much as 0.5-2% CaO can be formed in CaF_2 by the reaction with water vapour:

$$CaF_{2(s)} + H_2O_{(g)} \rightleftarrows CaO_{(s)} + 2HF_{(g)} . \tag{5.2}$$

while some CaO can also be formed in the CaF_2-Al_2O_3 system by the reaction

$$3CaF_{2(s)} + Al_2O_{3(s)} \rightleftarrows 3CaO_{(s)} + 2AlF_{3(g)} . \tag{5.3}$$

The difference in the liquidus temperatures reported by Kuo and Yen[120] and Mitchell and Burel[121] can also be traced to the different experimental techniques used by these workers. Mitchell and Burel's results, determined by the measurement of thermal arrests, are believed to be more accurate than those of previous workers, and their alumina saturated liquidus was used to design slags for Cell I. From Figure 3.11 it is also apparent that a large excess of alumina in the slag was avoided as this would have resulted in the loss of slag fluidity. The four slags at lower temperatures had to be used at temperatures higher than the liquidus of Mitchell and Burel due to the high viscosities of these slags at the reported liquidus temperatures. However, alumina saturation of the slags is virtually assured by the presence of solid alumina refractories in the cell.

In any event the errors introduced due to possible deviations of alumina activity from unity are small. Calculations using equation (5.1) show that even an alumina activity as small as 0.9 would introduce an error in the measured EMF of 2.7 mV at 1800°K, which corresponds to an error of 375 cal/mole in the calculated free energy of formation.

Finally, it must be noted that alumina activities of less than unity in the electrolyte will result in a more negative apparent standard free energy of formation. Thus, this factor cannot account for the discrepancy with thermochemical data shown in Figure 4.5.

(b) *Activity of aluminum in the anode.* The solubility of carbon in molten aluminum is small, one estimate[125] being less than 0.05 wt% at 1300°-1500°C - although a higher value of 0.32 wt% has been reported at 1200°C[126]. However, lower values were reported by the same workers[126] when they equilibrated their melt in an argon atmosphere. This was attributed to the presence of small amounts of oxygen in the gas. Thus, the carbon content of the aluminum anode is believed to be very small under the experimental conditions in this investigation and its effect on the activity of aluminum can be neglected.

On the other hand the phase diagram for the aluminum-platinum system reported by Huch and Klemm[127] indicate extensive solubility of Pt in liquid aluminum at 1500°C. However, the use of a platinum-alumina cermet to contact the liquid aluminum anode drastically reduced the dissolution of Pt in aluminum at the experimental temperature. Table 4.3 shows that the maximum dissolution of Pt in the anode metal was 2.54 wt% (0.0036 mole fraction Pt) at 1551°C while only 0.44 wt% dissolved at 1448°C.

Huch and Klemm[127] have found nine intermetallic phases in the Pt-Al system. They were all placed in the Pt rich portion of the diagram (Pt > 60% by wt) which indicates a strong negative deviation from ideality in this region. However, in the Al rich part there is an eutectic at 657°C and 9 wt% Pt which indicates a positive deviation from ideality at lower temperatures in this region. In any event, the activity of aluminum at greater than 0.9964 mole fraction cannot be very far from unity. Calculations using equation (5.1) show that even an aluminum activity of 0.90 would introduce an error of only 2.7 mV in the measured EMF at 1800°K. Thus, only small corrections to the cell EMF are expected from this source unless substantially small activity coefficients of aluminum exist at mole fractions of Al > 0.99.

(c) *Partial pressure of oxygen in the cathode.* High purity oxygen gas flowing past a Pt wire at a slightly higher than atmospheric pressure was the standard condition for the gas electrode. In principle, corrections are required for dilution of the oxygen gas by CaF_2 vapour, for the excess pressure of the oxygen caused by the immersion of the electrode tip under the melt and changes in the barometric pressure. However, these corrections are extremely small and well within the experimental precision of this investigation.

(d) *Thermal EMF.* Whenever there exists a temperature gradient across two non-identical electrical leads from an EMF cell to the measuring instrument, a thermal EMF is introduced into the measured cell EMF. In the initial design of Cell I, the graphite contact for the aluminum electrode gave rise to a platinum-graphite thermal EMF which had to be corrected for. The highest temperature at which values of this quantity are reported[128] in the literature is around 500°C. Therefore it was necessary to determine this thermal EMF in the temperature range of interest in this investigation, 1400°-1600°C, and the results obtained are shown in Figure 4.2.

Although no meaningful readings could be obtained from the platinum-graphite thermal EMF cell above 1400°C, the thermal EMF was obtained at the higher experimental temperatures by extrapolation of the essentially linear variation of the EMF below 1400°C, with an accuracy believed to be sufficient for this study. Differences in crystalline orientation, crystalline perfection, impurities, etc. of graphite are known to affect the thermal EMF[131]. Therefore the experiment was repeated with the same starting materials and the reproducibility of the thermal EMF below 1400°C was found to be ±0.2 mV. Thus, the error in the platinum-graphite thermal EMF in the temperature range 1400°-1600°C is placed at ±0.5 mV.

From Table 4.5 it can be seen that the corrections to the cell EMF due to the thermal EMF are quite substantial, in the range 0.025-0.027 V. These EMFs were added to the measured EMF as they were in opposition to cell EMF - graphite being positive with respect to platinum.

The reason for the failure of the thermal EMF cell above 1400°C is not known. The investigations of Raub and Falkenburg[129] show that Pt does not react with "exceedingly pure" graphite below the eutectic temperature of 1736°C. The deterioration of the Pt in contact with graphite at lower temperatures is believed to be due to impurities in the graphite[129].

(e) *Temperature gradient in the cell.* As reported in Section 4.1, a temperature gradient of ~5°C existed in the electrolyte layer in the vertical direction and a similar gradient is expected in the radial direction. As the anode, cathode and the thermocouple were placed about the same distance from the centre of the graphite crucible, the temperature difference between the electrodes is believed to be much smaller than 5°C. However, it is interesting to consider the effect of a temperature gradient between the electrodes on the cell EMF.

If T_1 is the overall cell temperature and T_2 the temperature of the oxygen electrode, the error in the cell EMF, ΔE, can be shown to be[130]

$$\Delta E = \frac{1}{4F}\left[\mu^\circ_{O_2}(T_2) - \mu^\circ_{O_2}(T_1)\right] \pm \alpha(T_2 - T_1) \tag{5.4}$$

where $\mu^\circ_{O_2}(T)$ is the standard chemical potential of oxygen at the temperature T and α is the average change of Pt-Al thermal EMF per °K at the cell temperature. The change in the chemical potential of oxygen can be estimated from

$$\Delta\mu^\circ_{O_2} = \mu^\circ_{O_2}(T_2) - \mu^\circ_{O_2}(T_1) = T_2 \mathrm{gef}_{T_2}(O_2) - T_1 \mathrm{gef}_{T_1}(O_2) \tag{5.5}$$

where $\mathrm{gef}_T(O_2)$ is the Gibbs energy function of oxygen. Using the Gibbs energy functions selected before (§2.7), $\Delta\mu^\circ_{O_2}$ is found to be 316 cal/mole O_2 for $T_1 = 1778$°K and $T_2 = 1773$°K. This is an error of 3 mV in the cell reading. The error from the second term of equation (5.4) can be estimated from the value of $\alpha_{Pt-Al} = 0.012$ mV/°C at 600°C[132], the highest temperature at which this data is available. The thermal EMF correction thus obtained is only 0.06 mV which is small compared to the above error. Goto and Pluschell[130] have similarly calculated the difference in EMF caused by a temperature difference of

10°C to be 5.3 mV in an oxygen concentration cell using lime stabilized zirconia as solid electrolyte. This is quite similar to the value of 3 mV for the 5°C temperature difference calculated above.

In addition, the small variation in cell EMF with oxygen flow rate can be understood in terms of the above calculations. At the higher flow rates the cold oxygen gas will reduce the oxygen electrode temperature, thus substantially changing the cell EMF. Therefore, small oxygen flow rates of 20-40 ml/min were used in this investigation.

5.2.2 Unambiguous cell reaction

In order to get any meaningful thermodynamic data from EMF measurements on electrochemical cells, it is imperative that the cell reaction is clearly and unambiguously defined. For example, a "mixed" potential of little thermodynamic significance will develop in a cell of the type

$$\text{A-B alloy} \mid A^{+n_1},\ B^{+n_2} \text{ ions in electrolyte} \mid O_{2(g)} \qquad (5.6)$$

when A and B are of similar electronegativity. Even if metal A is sufficiently more noble than metal B, a "mixed" potential will be observed below a certain activity of B in the alloy AB. In the case of a pure metal anode, such as used in this investigation, there is still a possibility of developing a "mixed" potential if there exist more than one oxidation state of the metal which are quite close to each other on the electronegativity scale. In the case of Cell I with an aluminum anode and oxygen cathode the possible species, representing different oxidation states of aluminum, are $Al_2O_{(g)}$, $AlO_{(g)}$, $Al_2O_{2(g)}$ and $AlO_{2(g)}$ in addition to solid Al_2O_3. The standard free energies of formation of these oxides at 1700°K and 1800°K are shown in Table 5.1, the data being selected from JANAF Thermochemical Tables[59]. From Table 5.1 it is apparent that Al_2O_3 is much more stable than the other oxides at 1400°-1600°C and therefore the cell EMF will virtually represent the formation of Al_2O_3 from the elements

$$2Al_{(\ell)} + \frac{3}{2}\,O_{2(g)} \rightleftarrows Al_2O_{3(s)} \tag{5.7}$$

which is obtained by combining the anode reaction

$$2Al_{(\ell)} + 3(O^{2-})_{slag} \rightleftarrows Al_2O_{3(s)} + 6e^- \tag{5.8}$$

with the cathode reaction

$$\frac{3}{2}\,O_{2(g)} + 6e^- \rightleftarrows 3(O^{2-})_{slag} \tag{5.9}$$

Another source of ambiguity in a cell reaction can arise due to polarization at the electrodes. The SiC electrode used by Chang and Derge[133] and the Fe-Si electrodes used by Sanbongi and Omori[134] can undergo surface changes in contact with an electrolyte if even small amounts of electricity are allowed to pass through the cell. Similarly, surface polarization is often observed in solid metal-metal oxide mixtures used as reference electrodes in oxygen concentration cells with solid electrolytes. Such surface polarization can be the source of

TABLE 5.1

THE STANDARD FREE ENERGY OF FORMATION, ΔG°_f, OF DIFFERENT ALUMINUM OXIDES AT 1700° AND 1800°K

Species	ΔG°_f, kcal/mole	
	At 1700°K	At 1800°K
α-$Al_2O_{3(s)}$	-270.61	-262.92
$Al_2O_{(g)}$	-60.77	-61.80
$AlO_{(g)}$	-9.83	-11.23
$Al_2O_{2(g)}$	-87.43	-86.22
$AlO_{2(g)}$	-45.23	-45.03

Note: All data taken from JANAF Tables[59].

serious errors due to the non-standard activity of the relevant component at the electrode surface.

In the present investigation, the use of a high impedance electrometer and a potentiometer with a step-down resistance box connected to a sensitive galvanometer ensured a very small polarizing cell current. The possibility of polarization at the liquid aluminum electrode is very small due to the high temperatures and convection in the liquid. However, reaction polarization of the oxygen electrode at relatively high current densities is possible[114].

In the case of cell I, a "sawtooth" variation of the cell EMF was observed with time when the oxygen electrode was pushed too far down into the slag. Such a variation has been observed before by Flood et al.[99] and Sridhar and Jeffes[106] with a platinum-oxygen electrode design similar to the present investigation. Jeffes and Sridhar[115] explain this EMF variation on the basis of a "mixed" potential at the Pt-oxygen electrode. Because of the small solubility of oxygen gas in the liquid electrolyte a sharp oxygen potential gradient exists in the electrolyte in which the platinum wire is immersed. This gives rise to a "mixed" EMF which varies periodically at the frequency of gas bubbling.

Sridhar and Jeffes solved this problem by retracting the Pt wire inside the sheath slightly. This allows the oxygen gas to be in contact with the whole length of the Pt wire while contact with the melt is made through a film of melt wetting the sheath. The EMF variation observed by Flood et al. disappeared when the cell atmosphere and the electrode gas was made the same, thereby presumably eliminating concentration gradients near the electrode. Delimarskii and Andreeva[108] obtained a constant EMF with a Pt tube electrode only when a high flow rate of oxygen (100 cm^3/min) was passed. This high flow rate was presumably necessary to establish a unit oxygen activity over the whole surface of the platinum electrode in contact with the melt. This will, however, lead to cooling of the oxygen electrode with the consequent error in cell EMF discussed earlier.

5.2.3 Compatibility of cell components and the mutual solubility of phases

The compatibility of cell components has already been discussed in Section 4.3. It must be noted that the operating range of the cell temperature was limited by the choice of cell components. The lower temperature limit when using CaF_2-Al_2O_3 electrolytes should, in principle, be the eutectic temperature of 1368°C[121]. However, in practice the slags in this system could not be used below 1425°C because of their high viscosity. On the other hand, using cell design II, a low melting silicate slag of composition 38 wt% CaO, 42 wt% SiO_2 and 20 wt% Al_2O_3 (Ternary eutectic, 1265°C) could be used as the electrolyte at lower cell temperatures.

The highest temperatures attainable in both the cells were limited by the rate of slag attack on the refractories. Both the electrolytes were quite stable even at the highest temperatures used in this study although a slight evaporation of CaF_2 was observed. The vapour pressure of pure CaF_2 at 1550°C is 0.7 mm Hg[57].

The design of Cell I, in which liquid aluminum was in contact with the electrolyte, restricted the choice of electrolyte components to those which could not be reduced by aluminum. The commonly used silicate electrolytes were thus ruled out. The standard free energy changes for the reactions:

$$2Al_{(\ell)} + 3CaF_{2(\ell)} \rightleftarrows 2AlF_{3(g)} + 3Ca_{(\ell,g)} \quad (5.10)$$

$$2Al_{(\ell)} + CaF_{2(\ell)} \rightleftarrows 2AlF_{(g)} + Ca_{(\ell,g)} \quad (5.11)$$

at 1700°K and 1800°K can be seen from Table 5.2 to be positive. Similarly, the oxidation of CaF_2 at the oxygen electrode, the reaction of CaF_2 and Al_2O_3 (Table 5.2), etc., have positive standard free energy changes, thus indicating the compatibility of CaF_2 with the other components of Cell I. In the Cell II most of these restrictions were removed by separating the electrolyte from the electrodes.

The mutual solubility of phases in the cell must be small in order to prevent the cell reaction from taking place <u>chemically</u> rather than <u>electrochemically</u>. Such a chemical reaction will change the concentrations of the active species in the electrodes and the electrolyte with a consequent drifting of cell EMF. An example of this effect is the cell used by Ranford and Flengas[109] with a Ni anode, $Pt\text{-}O_2$ cathode and a $NiO\text{-}SiO_2\text{-}Na_2O\text{-}K_2O$ electrolyte. The Ni anode was rapidly attacked presumably due to easy oxygen transfer through the melt by the following reactions

$$\text{(cathode)} \quad \frac{1}{2}\,O_2 + 2(Ni^{2+}) \rightleftarrows (O^{2-}) + 2(Ni^{3+}) \quad (5.12)$$

$$\text{(anode)} \quad Ni_{(s)} + 2(Ni^{3+}) \rightleftarrows 3(Ni^{2+})\ . \quad (5.13)$$

TABLE 5.2

$\Delta G°$ FOR POSSIBLE REACTIONS IN CELL I AT 1700° AND 1800°K

Reaction	$\Delta G°_{1700°K}$, kcal	$\Delta G°_{1800°K}$, kcal
$2Al_{(\ell)} + 3CaF_{2(\ell)} \rightleftarrows 2AlF_{3(g)} + 3Ca_{(\ell,g)}$	+155.80	+148.48
$2Al_{(\ell)} + CaF_{2(\ell)} \rightleftarrows 2AlF_{(g)} + Ca_{(\ell,g)}$	+42.27	+35.99
$CaF_{2(\ell)} + \frac{1}{2} O_{2(g)} \rightleftarrows CaO_{(s)} + F_{2(g)}$	+117.42	+117.10
$3CaF_{2(\ell)} + Al_2O_{3(s)} \rightleftarrows 3CaO_{(s)} + 2AlF_{3(g)}$	+99.34	+94.48

Note: All data except ΔG_f° (CaO) from JANAF Tables[59]; ΔG_f° (CaO) from BOHS[2].

This "chemical" solubility of oxygen in the melt is associated with the presence of transition metal ions in the electrolyte. This problem is absent in the electrolytes used in this investigation.

The "physical" solubility of oxygen in CaF_2-Al_2O_3 slags has not been studied, although some data is reported for the CaO-SiO_2-Al_2O_3 system[136]. The scanty data on solubilities of gases in molten salts have been reviewed by Battino and Clever[137] and Janz[138]. The solubility of gases in oxide and silicate melts have been reviewed by Sasabe and Goto[136] who have also determined the permeability and diffusivity of oxygen in PbO-SiO_2($-FeO$) and CaO-SiO_2-Al_2O_3 systems using solid electrolyte oxygen cells.

From the observation of the sawtooth variation of EMF with time in Cell I, it can be inferred that the "physical" solubility of oxygen in CaF_2-Al_2O_3 slags is small. The small solubilities of oxygen in these slags gives rise to a sharp oxygen potential gradient in the slag layer which cause a "mixed" potential to be set up on the platinum electrode (see Section 5.2.2).

Many metals, especially alkali and alkaline earth metals, have considerable solubilities in their molten salts and these have been adequately reviewed[138,139]. For example, Ca has extensive solubility in liquid CaF_2 which becomes a predominantly electronic conductor after dissolving a certain amount of Ca. However, no Ca is expected in the electrolytes used since: (1) the reduction of CaF_2 by Al at the cell temperature is not favourable (see Table 5.2) and (2) the cell atmosphere will rapidly oxidize any Ca present.

No data on the solubilities of Al in the $CaF_2-Al_2O_3$ system are available although some data reported in ternary chloride melts[138] and in cryolite-alumina melts[138,140] have been reviewed. The solubility of Al in cryolite was found to be small (~0.085 wt%) at 1020°C and was substantially reduced by the addition of alumina. In any event, very little aluminum is expected in the electrolyte under the experimental conditions of the present study.

5.2.4 Reversibility of electrode processes

Before a cell EMF can be related to any thermodynamic quantity, reversibility of the electrodes must be assured. Fortunately, in high temperature molten salts the electrode reversibility is the rule rather than the exception. Reversibility of an electrode depends upon the velocities of the oxidation and reduction reactions taking place which are considerably accelerated by increasing temperature. Thus, large exchange currents are quite common in molten salt electrodes which favour reversibility and reduce the possibilities of encountering significant overvoltages. However, reversibility of electrodes in molten salts is not guaranteed by the rapidity of the redox reactions. If some side reaction occurs at the same electrode at a rate similar to the process of interest, chances of which are also increased at higher temperatures, the electrode becomes irreversible and a "mixed" potential is set up. This has already been discussed in Section 5.2.2.

The overall cell reversibility, which implies individual electrode reversibility, was tested in the case of Cell I by imposing EMF greater or less than the equilibrium value. On removal of this constraint the cell returned to its initial value within a few seconds. The variation of oxygen flow rate had no significant effect on cell EMF except at very high flow rates, probably caused by cooling of the oxygen electrode (see Section 5.2.1). The cell EMF was found to be a single valued function of temperature within the observed maximum scatter of ±13 mV (see Figure 4.4), the EMF decreasing with increasing temperature. This agrees with the thermodynamic consideration that alumina is formed from its constituents with a decrease in entropy.

These tests, coupled with evidence from the literature that the aluminum and oxygen electrodes essentially behave in a reversible manner in similar melts, were taken as sufficient justification to assume cell reversibility. The previous uses of the oxygen electrode at high temperatures have already been reviewed in an earlier section (§ 2.10). The aluminum electrode has been used in many high temperature cells, some of which have been reviewed in Section 2.11. This electrode is known to be reversible[114,141] in melts similar to those of the present investigation.

However, after an initial plateau period of 6-15 minutes the cell EMF slowly degenerated. This is believed to be due to some irreversible process taking place on the $Pt-O_2$ electrode. When the $Pt-O_2$ electrode was replaced by a C-CO electrode in Cell II, a stable cell EMF was obtained. Deterioration of $Pt-O_2$ electrodes has been observed before[102,114]. For example, Hill et al. found "poisoning" of their $Pt-O_2$ electrode by deposition of iron compounds on the Pt wire in $Li_2SO_4-K_2SO_4$ melt containing CaO. The platinum wire near the melt in Cell I was found to be dulled and some reaction with the melt cannot be discounted. A fresh surface was therefore exposed in each experiment.

5.2.5 Partial electronic conductivity of the melt

The difference between the standard free energies of formation obtained from Cell I and those obtained from thermochemical data could be caused by mixed ionic and electronic conduction in the electrolyte. A 3% electronic conductivity would result in the Cell I values being about 7.5 kcal/mole too positive and make them consistent with the generally accepted thermochemical data[58,59] (see Figure 4.5).

There is, however, considerable evidence in the literature which indicates that the ionic transport number of the electrolyte is greater than 0.97 and sufficiently close to unity to preclude the possibility of any large systematic error. These will be discussed now.

The main component of the electrolyte, i.e. CaF_2, is known to be an ionic conductor. Ure[142] measured transport numbers in solid CaF_2 and concluded that CaF_2 is predominantly an ionic conductor, almost the entire current being carried by fluorine F^- ions. Wagner[143] and Hinze and Patterson[144] have shown that CaF_2 remains an ionic conductor over a wide range of conditions. Literature on the transport properties of CaF_2 and its successful use as a solid electrolyte has been reviewed elsewhere[145]. Literature on the conductivity of solid Al_2O_3 has been reviewed[146,147] and although there is disagreement on the extent of conduction by the oxygen O^{2-} ion, substantial electronic conductivity in Al_2O_3 in the temperature range 900°-1750°C is established. While measurements of the conductivity of alumina[148-150] show predominantly electronic conductivity, significant ionic conductivity is reported from EMF measurements at 1170°C[33] to 1550°C[151]. Matsumura[152] determined an ionic transport number, t_i, of $\sim$0.8 at $p_{O_2} \sim 1$ atm. at 900°C. Although both he and Schmalzried[33] demonstrated that Al_2O_3 becomes a predominantly ionic conductor above 1300°C, Fischer and Ackermann[153] have reported oxygen ion transport numbers of 0.6-0.7 at 1600°-1700°C from EMF measurements.

Therefore, in the present work we are concerned with the conductivity of an electrolyte formed by the addition of a semiconducting solid to a molten ionic liquid. Bell and Flengas[154,155] have shown that when semiconducting sulphides such as PbS and Ag_2S are added to their respective ionic molten chlorides, the total conductivity decreases initially, the conductivity remaining totally ionic. On further additions, the conductivity passes through a minimum as electronic conduction is initiated. The data reported by Mitchell and Cameron[156], for the CaF_2-Al_2O_3 system in the same composition range as that of the present work, shows a steady decrease in conductivity with the addition of Al_2O_3 to molten CaF_2.

The value of the conductivity itself is an indication of the nature of conductivity. From consideration of the maximum mobilities of ions a value of 10 ohm^{-1} cm^{-1} has been calculated[157] as the limit of conductivity of ionic liquids. On the other hand, predominantly electronic conductors have higher conductivities, usually several times this value. Mitchell and Cameron's[156] data show a drop in conductivity from $\sim$6 ohm^{-1} cm^{-1} for pure CaF_2 to $\sim$1.2 ohm^{-1} cm^{-1} for CaF_2-30 wt% Al_2O_3. The drop in conductivity on addition of alumina is due to reduction of the concentration of charge-carrying ions[156].

Another indication of the ionic character of the slags used, comes from the work of Mitchell and Beynon[158] who report a Faradaic efficiency of 100% in a CaF_2-Al_2O_3 slag.

Finally, the ionic character of the electrolytes used is indicated by the good agreement of the present results with those from EMF cells at ~1300°K. The results from these cells[74,110-114], which have been reviewed in Section 2.11, are plotted in Figure 5.1 along with the data from Cell I and the presently accepted thermochemical data[58,59]. Except for the work of Thonstad[114] the results from Cell I are in good agreement with those from lower temperature cells assuming a linear variation of ΔG_f° in the temperature range indicated. Thonstad could not obtain a stable and reproducible EMF from his cell and his value represents the initial reading after switching off the current subsequent to several hours of electrolysis. As the probability of substantial electronic conduction is less at the lower temperatures, the difference between the thermochemical and cell data is believed to be due to some other reasons. Further discussion on the excellent agreement between the Third Law analysis of Cell I results and $\Delta H^\circ_{298}(Al_2O_3)$ from various sources, is reserved for a later section (§ 5.6).

Except for the above results, the evidence of ionic conductivity of the CaF_2-Al_2O_3 electrolytes presented from the literature is, at best, qualitative. However, the direct determination of the ionic conductivity of these corrosive melts at high temperatures, with an accuracy substantially better than ±3%, is believed to be difficult. For this reason it was decided to get indirect experimental evidence

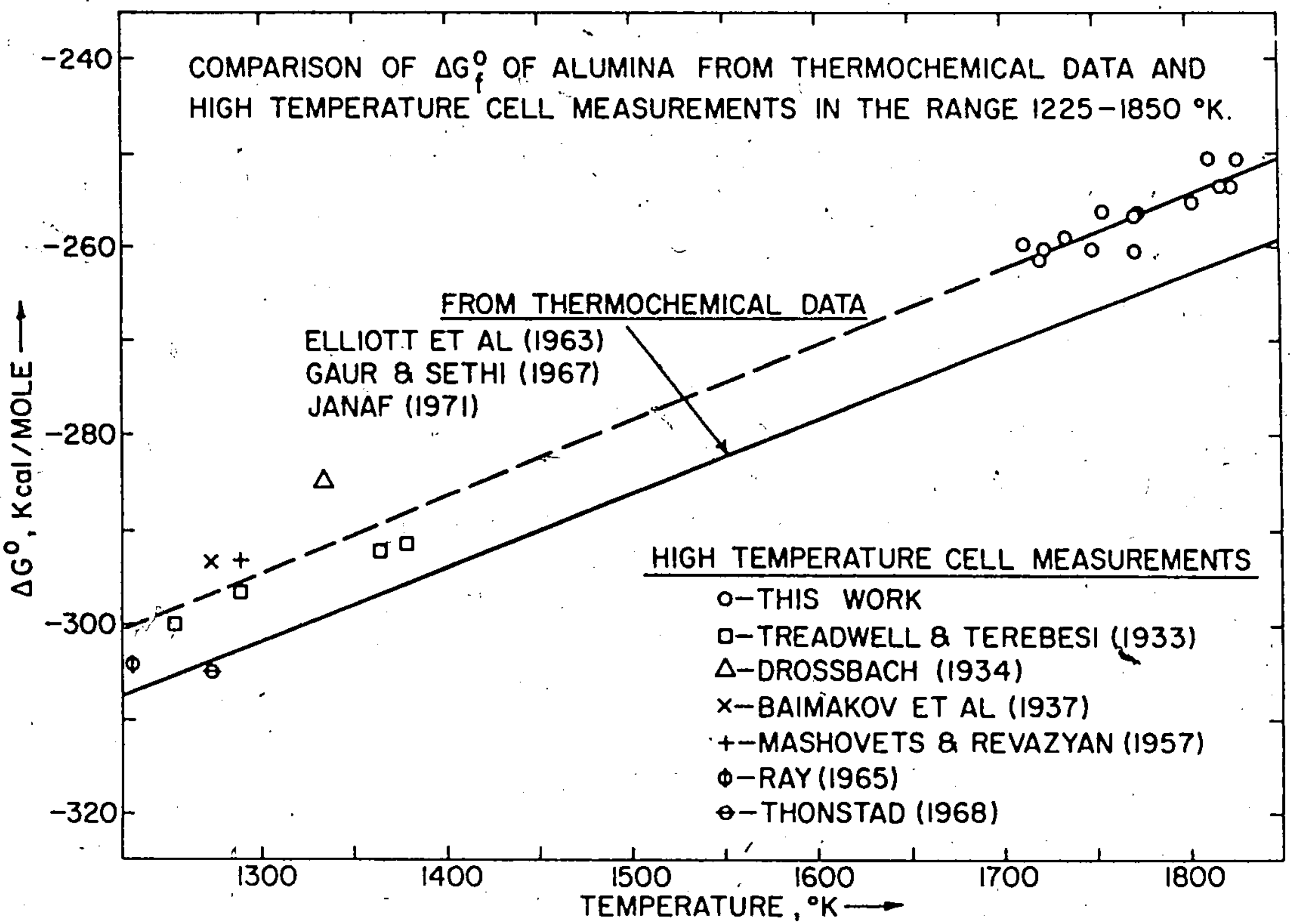

Figure 5.1: Comparison of ΔG_f^o (Al_2O_3) from thermochemical data and high temperature EMF cell measurements, (1225°- 1850°K).

by comparing the results from Cell I with those from cells using electrolytes known to be ionic. This led to the use of Cell II, results from which are discussed in the next section.

5.3 Cell II

The Cell II was studied in this investigation to check the results from Cell I which do not fully agree with presently accepted thermochemical data. Cell II, which can be represented by

$$C,\ Al_{(\ell)}\,|\,Al_2O_{3_{(s)}}\,|\,\underset{O^{2-}}{\text{Electrolyte containing}}\,|\,Al_2O_{3_{(s)}}\,|\,Fe\text{-}C_{satd.},\ CO_{(g)},\ C \tag{5.14}$$

is essentially an oxygen concentration cell using a liquid electrolyte in which the oxygen potential of the anode is determined by the Al-Al_2O_3 equilibrium while that of the cathode is given by the C-CO equilibrium. The anodic and cathodic reaction for this cell can be written as

$$\text{(Anode)}\qquad 2Al_{(\ell)} + 3(O^{2-}) \rightleftarrows Al_2O_{3_{(s)}} + 6e^- \tag{5.15}$$

$$\text{(Cathode)}\qquad 3CO_{(g)} + 6e^- \rightleftarrows 3(O^{2-}) + 3C \tag{5.16}$$

so that the total cell reaction is given by

$$2Al_{(\ell)} + 3CO_{(g)} \rightleftarrows Al_2O_{3_{(s)}} + 3C\ . \tag{5.17}$$

The standard free energy of this reaction was obtained from measurements of the cell EMF as all the components were kept at unit activity. Since the standard free energy of formation of CO is accurately known to within ±1 kcal/mole, the standard free energy of formation of alumina can be determined from Cell II data. The values of free energy of alumina thus obtained are compared with the data from Cell I in Figure 4.7 which also show the presently accepted thermochemical data[59]. From Figure 4.7 it can be seen that the Cell II data are in good agreement with the Cell I data, within the experimental error, and they are both significantly more positive than the thermochemical data.

Cell II was designed with a view to eliminating the possible sources of systematic error in Cell I. The separation of the electrode compartments from the electrolyte allowed the replacement of a CaF_2-Al_2O_3 electrolyte, whose electronic properties are unknown, by a well known ionic melt. The silicate melts containing alkali and alkaline earth metal ions are predominantly ionic conductors[159,130] and a slag in the CaO-SiO_2-Al_2O_3 system was chosen for the electrolyte. The electrolysis of CaO-SiO_2 slags[159] and the determination of transferance numbers[160] in CaO-SiO_2 and CaO-SiO_2-Al_2O_3 slags show that these slags are predominantly ionic conductors. For this reason CaO-SiO_2[161,162] and CaO-SiO_2-Al_2O_3[133,134,136,163-165] slags have been used in a number of EMF cells to determine thermodynamic properties of alloys or the slag system itself. Quite good agreement is obtained with determinations by other methods and confirm the highly ionic nature of these slags.

The composition of the slag chosen was 38 wt% CaO, 42 wt% SiO_2 and 20 wt% Al_2O_3 which is the composition of a ternary eutectic in the system at 1265°C. This allowed the temperature range of the determination of the standard free energy change to be extended to lower temperatures. Even at 1400°C the attack of this slag on recrystallized alumina refractory was not excessive and experiments could be carried out for over two hours. Unsaturated CaF_2-Al_2O_3 slags containing only 10 and 15 wt% Al_2O_3 were also used as electrolytes in Cell II as a check. The possibilities of significant electronic conductivity at these low concentrations of alumina are small.

In order to verify that the Pt-O_2 electrode was responsible for the deterioration of the EMF in Cell I after the initial constant period, the oxygen electrode was replaced by a C-CO electrode, which was separated from the electrolyte using an alumina sheath. The EMF of Cell II was found to be constant at constant temperature after the initial equilibration period. The reversibility tests, consisting of disturbing the equilibrium by imposing an external EMF, indicated that the electrodes were behaving in a reversible manner. Also, the same cell EMF was obtained when a given temperature was approached from a higher or lower value.

As identical electrode leads were used, no thermal EMF corrections are necessary in Cell II. As discussed in Section 5.2.1, the very small dissolution of graphite (contact) in liquid aluminum is not expected to change its activity significantly. The C-CO electrode and the reservoir were filled with CO at one atmosphere pressure which cannot change to any extent at the higher temperature. Thus, errors arising from non-standard conditions are expected to be negligible.

One of the satisfying aspects of the design of Cell II is the separation of the electrodes and the electrolyte which allows much greater flexibility than the earlier design. This separation also prevents any physical dissolution of the metal or the gas in the electrolyte which could subsequently react "chemically" at the other electrode.

Although the temperature gradient in the cell was not measured, it cannot be very different from that of Cell I. The errors in cell EMF arising from such gradients will be of the same order of magnitude as calculated for Cell I in Section 5.2.1. The errors in temperature and cell EMF measurements are the same as before. The cell temperature, however, was not determined to the same degree of accuracy as the induction unit was switched off before a reading could be taken. The temperature is estimated to be within ±10°C of the true value.

5.4 Second Law Analysis of the Present Data

The temperature variation of the standard free energy, ΔG°_T, data can be analysed by the "Second Law method" to give the enthalpy and entropy change, ΔH°_T and ΔS°_T, respectively, of the cell reaction in the experimental temperature range. The following well known thermodynamic relationships were used for that purpose

$$\Delta G^\circ_T = \Delta H^\circ_T - T\Delta S^\circ_T \tag{5.18}$$

$$\Delta H^\circ_T = \left[\frac{\partial(\Delta G^\circ/T)}{\partial(1/T)}\right]_P \quad \text{and} \quad \Delta S^\circ_T = -\left(\frac{\partial \Delta G^\circ}{\partial T}\right)_P \tag{5.19}$$

where the subscript P indicates constant pressure. From the equations it is apparent that the slope of the tangent of ΔG°_T curve at any temperature gives ΔS°_T at that temperature while the intercept of the tangent at absolute zero temperature gives the ΔH°_T. As ΔH°_T and ΔS°_T are not very sensitive functions of temperature, they can be assumed constant in a reasonable temperature range. The error from such an assumption has been shown[56] to be within the accuracy of most free energy data, although Kubaschewski et al.[57] propose an additional "T log T" term to better represent the free energy data. The experimental scatter in the present data does not warrant such a treatment and the data from Cell I has been treated by linear regression using formulae given in Appendix AII. The results are shown in Figure 4.5 and Section 4.6 along with the appropriate 95% confidence intervals. Some comments on the difference between the present data and the thermochemical data have already been made and further discussion will have to wait till the results of Third Law analysis are discussed.

The free energy data from Cell II are plotted along with Cell I data in Figure 4.7. It can be seen from the figure that data from both the cells are in very good agreement with each other within the experimental scatter. This has been taken as confirmation of (1) the predominantly ionic character of the CaF_2-Al_2O_3 electrolyte of Cell I, and (2) the essentially reversible value of cell EMF. It was shown in Section 5.2.5 that Cell I data are consistent with data from similar cells at lower temperatures (~1300°K). Thus, all the cell data seem to be consistent with each other.

The values of ΔH°_T and ΔS°_T obtained from the regression intercept and slope of Cell I data are now considered. The average value of ΔH°_T and ΔS°_T in the temperature range 1700°-1825°K are shown below along with those from JANAF Tables. Also shown are the 95% confidence intervals of the regression intercept and slope calculated using formulae given by Johnson and Leone[173].

	$-\Delta H^\circ_{av}$, kcal/mole		$-\Delta S^\circ_{av}$, kcal/mole-°K	
Present data (1700°-1825°K)	398[illegible]	(± 48)*	0.080	(± 0.027)
JANAF Tables (1700°-1800°K)	401.39		0.0778	

The present data appears to be in excellent agreement with the thermochemical data, ΔH°_{Av} and ΔS°_{Av}, being only 0.7% and 3% different. The fact that this agreement is only fortuitous can be seen from the rather large confidence intervals on ΔH°_{Av} and ΔS°_{Av} calculated from the present data. On the other hand, the largest value of the 95% confidence limit on ΔG° in the range 1713°-1827°K is ±1.9 kcal/mole, the smallest being ±1.0 kcal/mole. This apparent anomaly in the errors can be understood from the following considerations.

(1) The scatter in the data is too large to determine the temperature variation of ΔG° (i.e. ΔS°_{Av}) to any degree of accuracy. The value of ±0.027 kcal/mole-°K represents a ±34% variation in the ΔS°_{Av} value.

(2) This uncertainty in ΔS°_{Av} is magnified by three orders of magnitude

---

* Another estimate[174] ±1.0 kcal/mole (see Appendix AII).

in ΔH°_{Av} as the slope, ΔS°_{Av}, is used to extrapolate the data at 1700°-1850°K to 0°K to obtain ΔH°_{Av}. However, the accuracy of the ΔG°_T data in the temperature range 1700°-1850°K still remains at ±1.9 kcal/mole (max).

From this discussion it is apparent that a Second Law analysis of ΔG° data is not a good method of determining ΔH° values as an error in ΔG° could drastically change the ΔH° values. For this reason a Third Law analysis of the data was carried out.

5.5 Third Law Analysis

The Third Law analysis consists of converting free energy data at different temperatures to a common value of ΔH°_{298} using the known values of Gibbs energy functions of the products and the reactants. This method has the following advantages:

(1) Each experimental point is individually treated. This method can be even applied to a single observation.

(2) It can detect individual bad points in a set of experimental observations as points which are outside the normal scatter of values around an average ΔH°_{298}.

(3) It can reveal non-equilibrium or erroneous trends if the calculated ΔH°_{298} show some temperature dependence. This is based on the assumption that relatively accurate Gibbs energy functions are available.

The results of the Third Law analysis of Cell I data are shown in Table 4.8 and Figure 4.6. From this figure it is apparent that ΔH°_{298} values are independent of cell temperature. This was, however, checked out mathematically by calculating the correlation coefficient which is 0.05 in this case. The values of the average ΔH°_{298}, the standard deviation and the 95% confidence interval were calculated (see Appendix AII) and the results are summarized in Table 5.4.

Table 5.4 and Figure 4.6 also show the average ΔH°_{298}, the standard deviation and the 95% confidence interval of 10 independent determinations of ΔH°_{298} of alumina by "bomb" calorimetry, reviewed previously (§ 2.7.1). Although the presently accepted value of ΔH°_{298}, -400.40 kcal/mole (Holley and Huber[49] and Mah[51]), is 7.8 kcal/mole more negative than the average value of Cell I data, -392.55 kcal/mole, the average of <u>all</u> the calorimetric determinations is in excellent agreement with the present data.

The Third Law analysis of Cell II data is shown in Table 4.10 and summarized in Table 5.4 and Figure 4.10 in which the previous data are also included for comparison. The data from the three sources are in excellent agreement.

Finally, the standard free energy data from EMF measurements at ∿1300°K were also subjected to the Third Law analysis. The results are presented in Table 2.7, Table 5.4 and Figure 5.2. Again the agreement between the various sets of data is good.

Figure 5.3 summarizes the values of ΔH°_{298} obtained from all the sources.

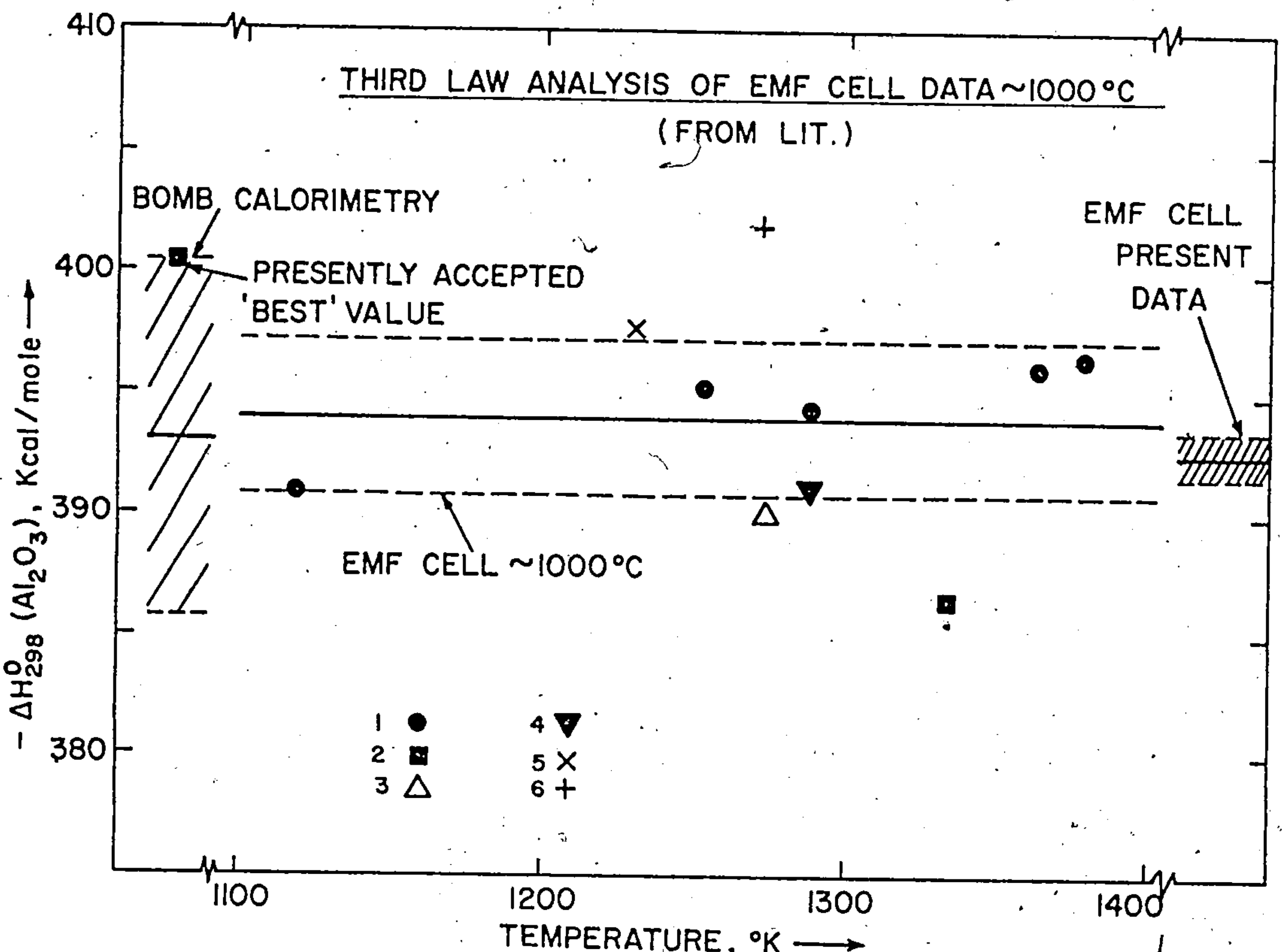

Figure 5.2: ΔH_f° (Al_2O_3) from the Third Law analysis of data from cells at ~1300°K (from literature). #1-Ref. 74, #2-Ref. 110, #3-Ref. 111, #4-Ref. 112, #5-Ref. 113, #6-Ref. 114.

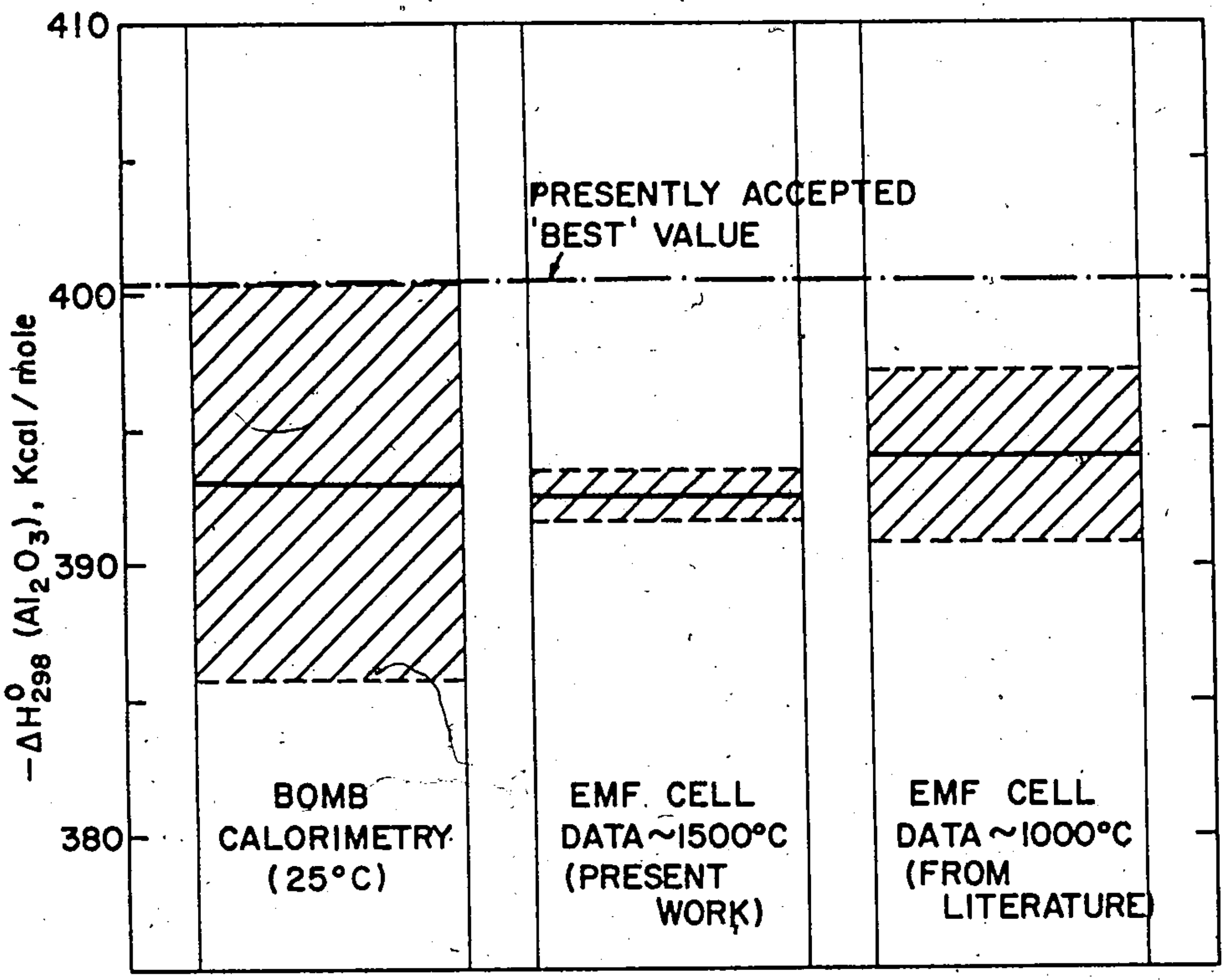

Figure 5.3: Comparison of ΔH°_{298} (Al_2O_3) obtained from different sources.

5.6 Critical Evaluation of "Bomb" Calorimetric Data

The ten determinations of ΔH°_{298} (Al_2O_3) by "bomb" calorimetry reported in the literature since 1901 have already been reviewed in Section 2.7.1. The type and purity of the materials used and the results obtained by the various workers are summarized in Table 2.4. In Figure 4.6 these values are plotted and the average of the ten determinations along with the 95% confidence interval of the data are shown. Also indicated in the figure is the presently accepted "best" value[58,59] of -400.4 kcal/mole based on the data of Holley and Huber[49] (-400.29 kcal/mole) and Mah[51] (-400.48 kcal/mole).

From Table 2.4 and Figure 4.6 it is apparent that while the estimated precision by the various authors never exceeds ±0.5%, the maximum divergence in these values is 27 kcal/mole or nearly 7%. As noted earlier, three values determined by <u>one</u> investigator (Roth) over a period of eleven years show a range of 22 kcal/mole. Some of the reasons for these discrepancies were given in Section 2.7.1 and they are now discussed in detail.

The metal sample must be as pure as possible since contamination may introduce a disproportionately large error into the results. Depending on the impurities the ΔH°_{298} value obtained can be higher or lower than the actual value. In order to explain the discrepancy with the present results, however, the impurities in the aluminum sample have to form more stable oxides than aluminum. This is unlikely.

The fluxing of molten Al_2O_3 with the crucible material can give rise to extrinsic heat effects resulting in an error in the calculated ΔH°_{298}. This can be avoided by the use of alumina crucibles, as is the case in the majority of the investigations reported (see Table 2.4). The crucibles used by Berthelot[42] and Wartenberg and Witzel[43] are not known while those used by Roth and Muller[45] were unsatisfactory in this respect.

Ignition aids are easily ignited materials used to start the combustion of rather inert substances. However, their use should be restricted as far as possible as they introduce additional errors, their heats of combustion, into the measurements.

The difference between the calibration run and the actual run can give rise to considerable error in the calculation of the total amount of heat liberated by the sample. For this reason the choice of proper sample size and control of experimental conditions are important considerations.

Incomplete combustion of the sample is one of the most common sources of error in bomb calorimetric studies. Fine particles from the sample may be thrown off the crucible by the violent combustion and will stop burning once they hit the cold surface of the bomb. Various estimates of this quantity by the investigators in case of aluminum are presented in Table 2.4, however, this quantity is difficult to determine accurately.

Another probable source of error is the percentage of the sample which is already oxidized. This will depend on the metal itself and the form of the sample used, i.e. powder, foil, etc, For this reason fine powder with a large surface area should be avoided.

Finally, the form of the combustion product obtained is a very important consideration when more than one polymorph can be formed.

Again, the estimation of the amounts of different crystalline products is difficult.

Critical evaluation of the data from aluminum combustion calorimetry given in the literature is almost impossible as it is difficult to determine to what extent each of these possible sources of error played a part in the individual determinations. Later investigators tend to discount the lower values obtained earlier by suggesting possible errors in those investigations arising from lower purity of metal and incomplete combustion of the sample. However, as there is no evidence to discount any particular value, equal weight was given to all the values reported. This results in an average value of ΔH°_{298} from bomb calorimetry of -393.08 ± 7.3 kcal/mole compared to the presently accepted "best" value of -400.4 ± 0.3 kcal/mole. These values are compared with the values obtained from the Third Law analysis of Cell I, Cell II and the cell measurements at ~1000°C reported in the literature, in Figures 4.6, 4.8 and 5.2, respectively. From these figures it is evident that the "average" value of -393.08 kcal/mole is in excellent agreement with all the electrochemical cell data.

5.7 ΔH°_{298} Calculated from Mineralogical Data

After the publication of the present results[175] discrepancies in the thermochemical data of several alumina bearing minerals have been brought to the attention of the author. Some of these discrepancies will now be presented.

In 1969 Zen[167] presented data for the following reactions:

$$\text{Kaolinite} + 2\ \text{Quartz} \rightleftarrows \text{Pyrophyllite} + H_2O \qquad (5.20)$$

$$\text{Pyrophyllite} \rightleftarrows \text{Andalusite} + 3\ \text{Quartz} + H_2O \qquad (5.21)$$

$$\text{Pyrophyllite} + 3\ \text{Corundum} \rightleftarrows 4\ \text{Kyanite} + H_2O \qquad (5.22)$$

in the temperature range 290°-525°C and the pressure range 0.6-7.0 k bar. The chemical formulae of the minerals are given in Table 5.3. Waldbaum[168] has used the data for equation (5.20) to calculate $\Delta H^\circ_{f,298}$ for pyrophyllite as -1338.28 ± 1.3 kcal/mole. Combining this value with the data of reaction (5.21) a value of -612.75 ± 1.6 kcal/mole has been obtained for $\Delta H^\circ_{f,298}$ (andalusite). Finally, using the data of Holm and Kleppa[169], Waldbaum has obtained

$$\Delta H^\circ_{f,298}\ (\text{corundum}) = -\ 393.76 \pm 1.7\ \text{kcal/mole}\ .$$

The equilibrium data[167] for reaction (5.22) was combined[168] with the data for kyanite (from solution calorimetric data[169] and enthalpy data[170]) to give

$$\Delta H^\circ_{f,298}\ (\text{corundum}) = -\ 391.50 \pm 3.0\ \text{kcal/mole}\ .$$

In a later paper, Zen[171] has calculated the standard free energy and enthalpy of formation at 298°K of a number of alumina bearing minerals

TABLE 5.3

SUMMARY OF $\Delta H^\circ_{f,298}$ (Al_2O_3) CALCULATED FROM MINERALOGICAL DATA[168]

No.	Reaction	$\Delta H^\circ_{f,298}$ (α-Al_2O_3), kcal/mole
1	$\underset{\text{Kaolinite}}{Al_2Si_2O_5(OH)_4} + \underset{\text{Quartz}}{2SiO_2} = \underset{\text{Pyrophyllite}}{Al_2Si_4O_{10}(OH)_2} + H_2O$ $\underset{\text{Pyrophyllite}}{Al_2Si_4O_{10}(OH)_2} = \underset{\text{Andalusite}}{Al_2SiO_5} + \underset{\text{Quartz}}{3SiO_2} + H_2O$	-393.76 ± 1.7
2	$\underset{\text{Pyrophyllite}}{Al_2Si_2O_{10}(OH)_2} + \underset{\text{Corundum}}{3Al_2O_3} = \underset{\text{Kyanite}}{4Al_2SiO_5} + H_2O$	-391.5 ± 3.0
3	$\underset{\text{Muscovite}}{KAl_3Si_3O_{10}(OH)_2} = \underset{\text{K-feldspar}}{KAlSi_3O_8} + \underset{\text{Corundum}}{Al_2O_3} + H_2O$ and other Muscovite-K-feldspar equilibria	-396.18 ± 1.0
4	Solution calorimetric data involving γ-Al_2O_3	-396.38 ± 0.8
	Average	-394.46

from reaction equilibria data. Two sets of standard free energies for the different minerals were obtained; one set was based on the calorimetric data for corundum and the other set was based on the calorimetric data of muscovite[172]. These two sets are different by 7-10 kcal/mole. Waldbaum, however, does not attribute the entire difference to corundum and estimates the following enthalpy change from the above data

$$\Delta H^{\circ}_{f,298} \text{ (corundum)} = -\ 396.18 \pm 1.0 \text{ kcal/mole .}$$

Waldbaum has also presented calculations of ΔH°_{298} (Al_2O_3) from solution calorimetric data. The calculation will not be presented here as it is believed sufficient values from mineralogical data have been presented to indicate the magnitude of the discrepancy with calorimetric data. The values of $\Delta H^{\circ}_{f,298}$ (Al_2O_3) calculated by Waldbaum are summarized in Table 5.3.

Table 5.4 and Figure 5.3 compare the ΔH°_{298} obtained from the various sources. The agreement between the data is excellent considering the diverse sources of the data.

5.8 ΔH°_{298} (Al_2O_3) from Different Sources

In 1961 Chipman[176] presented evidence based on five different equilibria which indicated that the oxygen "bomb" calorimetric determination of ΔH°_{298} (SiO_2) was about 5 kcal/mole more positive than the actual value. This discrepancy was resolved independently by

TABLE 5.4

SUMMARY OF $\Delta H^\circ_{f,298}$ (Al_2O_3) DATA FROM DIFFERENT SOURCES

Source	No. of data points	Average $-\Delta H^\circ_{f,298}$, kcal/mole	Standard Deviation, kcal/mole	95% Confidence limits, ±kcal/mole
Present study, Cell I	14	392.55	1.73	1.00
Present study, Cell II	6	392.71	2.20	2.31
Present study, all data	20	392.60	1.87	0.92
EMF cell at ∿1000°C (from literature)	10	394.06	4.44	3.18
Mineralogical Data	4	394.46	-	-
Oxygen bomb calorimetry				
(a) Presently accepted "best" value	2	400.40	-	0.3
(b) All data	10	393.08	10.23	7.32

Good[177] and Wise et al.[178] using different calorimetric methods. In this case, the 8 kcal change in the enthalpy of formation of quartz could be attributed to the presence of unburnt silicon.

However, from Table 5.4 it is apparent the proposed error in the presently accepted calorimetric value for Al_2O_3 is in the other direction. It is not known what could cause the measurement of enthalpy of alumina formation by oxygen bomb calorimeter to be more negative than the actual value and further resolution of this discrepancy must await determination by a different calorimetric method.

5.9 Deoxidation Equilibrium Constant Using the Present Value of $\Delta G^\circ_f\ (Al_2O_3)$

The free energy change for the reaction

$$2[Al]_{1w/o} + 3[O]_{1w/o} \rightleftarrows Al_2O_{3(s)} \qquad (5.23)$$

can now be calculated using the standard free energy of formation of alumina $\Delta G^\circ_f\ (Al_2O_3)$ determined in this investigation in the temperature range 1700°-1850°K and the data on solution of Al[16] and oxygen[2] in iron. The following equations may be considered

$$2Al_{(l)} + \frac{3}{2}O_{2(g)} \rightleftarrows Al_2O_{3(s)} \qquad \Delta G^\circ_1 = -398,560 + 80.02T \text{ cal} \qquad (5.24)$$

$$Al_{(l)} \rightleftarrows [Al]_{1w/o} \qquad \Delta G^\circ_2 = -15,100 - 6.67T \text{ cal}^{(16)} \qquad (5.25)$$

$$\frac{1}{2}\,O_{2(g)} \rightleftarrows [O]_{1w/o} \qquad \Delta G_3^\circ = -28{,}000 - 0.69T \text{ cal}^{(2)} \;. \tag{5.26}$$

The free energy change for reaction (5.23), ΔG°, is given by

$$\Delta G^\circ = \Delta G_1^\circ - 2\Delta G_2^\circ - 3\Delta G_3^\circ$$

$$= -284{,}360 + 95.43T \text{ cal} \tag{5.27}$$

from which $K = h_{Al}^2 h_O^3$ is calculated as

$$\log K = -\frac{62{,}160}{T} + 20.86 \;\; (\pm 0.2 \text{ at } 1873°K) \;. \tag{5.28}$$

This value of K is plotted in Figure 2.2 along with the thermochemical value[16] and the results of many experimental determinations of the same quantity. Using the presently accepted standard free energy of formation of alumina, a value of 4.5×10^{-14} can be calculated[16] for K at 1600°C which is an order of magnitude different from the value of 4.7×10^{-13} obtained from equation (5.28). The present results are in good agreement with the value of 1.2×10^{-13} recently obtained by Jacquemont et al.[32] using a ThO_2 (Y_2O_3) solid electrolyte oxygen concentration cell. From Tables 2.1 and 2.2 it can be seen that the present results are also in good agreement with the following experimental determinations: Swisher[13] $K' = 1.8\times10^{-13}$; Repetylo et al.[11] $K' = 5\times10^{-13}$; Geller and Dicke[17] $K' = 4.1\times10^{-13}$; and the extrapolated results of d'Entremont et al.[15] $K' = 2.5\times10^{-13}$. Comparison with Table 2.3 indicates that all the earlier estimations of

K using thermochemical data predict smaller values than those given above, the largest value of K in Table 2.3 being 8.9×10^{-14} at 1600°C[39].

CHAPTER VI

SUMMARY AND CONCLUSIONS

(1) Large variations in the reported values of the equilibrium constant, K, for the aluminum deoxidation of iron are due to errors in the analyses of small concentrations of aluminum and oxygen, the presence of reaction product in the samples and non-equilibrium conditions. A more reliable value of K can be calculated from the standard free energy of formation of alumina, ΔG_f° (Al_2O_3).

(2) There is no direct experimental determination of ΔG_f° (Al_2O_3) reported at steelmaking temperatures, the highest temperatures at which such determinations are reported being at aluminum extraction temperatures ~1000°C. These results are at variance with the thermochemical data which are calculated from the standard heat of formation at 298°K, ΔH_{298}°, and specific heat data. The uncertainty in the value of ΔH_{298}° makes the present thermochemical values uncertain.

(3) A high temperature electrochemical formation cell

$$\text{Cell I} \quad Pt_{(s)}, Al_{(\ell)} \mid Al_2O_3 \text{ in } CaF_{2(\ell)} \mid O_{2(g)}, Pt_{(s)}$$

has been designed and used under standard conditions to yield the standard free energy of formation of alumina in the temperature range 1713°-1827°K. The proper working of the cell has been checked by performing a number of tests. The deterioration of the cell EMF after an initial period of constant EMF is believed to be due to the deterioration of the oxygen electrode.

(4) Regression analysis of ΔG°_f (Al_2O_3) data from Cell I give the following relationship

$$\Delta G^\circ_f\ (Al_2O_3) = -398{,}560 + 80.02T\ (\pm\ 1{,}800)\ \text{cal/mole}$$

in the temperature range 1700°-1850°K.

(5) These free energy values are consistent with those determined at ~1000°C using a similar technique but are 3.3% more positive than the generally accepted thermochemical values at 1800°K.

(6) In order to confirm the absence of systematic errors in Cell I arising from any partial electronic conductivity of the CaF_2-Al_2O_3 electrolyte or the non-reversible behaviour of the oxygen electrode, the the following cell was designed and operated in the temperature range 1641°-1785°K.

$$\text{Cell II}\quad C_{gr},\ Al_{(\ell)}\,|\,Al_2O_3\,|\,\underset{(O^{2-})}{\text{Electrolyte containing}}\,|\,Al_2O_3\,|\,Fe\text{-}C_{satd},CO_{(g)},C_{gr}.$$

Highly ionic CaO-SiO_2-Al_2O_3 melts and CaF_2-Al_2O_3 melts were used as electrolytes.

(7) Using the well established standard free energy of formation of $CO_{(g)}$, ΔG°_f (Al_2O_3) was calculated from Cell II data. The results are in good agreement with those of Cell I, within the experimental error,

and they are both significantly more positive than the accepted thermochemical data.

(8) The Second Law analysis of the present data gives ΔH°_{Av} = -398.56 (±47.8) kcal/mole and ΔS°_{Av} = 0.0800 (±0.027) kcal/mole-deg which are in good agreement with the thermochemical data. However, this agreement is only fortuitous due to large errors associated with the results of the Second Law analysis of the present data.

(9) The Third Law analysis of the present data gives

Cell I ΔH°_{298} = -392.55 ± 1.00 kcal/mole

Cell II ΔH°_{298} = -392.71 ± 2.31 kcal/mole

Combined ΔH°_{298} = -392.60 ± 0.92 kcal/mole .

(10) These values are in good agreement with the Third Law analysis of data from electrochemical cells at ~1000°C reported in the literature.

(11) The present data is also in very good agreement with ΔH°_{298} (Al_2O_3) calculated from phase equilibria and solution calorimetric data in mineralogical systems.

(12) All these values are in variance with the presently accepted "best" value of ΔH°_{298} (Al_2O_3) = -400.40 (± 0.3) kcal/mole determined by oxygen bomb calorimetry. However, the average of ten determinations of ΔH°_{298} by bomb calorimetry reported in literature is in excellent agreement with the above results.

(13) Therefore, sufficient evidence now exists to indicate that the presently accepted ΔH°_{298} (Al_2O_3) may be 6-8 kcal/mole more negative than the true value. The ΔG°_f (Al_2O_3) will, then, be in error by the same amount. This can be resolved by an independent calorimetric determination of ΔH°_{298}, using a method other than oxygen bomb calorimetry.

(14) Using the present ΔG°_f (Al_2O_3) data and the data on aluminum and oxygen dissolution in iron, the following relationship can be obtained

$$\log K = -\frac{62,160}{T} + 20.86 \quad (\pm 0.2 \text{ at } 1873^\circ\text{K})$$

where $K = h^2_{Al} \cdot h^3_O$. The value of K at 1600°C is in good agreement with the most recent work of Jacquemont et al. and is an order of magnitude higher than earlier calculations.

REFERENCES

1 E. T. Turkdogan, J.I.S.I., 210, p 21, 1972

2 J. Chipman, Basic Open Hearth Steelmaking, (G. Derge, Ed.), AIME (Pub), p 640, 1964

3 C. Bodsworth and H. B. Bell, Physical Chemistry of Iron and Steel Manufacture, Longman (Pub), London 1972

4 H. Sawamura and N. Sano, Sub-comm. Phys. Chem. Steelmaking, 19th Comm., Third Div., Japan Soc. Promotion Sci., Sp. Rep. No. 3, Dec. 1963

5 J. Chipman, Metal Progress, p 211, 1949

6 G. R. Fitterer, Chemical Metallurgy of Iron and Steel, ISI Lond. (Pub), p 184, 1973

7 A. Jacquemont, C. Gatellier and M. Olette, Deoxidation Equilibrium in Liquid Iron, IRSID Report RE 109-3, 1975

8 M. W. Hessenbruch, Rev. Mét., 26, p 93, 1929

9 C. H. Herty et al., Co-op. Bull. No. 46, US Bur. Mines, Met. Advisory Board and Carnegie Inst. Tech., 1930

10 H. Wentrup and G. Hieber, Arch. Eisenh., 13, p 39, 1940

11 D. Repetylo et al., J. Met., p 45, May 1967

12 D. C. Hilty and W. Crafts, Trans. AIME, 188, p 414, 1950

13 J. H. Swisher, Trans. TMS-AIME, 239, p 123, 1967

14 N. A. Gokcen and J. Chipman, Trans. AIME, 197, p 173, 1953

15 J. C. d'Entremont, D. L. Guernsey and J. Chipman, Trans. TMS-AIME, 245, p 1501, 1969

16 R. J. Fruehan, Met. Trans., 1, p 3403, 1970

17 W. Geller and K. Dicke, Arch. Eisenh., 16, p 431, 1943

18 W. Geller, Arch Eisenh., 15, p 479, 1942

19 Z. Shibata and T. Yagihashi, Tetsu-to-Haganè, 39, p 393, 1953

20 M. N. Dastur and J. Chipman, Trans. AIME, 185, p 441, 1949

21 A. McLean and H. B. Bell, J.I.S.I., 203, p 123, 1965

22 S. E. Feldman and J. S. Kirkaldy, Can. Met. Quart., 13, p 625 1974

23 T. C. Wilder and J. F. Elliott, J. Electrochem. Soc., 107, p 628, 1960

24 Z. Buzek, Chemical Metallurgy of Iron and Steel, ISI Lond. (Pub), p 173, 1973

25 H. Schenck et al., Arch. Eisenh., 41, p 131, 1970

26 G. R. Belton and R. J. Fruehan, TMS-AIME, 245, p 113, 1969

27 L. E. Rohde et al., Arch. Eisenh., 42, p 165, 1971

28 T. B. Braun et al., as quoted by A. Vahed and D. A. R. Kay, Met. Trans. B, 6B, p 285, 1975

29 J. Chipman and F. C. Langenberg, The Physical Chemistry of Steelmaking, J. F. Elliott (Ed.), p 46, 1958

30 H. Sawamura et al., Fac. of Engg. Mem., 19, p 207, Kyoto Univ., Japan, 1957

31 K. Kiukkola and C. Wagner, J. Electrochem. Soc., 104, p 379-87; p 308-16, 1957

32 A. Jacquemont et al., C. R. Acad. Sc. Paris, 277, Ser. C, p 271, 1973

33 H. Schmalzried, Z. Phys. Chem., 38, p 87, 1963

34 H. Schenck, Physical Chemistry of Steelmaking (English Translation), BISRA, 1945

35 J. Chipman, Trans. ASM, 22, p 385, 1934

36 J. Chipman, BOH Steelmaking, Phys. Chem. of Steelmaking Comm., AIME, p 466, 1944

37 J. Chipman, ibid, p 621, 1951

38 O. Kubaschewski, J.I.S.I., 165, p 89, 1950

39 F. D. Richardson, ibid, 166, p 137, 1950

40 A. McLean and R. G. Ward, ibid, 204, p 8, 1966

41(a) L. Brewer, Chem. Revs., 52, (1), Feb. 1953

(b) E. Huber and C. E. Holley, Techniques of Metals Research, 4, part 1, R. F. Bunshah (Ed.), Interscience (Pub), 1970

42 M. Berthelot, Ann. Chim. Phys., 22, p 479, 1901

43 H. Wartenberg and G. Witzel, Z. Electrochem., 25, p 209, 1919

44 J. E. Moose and S. W. Parr, J. Am. Ch. Soc., 46, p 2656, 1924

45 W. A. Roth and F. Muller, Z. Phys. Chem., A144, p 253, 1929

46 A. Meichsner and W. A. Roth, Z. Electrochem., 40, p 19, 1934

47 W. A. Roth, U. Wolf and O. Fritz, ibid, 46, p 42, 1940

48 P. Snyder and H. Seltz, J. Am. Chem. Soc., 67, p 683, 1945

49 C. Holley and E. Huber, J. Am. Chem. Soc., 73, p 5577, 1951

50 A. Schneider and G. Gattow, Z. anorg. u. allegem. Chem., 277, p 41, 1954

51 A. D. Mah, J. Phys. Chem., 61, p 1572, 1957

52 M. de Kay Thompson, "The Total and Free Energies of Formation of the Oxides of Thirty-Two Metals", Electrochem. Soc. (Pub), N.Y., 1942

53 K. K. Kelley, US Bur. Mines Bull., No. 371 (1934); 434 (1941); 383 (1935); 393 (1936); 476 (1949); 477 (1950); and 584 (1960)

54 F. D. Rossini et al., Selected Values of Chemical Thermodynamic Properties, NBS Circ. 500, 1952

55 C. E. Wicks and F. E. Block, Thermodynamic Properties of 65 Elements - Their Oxides, Carbides and Nitrides, US Bur. Mines Bull. 605, 1963

56 F. D. Richardson and J. H. E. Jeffes, J.I.S.I., 160, p 261, 1948

57 O. Kubaschewski et al., Metallurgical Thermochemistry, (4th Ed.), Pergamon Press, 1967

58 J. F. Elliott et al., Thermochemistry for Steelmaking, V.1 (1960), V.2 (1963), Addison-Wesley (Pub)

59 D. R. Stull and H. Prophet (Ed.), JANAF Thermochemical Tables, (2nd Ed.), US Dept. Comm., 1971

60 F. T. Furukawa et al., J. Res. NBS, 57, p 67, 1956

61 D. A. Ditmars and T. B. Douglas, J. Res. NBS, 75A, p 401, 1971

62 D. C. Ginnings, J. Phys. Chem., 67, p 1917, 1963

63 C. H. Shomate and B. F. Naylor, J. Am. Chem. Soc., 67, p 72, 1945

64 M. Hoch and H. L. Johnston, J. Phys. Chem., 65, p 1184, 1961

65 A. Ferrier and M. Olette, C. R. Acad. Sc. Paris, 254, p 4293, 1962

66 P. B. Kantor et al., Ukr. Fiz. Zh., 7(2), p 205, 1962

67 R. A. McDonald, J. Chem. Eng. Data, 12, p 115, 1967

68 D. R. Stull and G. C. Sinke, Thermodynamic Properties of the Elements, Am. Chem. Soc. Monograph No. 18, Wash., 1956

69 R. Hultgren et al., Selected Values of Thermodynamic Properties of Metals and Alloys, Wiley (Pub), N.Y., 1963

70 E. H. Buyco and F. E. Davis, J. Chem. Eng. Data, 15, p 518, 1970

71 J. H. Awbery and E. Griffiths, Proc. Phys. Soc. (Lond.), 38, p 378, 1926

72 A. B. Newman and G. G. Brown, Ind. Eng. Chem., 22, p 995, 1930

73 P. Drossbach, Z. Elektrochem., 36, p 179, 1930

74 W. D. Treadwell and L. Terebesi, Helv. Chim. Acta, 16, p 922, 1933

75 W. Fischer and R. Gewehr, Z. anorg. allgem. Chem., 209, p 24, 1932

76 J. Chipman, Trans. ASM, 30, p 817, 1942

77 Y. H. Chou and J. F. Elliott, Acta Chim. Sinica, 22, p 23, 1956

78 R. Lorentz and F. Erbe, Z. Anorg. Chem., 183, p 311, 1929

79 M. Hillert, B. L. Averbach and M. Cohen, Acta Met., 4, p 31, 1956

80 J. Chipman and T. P. Floridis, Acta Met., 3, p 456, 1955

81 T. C. Wilder and J. F. Elliott, J. Electrochem. Soc., 107, p 628, 1960

82 O. J. Kleppa, J. Phys. Chem., 60, p 446, 1956

83 F. Vachet et al., C. R. Acad. Sc. Paris, 260, p 453, 1965

84 F. Woolley and J. F. Elliott, TMS-AIME, 239, p 1872, 1967

85 G. R. Belton and R. J. Fruehan, TMS-AIME, 245, p 113, 1969

86 T. P. Floridis and J. Chipman, TMS-AIME, 212, p 549, 1958

87 E. S. Tankins et al., TMS-AIME, 230, p 820, 1964

88 J. Chipman, J. Am. Chem. Soc., 55, p 3131, 1933

89 J. Lumsden, Thermodynamics of Molten Salt Mixtures, Academic Press (Pub), 1966

90 M. Blander (Ed.), Molten Salt Chemistry, Interscience, N.Y., 1964

91 B. R. Sundheim, Fused Salts, McGraw-Hill (Pub), N.Y., 1964

92 Yu. K. Delimarskii and B. F. Markov, Electrochemistry of Fused Salts, Sigma Press (Pub), 1961

93 R. W. Laity, Electrodes in Fused Salt Systems, in Reference Electrodes, edited by D. J. G. Ives and G. J. Janz, p 524, Academic Press, N.Y., 1961

94 T. B. Reddy, Electrochem. Tech., 1, p 325, 1963

95 C. Solomons, in "Techniques of Metals Research", 4, part 2, R. A. Rapp (Ed.), Interscience (Pub), p 35, 1970

96 C. Dijkhuis et al., Chem. Rev., 68, p 253, 1968

97 H. A. Laitinen and B. B. Bhatia, J. Electrochem. Soc., 107, p 705, 1960

98 H. Lux, Z. Elektrochem., 45, p 303, 1939

99 H. Flood et al., Acta Chem. Scand., 6, p 257, 1952

100 P. Csaki and A. Ditzel, Glastechn. Ber., 18, p 33 (& 65), 1940

101 R. Didtschenko and E. G. Rochow, J. Am. Chem. Soc., 76, p 3291, 1954

102 D. G. Hill et al., J. Electrochem. Soc., 105, p 408, 1958

103 L. N. Antipin, Zhur. Fiz. Khim., 29, p 1668, 1955

104 H. Ito and T. Yanagase, Trans. Jap. Inst. Metals, 1, p 115, 1960

105 V. I. Minenko and N. S. Ivanova, Ukr. khim. Zh., 29, p 1160, 1963 (Russ)

106 R. Sridhar and J. H. E. Jeffes, Trans. Instn. Min. Met., Sec. C, 76, p C44, 1967

107 B. M. Lepinskikh and O. A. Esin, Zh. neorg. Khim., 6, p 1223, 1961; Russ. J. inorg. Chem., 6, p 625, 1961

108 Yu. K. Delimarskii and V. N. Andreeva, Russ. J. inorg. Chem., 5, p 873, 1960

109 R. E. Ranford and S. N. Flengas, Can. J. Chem., 43, p 2879, 1965

110 P. Drossbach, Z. Elektrochem., 40, p 605, 1934

111 Yu. V. Baimakov et al., reported in ref. 112

112 V. P. Mashovets and A. A. Revazyan, Zh. Prikl. Khim. Leningr. (Eng. Trans), 30, p 1069, 1957

113 M. Rey, C. R. hebd. séanc. Acad. Sci. Paris, 260, p 5528, 1965

114 J. Thonstad, Electrochemica Acta, 13, p 449, 1968

115 J. H. E. Jeffes and R. Sridhar, in "Electromotive Force Measurements in High Temperature Systems", edited by C. B. Alcock, Am. Elsevier (Pub), 1968

116 C. M. Diaz and F. D. Richardson, Trans. Inst. Min. Met., p 196, 1967

117 F. A. Shunk, Constitution of Binary Alloys, Second Supplement, McGraw-Hill (Pub), N.Y., 1969

118 R. J. Fruehan et al., TMS-AIME, 245, p 1501, 1969

119 P. Pascal, Z. Electrochem., 19, p 610, 1913

120 Kuo Chu-Kun and Yen Tung-Sheng, Acta Chim. Sinica, 30, p 381, 1964

121 A. Mitchell and B. Burel, J.I.S.I., 208, p 407, 1970

122 W. E. Duckworth and G. Hoyle, Electro-slag Refining, Chapman and Hall (Pub), London, 1969

123 A. I. Vogel, A Text-Book of Quantitative Inorganic Analysis, p 510, 3rd Ed., Longmans (Pub), London, 1961

124 D. Ghosh, Reaction Sites in AC Electroslag Remelting, M.Eng. Thesis, McMaster University, Hamilton, 1972

125 M. Hansen, Constitution of Binary Alloys, 2nd Ed., McGraw-Hill (Pub), N.Y., 1958

126 I. Obinata and N. Komatsu, reported in ref. 117

127 R. Huch and W. Klemm, Z. Anorg. Allgem. Chem., 329, p 123, 1964

128 M. LaRosa, Nuovo Cimento, 12, p 284, 1916

129 E. Raub and G. Falkenburg, Z. Metallk., 55, p 186, 1964

130 K. S. Goto and W. Pluschkell, Physics of Electrolytes, edited by J. Hladik, 2, p 540, Academic Press (Pub), London, 1972

131 N. R. Thielke and R. L. Shepard, High Temperature Thermometry Seminar (Oct 1959), W. R. Grimes and D. R. Cuneo (Eds.), TID-7586 (Part 1), p 44, Oak Ridge, 1960

132 Temperature - Its Measurement and Control in Science and Industry, Am. Inst. Phys., Reinhold (Pub), N.Y., 1941

133 L. C. Chang and G. Derge, Trans. AIME, 172, p 90, 1947

134 K. Sanbongi and Y. Omori, Sci. Rep. Tohoku Univ., A11, p 244, 1959

135 A. Mitchell, Proc. Intern. Symp. on ESR Processing, Mellon Inst., Part II, paper 1, 1967

136 M. Sasabe and K. S. Goto, Met. Trans., 5, p 2225, 1974

137 R. Battino and H. L. Clever, Chem. Rev., 66, p 395, 1966

138 G. J. Janz, Molten Salts Handbook, Academic Press (Pub), N.Y., 1967

139 M. A. Bredig, in ref. 90, Chapter 5

140 A. M. Arthur, Met. Trans., 5, p 1225, 1974

141 R. Piontelli, Ann. N.Y. Acad. Sci., 79, p 1025, 1960

142 R. W. Ure, J. Chem. Phys., 26, p 1363, 1957

143 C. Wagner, J. Electrochem. Soc., 115, p 933, 1968

144 J. W. Hinze and J. W. Patterson, J. Electrochem. Soc., 120, p 96, 1973

145 Y. D. Tretyakov and A. R. Kaul, Physics of Electrolytes, Vol. 2, (J. Hladik, Ed.), p 623, Academic Press (Pub), London, 1972

146 B. Korousic, Min. Met. Quart., No. 1, p 47, 1970

147 T. H. Etsell and S. N. Flengas, Chem. Rev., 70, p 339, 1970

148 J. Pappis and W. D. Kingery, J. Am. Ceram. Soc., 44, p 459, 1961

149 W. D. Kingery and G. E. Meiling, J. Appl. Phys., 32, p 556, 1961

150 P. J. Harrop and R. H. Creamer, Brit. J. Appl. Phys., 14, p 335, 1963

151 R. Baker and J. M. West, J.I.S.I., 204, p 212, 1966

152 T. Matsumura, Can. J. Phys., 44, p 1685, 1966

153 W. A. Fischer and W. Ackermann, Arch. Eisenh., 39, p 273, 1968

154 M. C. Bell and S. N. Flengas, J. Electrochem. Soc., 111, p 575, 1964

155 M. C. Bell and S. N. Flengas, ibid, 113, p 31, 1966

156 A. Mitchell and J. Cameron, Met. Trans., 2, p 3361, 1971

157 A. F. Ioffe and A. R. Regel, Progress in Semiconductors, 4, A. F. Gibson (Ed.), Wiley (Pub), N.Y., 1960

158 A. Mitchell and G. Beynon, Met. Trans., 2, p 3333, 1971

159 J. O'M. Bockris et al., Trans. Farad. Soc., 48, p 536, 1952

160 O. A. Esin and A. K. Kirianov, Izv. Akad. Nauk. SSSR, Otdel. Tekn. Nauk., No. 12, p 28, 1955

161 K. Schwerdtfeger and H. J. Engell, Arch. Eisenh., 35, p 533, 1964

162 K. Schwerdtfeger and H. J. Engell, TMS-AIME, 233, p 1327, 1965

163 K. Sanbongi and Y. Omori, Sci. Rep. Tohoku Univ., A11, p 339, 1959; A13, p 174, 1961

164 K. Sanbongi and M. Ohtani, ibid, A5, p 263, 1953; A5, p 350, 1953; A7, p 204, 1955

165 M. Ohtani, ibid, A7, p 487, 1955

166 G. K. Sigworth and J. F. Elliott, Metal Science, 8, p 298, 1974

167 E-an Zen, Am. Mineral., 54, p 1592, 1969

168 D. R. Waldbaum, unpublished report, 1971

169 J. L. Holm and O. J. Kleppa, Am. Mineral., 51, p 1608, 1966

170 R. A. Robie and D. R. Waldbaum, Thermodynamic Properties of Minerals and Related Substances, US Geol. Surv. Bull., No. 1259, p 256, 1968

171 E-an Zen, Am. Mineral., 57, p 524, 1972

172 R. Barany, US Bur. Mines Rep. Invest. 6356, p 6, 1964

173 N. L. Johnson and F. C. Leone, Statistics and Experimental Design, Vol. I, Wiley (Pub), N.Y., 1964

174 A. D. Rickmers and H. N. Todd, Statistics, McGraw-Hill (Pub), N.Y., 1967

175 D. Ghosh and D. A. R. Kay, Metal-Slag-Gas Reactions and Processes, Z. A. Foroulis and W. W. Smeltzer (Eds.), Electrochem. Soc. (Pub), 1975

176 J. Chipman, J. Am. Chem. Soc., 83, p 1762, 1961

177 W. D. Good, J. Phys. Chem., 66, p 380, 1962

178 S. S. Wise et al., ibid, 66, p 381, 1962

179 H. Kojima et al., Can. J. Chem., 46, p 2968, 1968

180 R. C. Weast (Ed.), Handbook of Chemistry and Physics, CRC (Pub), 1973

181 H. F. Stimson, J. Res. NBS A, 65A, p 139, 1961

APPENDIX AI

X-RAY ANALYSIS OF CaF_2-Al_2O_3 ELECTROLYTE

X-ray diffraction analysis of the electrolyte samples were done to identify the phases present. The 'pure' starting materials were also analysed. A Philips diffractometer was used for the study. Typical results are shown in Tables AI.1, AI.2 and AI.3.

From the tables it can be seen that the patterns of CaF_2 and Al_2O_3 match quite closely with the standard ASTM patterns although the intensity ratio differ to some extent. Only an approximate method of taking the height of peaks (instead of area underneath them) was used to determine intensity ratios. In addition, since the intensities depend on sample preparation, these discrepancies are not surprising.

No CaO was detected in the 'pure' CaF_2. However, Table AI.3 shows the presence of $CaO \cdot 6Al_2O_3$ in the slag in addition to CaF_2 and Al_2O_3. All the major lines of $CaO \cdot 6Al_2O_3$ (I/I_0 > 0.3) were observed, although intensity ratios were quite different from the standard pattern.

TABLE AI.1

X-RAY DIFFRACTION PATTERN OF 'PURE' CaF_2

(BDH - AS RECEIVED)

Radiation: CuK_α, $\lambda = 1.5418$ Å; Scanning Speed - 1°/min

Count Rate: 400 Cps; Time Constant: 4 s

No.	CaF_2 (BDH-as received)			ASTM Ø4-0864	
	2θ, deg.	d, Å	$I/I_0 \times 100$	d, Å	$I/I_0 \times 100$
1	28.35	3.148	100	3.153	94
2	47.1	1.929	86	1.931	100
3	55.95	1.643	23	1.647	35
4	68.8	1.365	8	1.366	12
5	76.0	1.252	7	1.253	10
6	87.5	1.115	9	1.115	16
7	94.4	1.0507	3	1.0512	7
8	106.0	0.9653	2	0.9657	5
9	113.2	0.9234	3	0.9233	7
10	126.4	0.8637	4	0.8637	9

TABLE AI.2

X-RAY DIFFRACTION PATTERN OF α-Al_2O_3

(FISHER)

Radiation: CuK_α, λ = 1.5418 Å; Scanning speed - 1°/min

Count rate: 400 Cps; Time Constant: 4 s

No.	α-Al_2O_3 (Fisher-as received)			ASTM #10-173	
	2θ, deg.	d, Å	I/I_0×100	d, Å	I/I_0×100
1	25.7	3.466	75	3.479	75
2	35.3	2.543	98	2.552	90
3	38.0	2.368	43	2.379	40
4	ND*	-	-	2.165	<1
5	43.5	2.080	100	2.085	100
6	ND	-	-	1.964	2
7	52.7	1.737	42	1.740	45
8	57.65	1.600	76	1.601	80
9	ND	-	-	1.546	4
10	ND	-	-	1.514	6
11	61.5	1.508	7	1.510	8
12	66.65	1.403	26	1.404	30
13	68.35	1.372	39	1.374	50
14	ND	-	-	1.337	2
15	ND	-	-	1.276	4
16	77.20	1.236	12	1.239	16
17	ND	-	-	1.2343	8
18	80.8	1.189	4	1.1898	8
19	ND	-	-	1.1600	<1
20	84.5	1.147	3	1.1470	6
21	ND	-	-	1.1382	2
22	86.6	1.124	3	1.1255	6
23	ND	-	-	1.1246	4

TABLE AI.2 - continued

No.	α-Al_2O_3 (Fisher-as received)			ASTM #10-173	
	2θ, deg.	d, Å	$I/I_0\times100$	d, Å	$I/I_0\times100$
24	89.2	1.098	4	1.0988	8
25	ND	-	-	1.0831	4
26	91.3	1.078	7	1.0781	8
27	95.3	1.043	11	1.0426	14
⋮	⋮	⋮	⋮	⋮	⋮

* ND - Not detected or trace.

TABLE AI.3

X-RAY DIFFRACTION PATTERN OF SLAG SAMPLE

Radiation: CuK_{α}, λ = 1.5418 Å; Scanning speed - 1°/min

Count rate: 400 Cps; Time Constant: 4 s

Line No.	2θ, deg.	d, Å	$I/I_0 \times 100$	Matches the ASTM Standard line of *
1	20.2	4.403	2	CHA
2	22.2	4.010	2	CHA
3	25.7	3.466	7	A
4	28.35	3.148	100	CF
5	32.3	2.772	6	CHA
6	34.3	2.614	2	CHA
7	35.3	2.543	7	A
8	36.3	2.475	3	CHA
9	38.0	2.368	7	A
10	39.5	2.281	4	CHA
11	40.9	2.206	1	CHA
12	42.9	2.106	2	CHA
13	43.5	2.080	9	A
14	47.1	1.929	91	CF
15	52.7	1.737	4	A
16	55.9	1.645	29	CF
17	57.65	1.600	40	A
18	58.8	1.570	3	CHA
19	60.4	1.533	2	CHA
20	61.4	1.510	10	A
21	64.2	1.451	1	CHA
22	66.6	1.404	2	A
23	67.4	1.389	1	CHA
24	68.3	1.373	3	A

TABLE AI.3 - continued

Line No.	2θ, deg.	d, Å	$I/I_0 \times 100$	Matches the ASTM Standard line of *
25	68.8	1.365	8	CF
26	76.0	1.252	7	CF
27	77.1	1.237	3	A
28	87.5	1.115	17	CF
29	94.4	1.051	5	CF
30	95.3	1.043	2	A
31	106.0	0.965	7	CF
32	113.1	0.924	7	CF
33	126.3	0.864	7	CF
⋮	⋮	⋮	⋮	⋮

* CF - Calcium fluoride (CaF_2)

A - α-Alumina (Al_2O_3)

CHA - Calcium hexaluminate ($CaO \cdot 6Al_2O_3$)

APPENDIX AII

STATISTICAL METHODS

This section summarizes the statistical methods used in this investigation to treat the experimental data. These methods are described in detail by Johnson and Leone[173].

AII.1 Treatment of Free Energy of Formation Data

The standard free energy of formation data calculated from cell EMFs were treated by linear regression analysis. Taking $\Delta G°$ as the dependent variable y and the temperature as the independent variable x, the equation of the regression line is

$$E(y/x_i) = a + bx_i \qquad \text{(AII.1)}$$

where a is the estimate of the intercept;

b is the estimate of the slope; and

$E(y/x_i)$ represents the estimate of y ($\equiv \Delta G°$) at any temperature x_i. In addition to the basic assumption that $\Delta G°$ is a linear function of temperature, the thermodynamic implications of which have already been discussed in Section 5.4, the following assumptions were made about the data[173]:

(1) The x_i values (i.e. temperature) are controlled and/or observed without error.

(2) The deviations $y_i - E(y/x_i)$ are mutually independent.

(3) These deviations have the same variance σ^2 whatever be the value of x_i.

(4) These deviations are normally distributed.

By the method of least squares the following estimate of the slope and intercept can be derived[173] for n data points (x_i,y_i)

$$b = \frac{n\Sigma x_i y_i - \Sigma x_i \cdot \Sigma y_i}{n\Sigma x_i^2 - (\Sigma x_i)^2} \quad \text{(AII.2)}$$

$$a = \bar{y} - b\bar{x} \quad \text{(AII.3)}$$

where Σ represents the sum from $i=1$ to n;

$\bar{y}$ is the mean of y given by $\Sigma y_i/n$; and

$\bar{x}$ is the mean of x given by $\Sigma x_i/n$.

The standard deviation about the fitted line, S, is given by

$$S = \sqrt{\Sigma(y_i-a-bx_i)^2/(n-2)}$$

$$= \sqrt{[\Sigma y_i^2 - a\Sigma y_i - b\Sigma x_i y_i]/(n-2)} \quad \text{(AII.4)}$$

The 100(1-α) percent confidence interval (C.I.) about the regression line at any point x_0 is given by

$$\text{C.I.} = \pm t_{n-2,1-\alpha/2}\left(\frac{1}{n} + \frac{(x_0-\bar{x})^2}{\Sigma(x_i-\bar{x})^2}\right)^{1/2} S \quad \text{(AII.5)}$$

where $t_{n-2,1-\alpha/2}$ is Student's t-distribution with n-2 degrees of freedom.

The 100(1-α) percent confidence interval for the slope and the intercept were calculated using

$$C.I.(\text{slope}) = \pm \frac{t_{n-2,1-\alpha/2} \cdot S}{\sqrt{\Sigma(x_i-\bar{x})^2}} \tag{AII.6}$$

and

$$C.I.(\text{intercept}) = \pm t_{n-2,1-\alpha/2}\left(\frac{1}{n} + \frac{\bar{x}^2}{\Sigma(x_i-\bar{x})^2}\right)^{1/2} S\ . \tag{AII.7}$$

However, an alternate formula for the confidence interval for the intercept has been proposed by Rickmers and Todd[174]

$$C.I.(\text{intercept}) = \pm t_{n-2,1-\alpha/2} \cdot S/\sqrt{n} \tag{AII.8}$$

which gives a much smaller interval for the intercept of the present data than equation (AII.7). Equation (AII.7) seems to take care of the distance of the data points from x=0; the further the data points from x=0 the lower is the confidence on the value of intercept a. However, the confidence on y is unaffected by its distance from x=0.

Finally, the correlation coefficient was calculated using the formula

$$r = \frac{n\Sigma x_i y_i - \Sigma x_i \cdot \Sigma y_i}{\{[n\Sigma x_i^2 - (\Sigma x_i)^2][n\Sigma y_i^2 - (\Sigma y_i)^2]\}^{1/2}}\ . \tag{AII.9}$$

Before closing it is interesting to note the following points about the above analysis:

(1) Although there was obviously an error in the measurement of

temperature, it does not invalidate the above analysis. Any error in the temperature measurement can be considered as an error in the free energy assuming the temperature was correct. Thus, the errors calculated are the sum total of EMF and temperature measurements.

(2) The confidence limits calculated from the above analysis only represent the "random" error in the experimental data and do not include any systematic errors.

AII.2 Treatment of ΔH°_{298} Data From All Sources

ΔH°_{298} calculated from the Third Law analysis of the present cell data were first treated by the regression analysis given above. After making sure that ΔH°_{298} has no significant correlation with the experimental temperature, the data were treated by normal statistical methods[173] for a single variable. If (x_i), i=1 to n, represents the n data points, the mean $\bar{x}$ is given by

$$\bar{x} = \Sigma x_i / n \quad \text{(AII.10)}$$

The standard deviation S is given by

$$S = \sqrt{\Sigma (x_i - \bar{x})^2 / (n-1)} \quad \text{(AII.11)}$$

and the 100(1-α) percent confidence interval about the mean is given by

$$C.I. = \pm t_{n-1,1-\alpha/2} \cdot S/\sqrt{n} \tag{AII.12}$$

where the symbols have the same meaning as before.

The data from the Third Law analysis of the results obtained from cells at $\sim$1000°C were also treated in the same way without the initial regression analysis. The mean, standard deviation and the confidence intervals of the "bomb" calorimetric data were obtained using equations (AII.10) to (AII.12).